

**PRESSURE TRANSIENT ANALYSIS OF BINGHAM FLUIDS USING TIAB'S DIRECT
SYNTHESIS APPROACH**

A thesis submitted to the faculty at African University of Science and Technology in partial
fulfilment of the requirements for the degree of Master of Science in the Department of
Petroleum Engineering

By

PROSPER KUFAMUNI

Supervised by

Dr. Alpheus Igbokoyi



African University of Science and Technology

www.aust.edu.ng

P.M.B 681, Garki, Abuja F.C.T, Nigeria

Abuja, Nigeria

July, 2019

CERTIFICATION

This is to certify that the thesis titled “PRESSURE TRANSIENT ANALYSIS OF BINGHAM FLUIDS USING TIAB’S DIRECT SYNTHESIS APPROACH” submitted to the school of postgraduate studies; African University of Science and Technology (AUST), Abuja, Nigeria for the award of the Master’s degree is a record of original research carried out by Prosper Kufamuni in the Department of Petroleum Engineering.

**PRESSURE TRANSIENT ANALYSIS OF BINGHAM FLUIDS USING TIAB'S DIRECT
SYNTHESIS APPROACH**

By

Prosper Kufamuni

A THESIS APPROVED BY THE PETROLEUM ENGINEERING DEPARTMENT

RECOMMENDED:

.....

Supervisor: Dr. Alpheus Igbokoyi

.....

Committee Member: Prof David O. Ogbe

.....

Head, Department of Petroleum Engineering

APPROVED:

.....

Chief Academic Officer

.....

Date

©2019

Prosper Kufamuni

ALL RIGHTS RESERVED

ABSTRACT

This study investigated transient flow response of heavy oil that exhibit Bingham fluid characteristics. Four wellbore conditions in naturally fractured reservoirs were considered which include horizontal well, hydraulically fractured well, partially penetrating and fully penetrating vertical wells. Physical models were established and corresponding mathematical models were presented taking cognisance of minimum threshold pressure, λ_B . The model was solved analytically by successive application of Laplace and Fourier transforms. The solution was inverted from Laplace space to real domain by using Stehfest algorithm and was extended to obtain solutions for all the four wellbore conditions. Also, equations used for Tiab's Direct Synthesis (TDS) technique were derived, considering λ_B . It was established that the pressure derivative on log-log plot of a heavy oil reservoir with λ_{BD} is higher than that for oil behaving like Newtonian fluid by a factor of $(\lambda_{BD} + 1)$ at any time on pressure derivative curve for all four wellbore conditions.

Keywords: Bingham fluids, Pressure Transient Analysis, minimum threshold pressure, Tiab's Direct Synthesis technique, horizontal well, hydraulically fractured well, partially penetrating vertical well, fully penetrating vertical well.

DEDICATION

I dedicate this work to my sister

Tarisai Kufamuni

ACKNOWLEDGEMENT

I give the Almighty God through Jesus Christ our Lord and Saviour, all the Praise and Honour for His great Mercies that He showed me throughout the duration of my study at AUST. He has been my Provider and kept me like an apple of His eye. It wouldn't have been possible without God. I praise His holy name. I thank the African Development Bank (AfDB) for the Scholarship which I benefitted from. I also thank The World Bank through the PAMI fund for internship grant that they provided me to have an industrial hands-on experience.

I have special appreciation for the following individuals and friends:

- My main supervisor Dr. Alpheus Igbokoyi for his unwavering support, his availability and eagerness to assist and his encouragement during the course of this study. He has helped me achieve something that I initially thought was unsurmountable. This study has earned me a better understanding of well test analysis and I believe it will be very useful in my career. I pray God will bless him richly.
- My well test lecturer Dr Xingru Wu whose well test class was of great help.
- Prof. Djebbar Tiab whose class notes on pressure transient analysis was useful.
- All my classmates, particularly Emmanuel Adeyeye Adeyemi and Godfrey Osemudiamhen Eseigbe for their brotherly love and support throughout the course of the program.
- The AUST community for their numerous contributions towards the success of my study at AUST.

Last but most notably, my family particularly my parents for always standing by me and giving me reasons to soldier on even when my strength seemed almost spent.

TABLE OF CONTENTS

CONTENTS

| | |
|--|------------|
| ABSTRACT..... | iv |
| DEDICATION | v |
| ACKNOWLEDGEMENT | vi |
| TABLE OF CONTENTS..... | vii |
| LIST OF FIGURES..... | x |
| LIST OF TABLES | xii |
| CHAPTER 1 INTRODUCTION | 1 |
| 1.1 Background | 1 |
| 1.2 Statement of the Problem | 4 |
| 1.3 Objectives..... | 4 |
| CHAPTER 2 LITERATURE REVIEW..... | 5 |
| 2 | 5 |
| 2.1 Review of rheology of Non-Newtonian fluids..... | 5 |
| 2.1.1 Time independent fluids | 5 |
| 2.1.2 Time dependent fluids | 5 |
| 2.2 Flow of Bingham Plastic fluids | 7 |
| 2.3 Pressure transient analysis of Horizontal wells | 8 |
| 2.3.1 Flow regimes | 9 |
| 2.4 Sensitivity to different well and reservoir parameters | 12 |
| 2.4.1 Well length and position | 12 |
| 2.4.2 Sensitivity to anisotropy. | 14 |
| 2.4.3 Effect of wellbore storage..... | 15 |
| 2.5 Analytical solutions | 15 |
| 2.5.2 Pressure transient analysis of partially penetrating vertical well (PPVW) in naturally fractured reservoirs (NFR)..... | 22 |
| 2.5.3 Application of Tiab’s Direct Synthesis Technique in Pressure Transient Analysis | 28 |
| 2.6 Hydraulically fractured Wells | 31 |
| 2.6.1 Flow patterns in hydraulically fractured wells..... | 32 |
| 2.6.2 Dual Porosity Behaviour in Pressure Transient Analysis..... | 33 |
| CHAPTER 3 METHODOLOGY | 35 |
| 3 | 35 |
| 3.1 Incorporating minimum threshold pressure into inner boundary condition | 35 |
| 3.2 Physical Model formulation | 37 |

| | | |
|--|--|-----------|
| 3.2.1 | Assumptions..... | 37 |
| 3.2.2 | Physical model for horizontal well..... | 37 |
| 3.2.3 | Physical Model for hydraulically fractured Model..... | 38 |
| 3.2.4 | Physical model for partially penetrating vertical well | 39 |
| 3.2.5 | Physical Model for fully penetrating vertical well in a naturally fractured reservoir. ... | 40 |
| 3.3 | Mathematical models | 40 |
| 3.4 | Dimensionless Mathematical Model | 41 |
| 3.4.1 | Solution to the Dimensionless Mathematical Model | 44 |
| 3.4.2 | Transformation into Fourier space: | 46 |
| 3.4.3 | Solution to Dimensionless Mathematical Model..... | 48 |
| 3.4.4 | Extension of Point Source Solution..... | 51 |
| 3.5 | Investigating effects of parameters on pressure transient analysis..... | 54 |
| 3.5.1 | Investigating effect of λBD on Pressure Transient Analysis | 54 |
| 3.5.2 | Effect of ω , on the pressure response | 54 |
| 3.5.3 | Effect of interporosity flow parameter, (λ) on the pressure response for the four cases | 54 |
| 3.6 | TDS Technique | 55 |
| CHAPTER 4 RESULTS AND DISCUSSION..... | | 57 |
| 4 | | 57 |
| 4.1 | Effect minimum threshold pressure on pressure transient response of HW..... | 57 |
| 4.2 | Effect of well length on the flow regimes of HW in NFR | 59 |
| 4.3 | Effect of minimum threshold pressure in hydraulically fractured well in naturally fractured reservoir..... | 60 |
| 4.4 | Effects of minimum threshold pressure on partially penetrating vertical wells in NFR | 61 |
| 4.5 | Effect of penetration ratio in partially penetrating vertical wells in NFR..... | 63 |
| 4.6 | Effect of minimum threshold pressure on a fully penetrating vertical well in NFR..... | 64 |
| 4.7 | Effects of Storativity ratio | 65 |
| 4.7.1 | Horizontal Well | 66 |
| 4.7.2 | Hydraulically fractured well | 67 |
| 4.7.3 | Partially Penetrating Vertical Well..... | 68 |
| 4.7.4 | Fully Penetrating Vertical Well..... | 68 |
| 4.8 | Effects of interporosity flow parameter, λ | 69 |
| 4.8.1 | Horizontal well | 69 |
| 4.8.2 | Hydraulically fractured well | 70 |
| 4.8.3 | Partially penetrating vertical well | 70 |
| 4.8.4 | Fully penetrating vertical well..... | 71 |

| | | |
|---|--|-----------|
| 4.9 | Establishment of the pressure derivative at late radial flow | 71 |
| 4.9.1 | Horizontal Well | 72 |
| 4.9.2 | Hydraulically Fractured Well..... | 73 |
| 4.9.3 | Partially Penetrating Vertical Well..... | 74 |
| 4.9.4 | Fully penetrating vertical well..... | 74 |
| 4.10 | Derivation of permeability formular during early radial flow..... | 75 |
| 4.11 | Derivation of equation for average radial permeability | 77 |
| 4.12 | Derivation of equation for fracture length in hydraulically fractured well | 78 |
| 4.13 | Derivation of equation for storativity ratio | 79 |
| 4.14 | Derivation of equation for interporosity flow parameter | 80 |
| 4.15 | Example of Application | 80 |
| 4.15.1 | Calculating permeability during infinitely acting late radial flow | 82 |
| 4.15.2 | Calculating storativity ratio..... | 83 |
| 4.15.3 | Calculating interporosity flow parameter..... | 84 |
| CHAPTER 5 CONCLUSION AND RECOMMENDATIONS | | 85 |
| 5 | | 85 |
| 5.1 | Conclusions | 85 |
| 5.2 | Recommendations | 85 |
| REFERENCES | | 87 |
| APPENDIX A..... | | 89 |
| APPENDIX B..... | | 92 |
| APPENDIX C..... | | 93 |

LIST OF FIGURES

| | |
|---|----|
| Figure 2.1 Shear stress-shear rate relationship for Bingham plastic, pseudo-plastic, Newtonian and Dilatant fluids. (J. . Wu, 1990)..... | 6 |
| Figure 2.2 Early radial flow regime (Houzé et al., 2018)..... | 9 |
| Figure 2.3 Hemi-radial flow regime (Houzé et al., 2018)..... | 10 |
| Figure 2.4 Linear flow regime..... | 11 |
| Figure 2.5 Late radial flow regime | 12 |
| Figure 2.6 Pressure and pressure derivative curves on log-log plots (Mattar & Dean, 2008)..... | 12 |
| Figure 2.7 Log-log response for horizontal wells, variable well length. (Houzé et al., 2018)..... | 13 |
| Figure 2.8 Horizontal well pressure response to well placements (Houzé et al., 2018)..... | 14 |
| Figure 2.9 Horizontal well bi-logarithm response to variable to vertical anisotropy. | 14 |
| Figure 2.10 Horizontal well log-log response to wellbore storage..... | 15 |
| Figure 2.11 The pressure response for horizontal well of infinite conductivity | 19 |
| Figure 2.12 Log-log curves for flow regime recognition | 21 |
| Figure 2.13 Log-log curve of pressure and pressure derivative showing effect of variable dimensionless threshold pressure..... | 21 |
| Figure 2.14 Log-log curve of showing effects of wellbore length. | 22 |
| Figure 2.15 Different types of partially penetrating vertical wells based on the position in the perforated interval, hw (Slimani & Tiab, 2008) | 23 |
| Figure 2.16 Different types of partially penetrating vertical wells based on the position in the perforated interval, hw (Slimani & Tiab, 2008)..... | 24 |
| Figure 2.17 Dual porosity Model Diagnostic Plots; Build-up Test and its derivative.(Rebolledo & Ershaghi, 2015) | 26 |
| Figure 2.18 Effect of interporosity flow parameter on pressure derivative. (Slimani & Tiab, 2008) | 27 |
| Figure 2.19 Effect of dimensionless storage coefficient on pressure derivative | 28 |
| Figure 2.20 flow regimes in hydraulically fractured well..... | 32 |
| Figure 2.21 Model Reservoir (Warren & Root) Figure 2.22 Actual reservoir | 34 |
| Figure 0.1 Horizontal well in an underground formation (Nie et al., 2018) | 38 |
| Figure 0.2 Infinite conductivity vertical fracture in an infinite slab reservoir..... | 39 |
| Figure 0.3. Partially penetrating vertical well schematic. (Houzé et al., 2018). | 40 |
| Figure 4.1 Effect of λBD pressure on reservoir pressure response of horizontal well | 58 |
| Figure 4.2 CASE1: Effect of LD on flow regimes in horizontal wells | 59 |
| Figure 4.3 CASE2: Effect of LD on flow regimes in horizontal wells | 60 |
| Figure 4.4 Effect of λBD pressure on reservoir pressure response of hydraulically fractured well | 61 |
| Figure 4.5 Effect of λBD on pressure response of Partially Penetrating well | 62 |
| Figure 4.6 Pressure response to completed interval in a PPVW in NFR | 64 |
| Figure 4.7 Effect of λBD pressure on reservoir pressure response of fully penetrating vertical well | 65 |
| Figure 4.8 Effect of storativity on pressure response of a horizontal well | 66 |
| Figure 4.9 Effect of storativity ratio on pressure response of hydraulically fractured well..... | 67 |
| Figure 4.10 Effect of storativity on pressure response of a partially penetrating vertical well..... | 68 |
| Figure 4.11 Effect of storativity ratio on pressure response of a fully penetrating vertical well | 68 |
| Figure 4.12 Effect of interporosity flow parameter on horizontal well | 69 |
| Figure 4.13 Effects of interporosity flow parameter in hydraulically fractured well. | 70 |
| Figure 4.14 Effect of interporosity flow parameter in a partially penetrating vertical well..... | 70 |
| Figure 4.15 Effect of interporosity flow parameter for vertical well | 71 |

| | |
|--|----|
| Figure 4.16 Pressure derivative value for Horizontal well in a reservoir with minimum threshold pressure | 72 |
| Figure 4.17 Pressure derivative value for hydraulically fractured well in a reservoir with minimum threshold pressure | 73 |
| Figure 4.18 Pressure derivative value for partially penetrating vertical well in a reservoir with minimum threshold pressure | 74 |
| Figure 4.19 Pressure derivative value for fully penetrating vertical well in a reservoir with minimum threshold pressure | 74 |

LIST OF TABLES

Table 1: Pressure drawdown data..... 92

CHAPTER 1

INTRODUCTION

1.1 Background

Pressure transient analysis involves perturbing one or more drilled wells, observing the response at the perturbed well/adjacent well and making analysis that leads to estimation of reservoir parameters. Studies on pressure transient analysis of various fluid flow behaviour in porous media have indicated an anomaly in flow behaviour of Bingham fluids as opposed to Newtonian fluids (Mendes et al., 2002a; Nie et al., 2018; Wu et al., 1992; . The behaviour of heavy oil approaches that of Bingham fluids in porous media (Mendes et al., 2002a; Owayed & Tiab, 2008a; Wu et al., 1992) and the study of heavy oil has attracted the attention of many researchers due to an increase in global energy demands triggering development of heavy oil fields.

Bingham fluids exhibit a minimum threshold pressure, λ_B which arises due to an inherent yield stress of the fluid. The minimum threshold pressure increases the amount of pressure required to cause the fluid to flow. Pressure gradient above λ_B is required to flow the fluid in the formation towards the wellbore (Escobar, 2012).

(Wu, 1990) proposed a ratio of velocity to pressure gradient, where the pressure gradient component incorporated the minimum threshold pressure. The ratio constitutes what is known as modified Darcy's law for Bingham fluid flow. The modified Darcy's law also takes into account the threshold pressure gradient which is a function of fluid properties and the pore geometry (Mendes et al., 2002a). This modification enables Darcy's law to provide for the extra pressure drop associated with the fluid and formation characteristics.

For very low values of λ_B the behaviour of Bingham fluids approximate that of Newtonian fluids. However, for large values of λ_B a deviation in the pressure response is

observed. For this reason the pressure transient analysis models used for analysing transient pressure of Newtonian fluids may not be appropriate for Bingham fluids.

Many researchers have worked on developing models for simulating pressure transient behaviour for non-Newtonian fluids in the past three decades. These models were modification of the models that were developed for Newtonian fluids. Gringarten & Ramey(1973) were the first to introduce the application of source and Green's function in solving transient unsteady state flow problems in porous media (Owayed & Tiab, 2008a). They established that an infinite line source can be visualized as an intersection of two perpendicular planes that are perpendicular to two of the three principal axes of permeability, while the point source can be considered as an intersection of three mutually perpendicular planes that are perpendicular to the three axes of permeability. Subsequently, (Ozkan, 1988) introduced a new solution to the diffusivity equation using Laplace space to overcome challenges that were faced with the application of Gringarten and Ramey's solutions to complex geometrical configurations such as dual-porosity and dual-permeability in porous media. (Goode & Thambynayagam, 1985) also presented analytical solution for the response during pressure drawdown and build-up of a horizontal well using Fourier and Laplace transform, respectively. Zhao et al., (2013) used the perturbation technique to solve for either constant pressure or constant rate or infinite lateral boundary conditions with closed vertical boundaries. The solutions presented by (Ozkan, 1988)), (Goode & Thambynayagam, 1985), (Ozkan & Raghavan, 1991), (Guo, Nie, & Jia, 2012), and (Zhao et al., 2013) were all suitable for analysing pressure behaviour of Newtonian fluids without considering the effects of λ_B .

Extension of analytical solutions for analysing pressure transient behaviour of Newtonian fluids to analyse Bingham fluids is currently been worked on by various researchers. (Zhao et al., 2013) presented mathematical model to analyse pressure transient behaviour of horizontal well in a low permeability reservoir with minimum threshold pressure. They used the Fourier and Laplace transforms, respectively and inverted the solution in Laplace domain to real domain by using Stehfest algorithm (Stehfest, 2002). (Nie et al., 2018)

extended the work of (Guo et al., 2012) and presented a mathematical model to analyse pressure transient behaviour for Bingham fluids for a horizontal well in a heavy oil reservoir.

To the best knowledge of the author, no publication has been made for modelling Bingham porous-flow for, partially penetrating and fully penetrating, hydraulically fractured well in a naturally fractured reservoir. The study of pressure transient behaviour of Bingham fluids on various wellbore conditions is very important for heavy oil production. In this study, four wellbore types in naturally fractured reservoirs were considered and these include; hydraulically fractured, partially penetrating, fully penetrating and horizontal well.

1.2 Statement of the Problem

Pressure transient analysis models that have been built are mostly for Newtonian fluids. Since Bingham fluids behave differently, using the same models that are used for Newtonian fluids would produce inaccurate results. Some research has been done on pressure transient analysis of horizontal wells in heavy oil reservoirs. However, more work needs to be done in other well types. This study seeks to present analytical solutions and to analyse pressure transient behaviour of Bingham fluids taking cognisance of the minimum threshold pressure.

1.3 Objectives

The objectives of this work are to:

- Incorporate the minimum threshold pressure gradient into the inner boundary condition of a horizontal well equation.
- Develop mathematical models that can be used to solve pressure transient analyses problems for horizontal, partially penetrating, fully penetrating, hydraulically fractured wells in naturally fractured heavy oil reservoirs.
- Derive equations for TDS technique considering minimum threshold pressure gradient.
- Analyse the pressure response from the pressure and pressure derivative log-log plots using TDS approach to obtain some reservoir properties.

CHAPTER 2

LITERATURE REVIEW

2.1 Review of rheology of Non-Newtonian fluids

Fluids are usually categorised into two groups based on their characteristic response to applied stress i.e. Newtonian or Non-Newtonian. Newtonian fluids obey the Newtonian law of viscous resistance and have a constant viscosity while non-Newtonian fluids do not obey the Newtonian law of viscous resistance and their viscosity varies. The relationship between shear stress and shear rate is given by equation 2.1.

$$\tau = \mu\dot{\gamma} \tag{2.1}$$

Where τ is the shear stress, μ is the dynamic viscosity and $\dot{\gamma}$ is the shear rate.

There are three groups of Non Newtonian fluids namely; time independent, time dependent and viscoelastic (Wu, 1990).

2.1.1 Time independent fluids

Time independent fluids have a unique shear rate which is not a linear function to the instantaneous shear stress at any point. Fluids that include Bingham plastic, pseudo-plastic and dilatant fluids are categorised as time independent fluids.

2.1.2 Time dependent fluids

The relationship between shear rate and shear stress is complex. The shear rate does not solely depend on shear stress but is also dependent on shear time and history of their shear rate-shear stress relationship (Wu, 1990). They can be further classified into two groups i.e. thixotropic and rheopetic depending on whether shear stress increases or decreases with shear time (Wu, 1990). Figure 2-1 shows the variation of shear stress with shear time for both of them.

2.1.3 Viscoelastic fluids

Viscoelastic fluids exhibit a combination of viscous and elasticity characteristics. They partially recover after a deformable shear stress is removed from them. The rheological properties at any instant will be a function of recent history of the material and cannot be described by relationships between shear stress and shear rate alone but will require inclusion of the time derivative of both quantities (Wu, 1990). A typical model of a viscoelastic model is given by equation 2.2.

$$\tau = \mu \frac{d\dot{\gamma}}{dt} - \frac{\mu}{\lambda} \frac{d\tau}{dt} \quad (2.2)$$

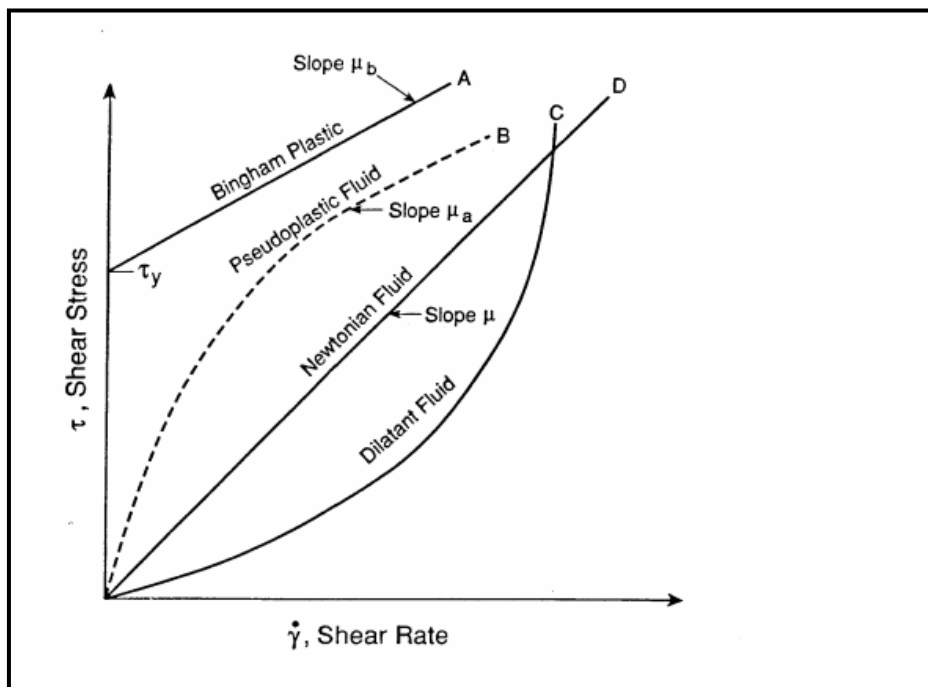


Figure 2.1 Relationship between shear rate and shear stress for different fluid types (Wu, 1990).

2.2 Bingham Plastic fluids flow dynamics

(Mendes et al., 2002a) performed experiments to determine the relationship between flow rate and pressure drop for a flowing Bingham fluid. In that study, grease of Bingham rheological behaviour was used and an array of cylindrical rods used to mimic connected pore spaces in the formation. It was observed that flow only occurs when the pressure gradient exceeds the minimum threshold pressure gradient. It was also established that viscosity of heavy oil is a function of the difference between applied pressure gradient and threshold pressure gradient. For pressure gradients slightly above the threshold value, viscosity of the fluid decreased sharply with the deformation rate and the fluid permeability increases as well. It was concluded that the viscosity decrease was due to the domination of yield stress within that range of pressure gradient.

Bingham plastic fluids are among the most common time independent fluids. They exhibit a finite yield stress at zero shear rate which implies that there is no gross movement of fluids until a yield stress τ_y is exceeded (Owayed & Tiab, 2008b). They are characterized by τ_y (yield stress) and Bingham plastic model μ_B (Escobar, 2012).

The rheological equation for Bingham plastic fluid is given equation 2.3;

$$\tau = \tau_y + \mu_B \dot{\gamma} \quad (2.3)$$

According to (Wu, 1990), the physical behaviour of Bingham fluids can be explained by considering their internal structure in three dimensions. The internal structure tends to collapse when the shear stress exceeds the yield stress thereby allowing shear movement to occur (Wu, 1990).

Bingham fluids do not obey Darcy's law and therefore to describe their flow in porous media, the Darcy equation should be modified. Equation 2.1 is known as the modified Darcy's law.

$$\vec{u} = \begin{cases} -\frac{k}{\mu} * \left(1 - \frac{\lambda_B}{|p|}\right) * |p| & \text{for } |p| > \lambda_B \\ 0 & \text{for } |p| < \lambda_B \end{cases} \quad (2.4)$$

(Owayed & Tiab, 2008b).

From equation 2.4, it is clear that the fluid will only flow when $|p|$ exceeds the minimum pressure gradient λ_B of the fluid. A relationship between λ_B and yield shear stress and pore was presented by Buckingham as shown on equation 2.5 (Wu, 1990).

$$\lambda_B = \tau_y / \left(\frac{3R}{8}\right) \quad (2.5)$$

From equation 2.5, it is clear that minimum pressure gradient λ_B is a function of fluid properties and formation properties i.e. yield stress of the fluid and formation pore radius. The parameters λ_B and τ_y are obtainable experimentally and from well tests (Owayed & Tiab, 2008b). Research has established that heavy oil exhibit Bingham plastic characteristics and as such, the flow behaviour can be modelled by equation 2.2 (Owayed & Tiab, 2008b),(Wu, 1990).

2.3 Pressure transient analysis of Horizontal wells

Three basic steps are involved in pressure transient analysis of horizontal wells. These steps include: identification of flow regimes from completion data, application of proper analytical and graphical procedures to the data and evaluation of the uniqueness and sensitivity of the results to properties derived from the analysis (Lee, Rollins, & Spivy, 2003). There are five flow regimes that are possible in horizontal wells, however not all of these may be present in a given test. This is because wellbore storage effects, end effects and transition effects may obscure certain flow regimes. Results from horizontal well tests are seldom unique

(Lee et al., 2003). As such, it is important to evaluate the sensitivity and distinctiveness of results.

2.3.1 Flow regimes

Five flow regimes that can occur in horizontal well test are: early radial flow, hemi radial flow, early linear flow, late pseudo-radial flow and late linear flow. In horizontal wells, initial flow occurs radially in the vertical plane towards the wellbore i.e. y-z plane. This is contrast to vertical well whose radial flow occurs in the horizontal plane i.e. x-y plane. The average permeability combines vertical and a radial component with horizontal anisotropy, however the horizontal anisotropy is often ignored (Houzé, Viturat, & Fjaere, 2018). The thickness-permeability product is defined with the average permeability in the vertical plane and is given as:

$$(kh)_{early} = 2L\sqrt{k_v k_h} \quad (2.6)$$

On the pressure derivative curve of log-log plot, early radial flow is represented by a horizontal line. From this flow regime, mechanical skin factor, geometrical vertical and horizontal permeability product can be obtained. However, due to wellbore storage effects, this flow regime is often distorted. A schematic of early radial flow regime is shown in figure 2.2.

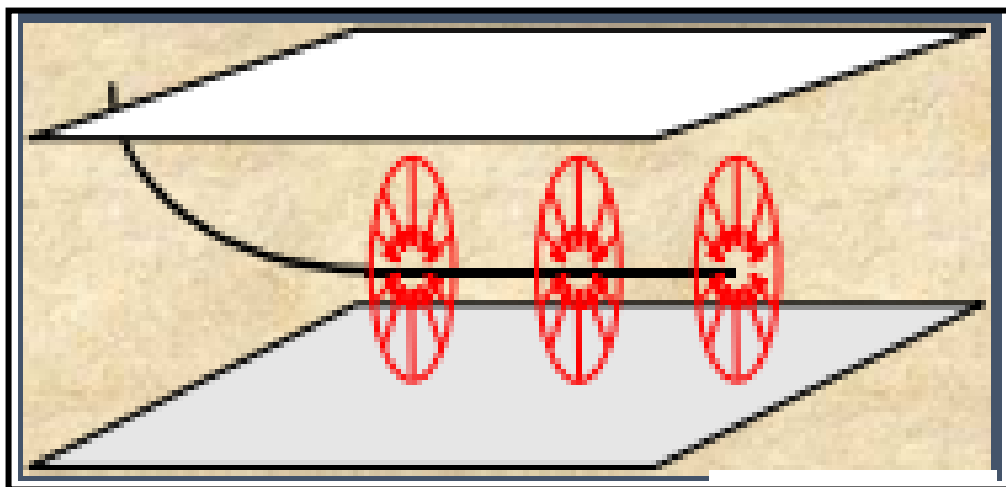


Figure 2.2 Early radial flow regime (Houzé et al., 2018)

If the wellbore is located closer to one of the vertical boundaries relative to the other, hemi-radial flow occurs. Fig. 2.3 is a schematic for hemi-radial flow. . The thickness-permeability product during this flow regime is given as:

$$(kh)_{linear} = L^2k \quad (2.7)$$

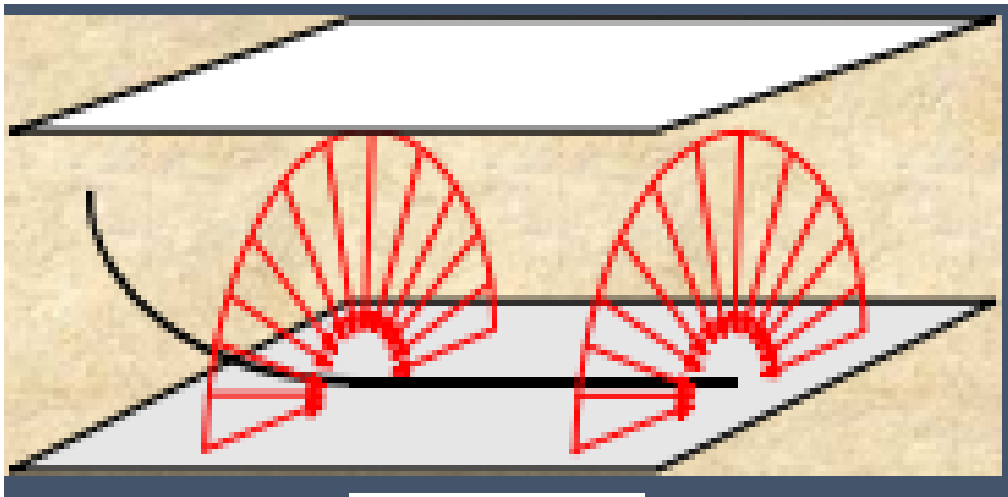


Figure 2.3 Hemi-radial flow regime (Houzé et al., 2018)

Once the transient reaches both top and bottom boundary, early linear flow begins. This flow is indicated by a 0.5 slope on both pressure change and pressure derivative curves on log-log plot. The early linear flow can be analysed to estimate length of producing interval, as long as the horizontal plane can be considered isotropic (Mattar & Dean, 2008).

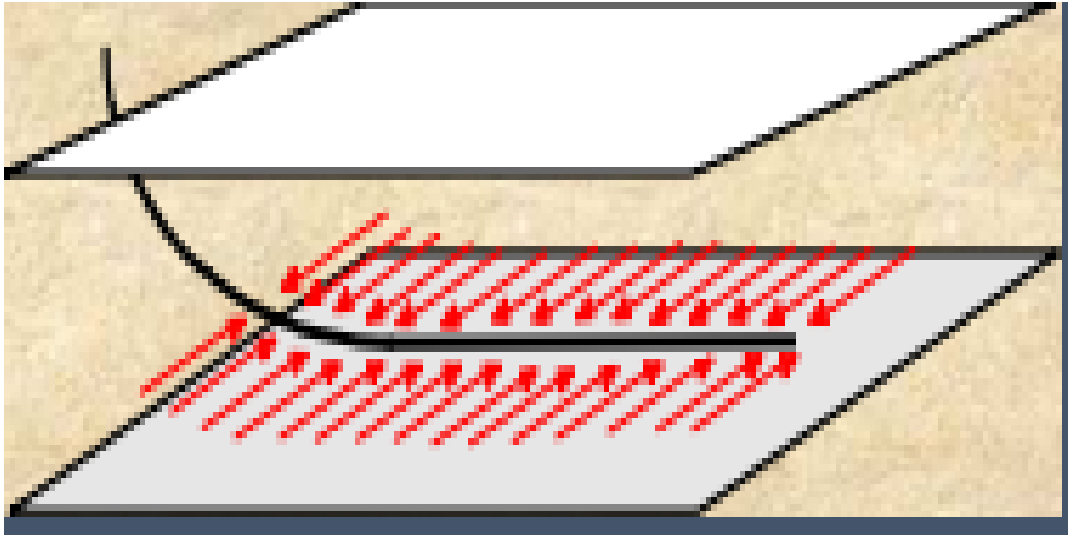


Figure 2.4 Linear flow regime (Houzé et al., 2018)

As the transient propagates deeper into the formation, a third flow regime called late radial flow will appear. This flow regime occurs in the x-y plane. It is characterised by a horizontal line on the derivative curve of log-log plot. Average horizontal permeability and total skin factor (mechanical and geometrical skin) factors can be found from this flow regime. This flow regime is equivalent to that in a vertical well and the permeability-thickness product is given as:

$$(kh)_{late} = k_H h \quad (2.8)$$

Figure 2-5 shows late radial flow regime while figure 2-6 shows pressure and pressure derivative curves on log-log plots.

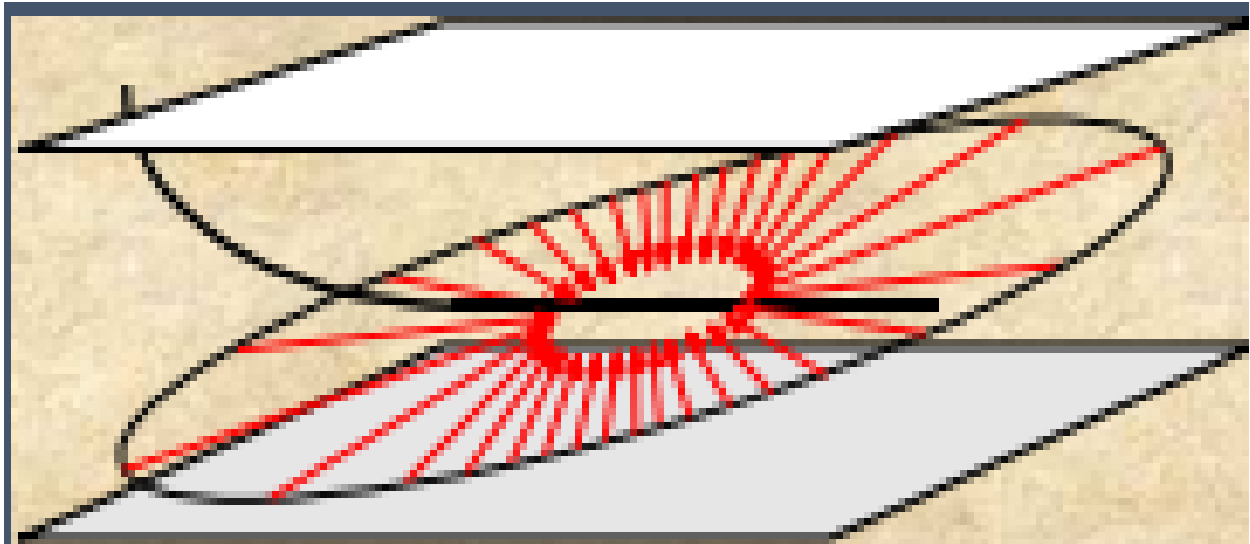


Figure 2.6 Late radial flow regime(Houzé et al., 2018)

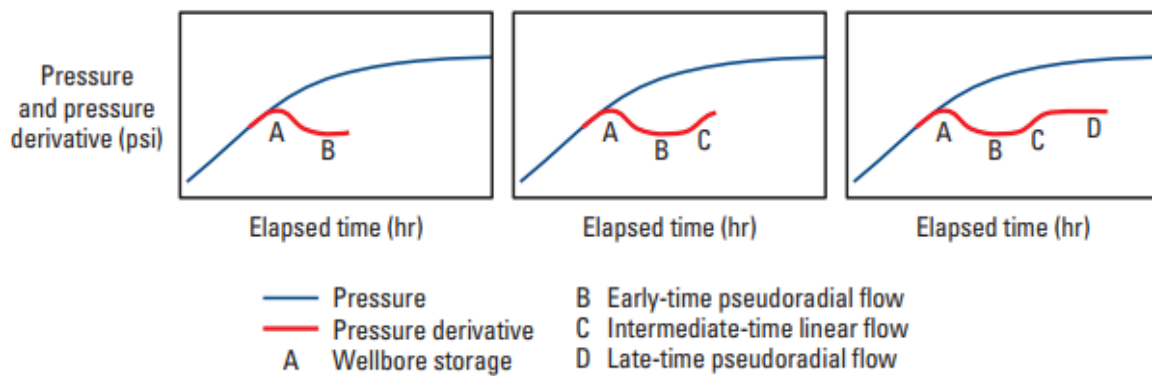


Figure 2.6 Pressure and pressure derivative on bi-logarithm plots (Mattar & Dean, 2008)

2.4 Sensitivity to different well and reservoir parameters

2.4.1 Well length and position

Ideally, the well is placed at the centre between the upper and bottom boundaries. In this case the boundaries will be seen simultaneously and a clear transition from early radial to

linear flow regime will be observed. Figure 2.7 shows horizontal well log-log response for variable well length.

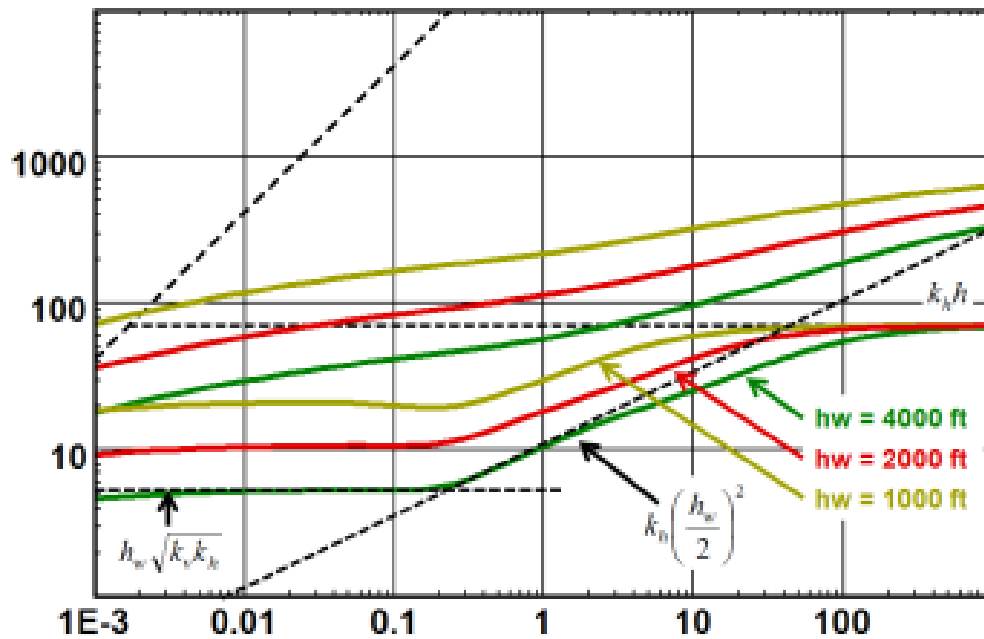


Figure 2.7 Log-log responses for horizontal wells, variable well length. (Houzé et al., 2018)

If the well is not placed at the centre, there is a tendency of one of the boundaries to be felt before the other. One such case is when one of the boundaries is an aquifer or gas cap. In this case, the well will be placed close to the other boundary and a doubling of the derivative occurs (Houzé et al., 2018). Figure 2.8 shows horizontal well log-log response to variable well placements.

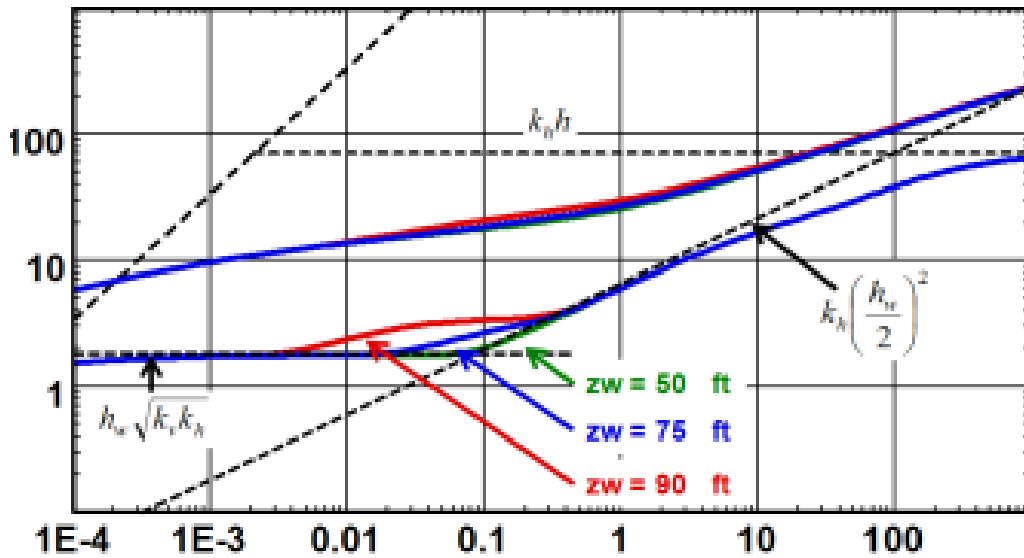


Figure 2.8 Horizontal well pressure response to well placements (Houzé et al., 2018)

2.4.2 Sensitivity to anisotropy.

The response to vertical anisotropy is an interesting phenomenon, when the permeability contrast between vertical and horizontal plane increases. The shape of the pressure derivative on the log-log plot will lose the classical finger print of the horizontal well as shown on figure 2.9

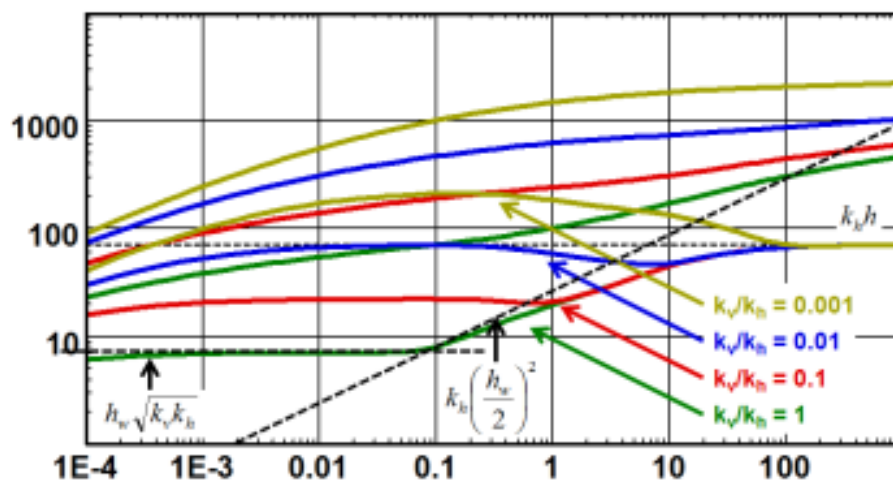


Figure 2.9 Horizontal well bi-logarithm response to variable to vertical anisotropy (Houzé et al., 2018)

2.4.3 Effect of wellbore storage

Wellbore storage is well known for obscuring the early radial flow regime. (Houzé et al., 2018) also indicated that significant wellbore storage will mask the half unit slope straight line of the linear flow. This challenge may be surmounted if the reliability of the known data is high. Figure 2.10 shows the horizontal well log-log response to variable wellbore storage.

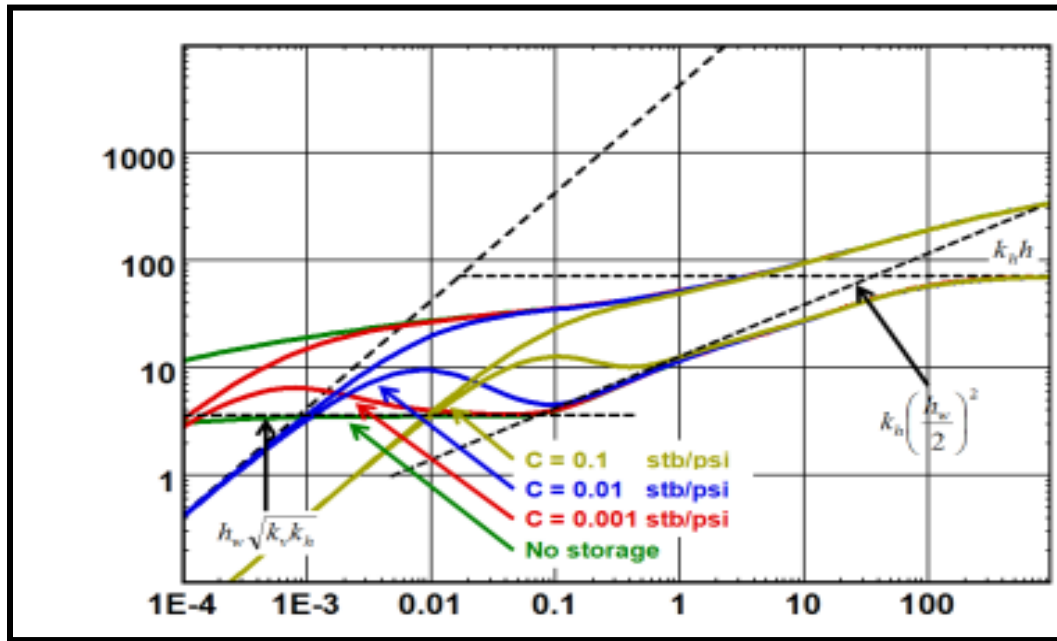


Figure 2.10 Horizontal well log-log response to wellbore storage (Houzé et al., 2018)

2.5 Analytical solutions

(Ozkan, 1988) presented a library of solutions to obtain pressure distributions in homogeneous and naturally fractured reservoirs for various wellbore conditions. A horizontal well in an infinite reservoir with closed boundaries at $z_D = 0$ and $z_D = 1$ was assumed.

Given $\bar{x}_D = x_D - x_{wD} - \alpha\sqrt{k/k_x}$, $\bar{y}_D = y_D - y_{wD}$, $q = \bar{q}L_h$, $u = sf(s)$.

A point source solution was developed and given as:

$$\Delta\bar{P} = \frac{\check{q}\mu}{4\pi kLs} \left[\sum_{n=-\infty}^{+\infty} \frac{\exp[-\sqrt{u}\sqrt{r_D^2+(z_D-z_{wD}-2nh_D)^2}]}{\sqrt{r_D^2+(z_D-z_{wD}-2nh_D)^2}} + \frac{\exp[-\sqrt{u}\sqrt{r_D^2+(z_D+z_{wD}-2nh_D)^2}]}{\sqrt{r_D^2+(z_D+z_{wD}-2nh_D)^2}} \right] \quad (2.9)$$

Where:

$$r_D = \sqrt{(x_D - x_{wD})^2 + (y_D - y_{wD})^2} \quad (2.10)$$

$$h_D = \frac{h}{L} \sqrt{k/k_x} \quad (2.11)$$

$$x_D = \frac{2x}{L_h} \sqrt{k/k_x} \quad (2.12)$$

$$y_D = \frac{2y}{L_h} \sqrt{k/k_y} \quad (2.13)$$

$$z_D = \frac{z}{h} \quad (2.14)$$

Poisson's summation formula was used such that the pressure distribution for a continuous point source located at (x_{wD}, y_{wD}, z_{wD}) in a laterally infinite reservoir with closed top and bottom boundaries was given as shown in 2.15:

$$\Delta\bar{p} = \frac{\check{q}u}{2\pi kLhDs} \left[\frac{K_0(r_D\sqrt{u})}{\sqrt{u + \frac{n^2\pi^2}{h_D^2}}} + 2 \sum_{n=1}^{\infty} K_0 \left(r_D \sqrt{u + \frac{n^2\pi^2}{h_D^2}} \right) \cos n\pi \frac{z_D}{h_D} \cos n\pi \frac{z_{wD}}{h_D} \right] \quad (2.15)$$

K_0 is a Bessel function of order zero which is given by (Abramowitz & Stegun, I., 1964). K_0 is defined as shown in 2.16:

$$\int_0^x K_0(u)du = \left[\begin{array}{l} - \left(\ln \left(\frac{x}{2} \right) + \gamma \right) x \sum_{k=0}^{\infty} \frac{\left(\frac{x}{2} \right)^{2k}}{(k!)^2 (2k+1)} + \\ x \sum_{k=0}^{\infty} \frac{\left(\frac{x}{2} \right)^{2k}}{(k!)^2 (2k+1)} + x \sum_{k=1}^{\infty} \frac{\left(\frac{x}{2} \right)^{2k}}{(k!)^2 (2k+1)} \sum_{n=1}^{\infty} \frac{1}{n} \end{array} \right] \quad (2.16)$$

This solution is a general solution that can be extended for various wellbore conditions by integrating throughout the entire length of the well. Some of the various equations as presented for closed upper and bottom boundaries by (Ozkan, 1988) are given in below:

Solution for fully penetrating vertical well

$$\Delta \bar{p} = \frac{\tilde{q}uh}{2\pi kLh_D S} k_0(r_D \sqrt{u}) \quad (2.17)$$

Solution for partially penetrating vertical well

$$\Delta \bar{p} = \left[\begin{array}{l} \frac{\tilde{q}uh_w}{2\pi kLh_D S} K_0(r_D \sqrt{u}) + \\ \frac{2\tilde{q}\mu h}{\pi^2 kLh_D S} \sum_{n=1}^{\infty} \left[\frac{1}{n} K_0 \left(r_D \sqrt{\mu + \frac{n^2 \pi^2}{h_D}} \right) \sin n\pi \frac{h_w}{2h} \cos n\pi \frac{z_w}{h} \cos n\pi \frac{z}{h} \right] \end{array} \right] \quad (2.18)$$

Solution for partially penetrating vertical fracture

$$\Delta \bar{p} = \left\{ \begin{array}{l} \frac{\tilde{q}uh_w}{2\pi kLh_D S} \int_{-L_{xf}/L}^{+L_{xf}/L} K_0 \left[\sqrt{u} \sqrt{\left(x_D - x_{wD} - \alpha \sqrt{\frac{k}{k_x}} \right)^2 + (y_D - y_{wD})^2} \right] d\alpha + \\ \frac{2\tilde{q}\mu h}{\pi^2 kLh_D S} \sum_{n=1}^{\infty} \left[\frac{1}{n} \sin n\pi \frac{h_w}{2h} \cos n\pi \frac{z_w}{h} \cos n\pi \frac{z}{h} \right] \\ \int_{-L_{xf}/L}^{+L_{xf}/L} \left[K_0 \left(\sqrt{\mu + \frac{n^2 \pi^2}{h_D}} \right) \sqrt{\left(x_D - x_{wD} - \alpha \sqrt{\frac{k}{k_x}} \right)^2 + (y_D - y_{wD})^2} \right] d\alpha \end{array} \right\} \quad (2.19)$$

Solution for horizontal well

$$\Delta \bar{p} = \frac{\tilde{q}u}{2\pi kLh_D s} \left\{ \begin{array}{l} \int_{-\frac{L_h}{2L}}^{+\frac{L_h}{2L}} K_0 \left[\sqrt{u} \sqrt{\left(x_D - x_{wD} - \alpha \sqrt{\frac{k}{k_x}}\right)^2 + (y_D - y_{wD})^2} \right] d\alpha + \\ 2 \sum_{n=1}^{\infty} \cos n\pi \frac{z}{h} \cos n\pi \frac{z_w}{h} \\ \int_{-\frac{L_h}{2L}}^{+\frac{L_h}{2L}} K_0 \left(r_D \sqrt{\mu + \frac{n^2 \pi^2}{h_D}} \right) \sqrt{\left(x_D - x_{wD} - \alpha \sqrt{\frac{k}{k_x}}\right)^2 + (y_D - y_{wD})^2} d\alpha \end{array} \right\} \quad (2.20)$$

The solution was inverted from Laplace space to real space using Stehfest algorithm (Stehfest, 2002) and the solution used to produce plots of dimensionless pressure and vs dimensionless time. The pressure response for horizontal well of infinite conductivity is shown in figure 2.11. Dimensionless horizontal wellbore length L_D was varied in the range $0.1 \leq L_D \leq 100$.

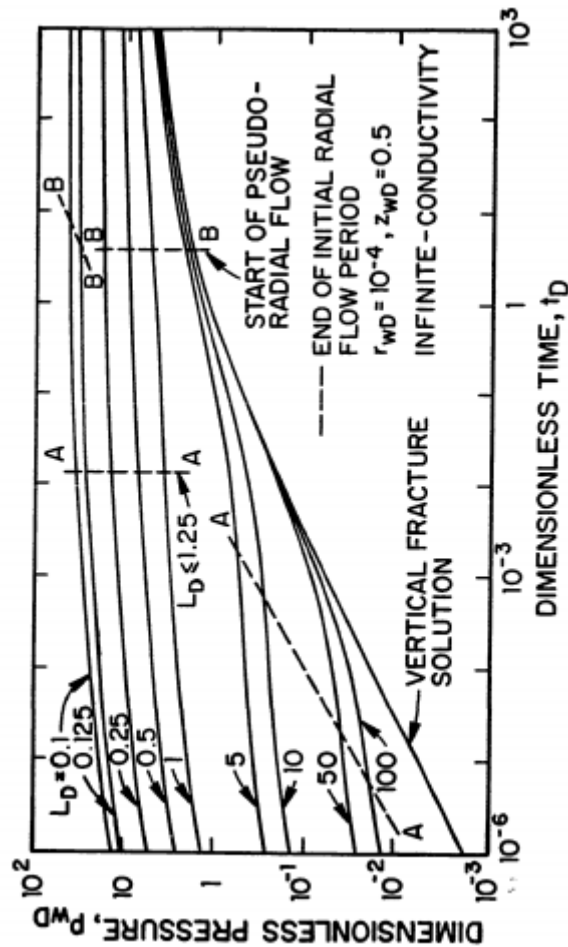


Figure 2.11 The pressure response for horizontal well of infinite conductivity (Ozkan, 1988)

Subsequently, (Nie et al., 2018) studied hydrodynamic characteristics of the flow mechanics in porous media in a heavy oil reservoir. They developed a physical model for a horizontal well in a heavy oil reservoir and solved the corresponding mathematical model. A homogeneous formation with a perfectly parallel horizontal well to the closed horizontal boundaries was assumed.

They used the method of Laplace transform and separation of variables and presented the solution in Laplace space as shown in 2.21:

$$\bar{p}_D = \sum_{n=0}^{\infty} \int_{-L/2r_w}^{L/2r_w} \bar{R}(x_D, \lambda_n) dx_D \cdot \bar{z}_w(\lambda_n) \quad (2.21)$$

\bar{R} is given as:

$$\bar{R}(x_D, \xi_n) = A_n I_0(x_D \sqrt{\xi_n}) + B_n K_0(x_D \sqrt{\xi_n}) + \bar{R}^* \quad (2.22)$$

Where,

$$\bar{R}^* = \frac{\pi \lambda_{BD} e^{-s}}{2u \sqrt{\xi_n}} I_0(\xi_n) \quad (2.23)$$

$$\bar{z} = C \cos \left[\sqrt{\lambda_n} \left(\frac{r_w}{h} + z_{wD} \right) \right] + D \sin \left[\sqrt{\lambda_n} \left(\frac{r_w}{h} + z_{wD} \right) \right] \quad (2.24)$$

$$\xi_n = u e^{-2s} + \frac{\lambda_n}{h^2_D}, n = 0, 1, 2 \dots \quad (2.25)$$

Dimensionless bottom hole pressure (p_{wD}) in real space was obtained by inverting the solution from Laplace domain to real domain using Stehfest numerical inversion (Stehfest, 2002). Log-log plots of pressure and dimensionless pressure derivative were drawn as shown on figure 2.12 to 2.14.

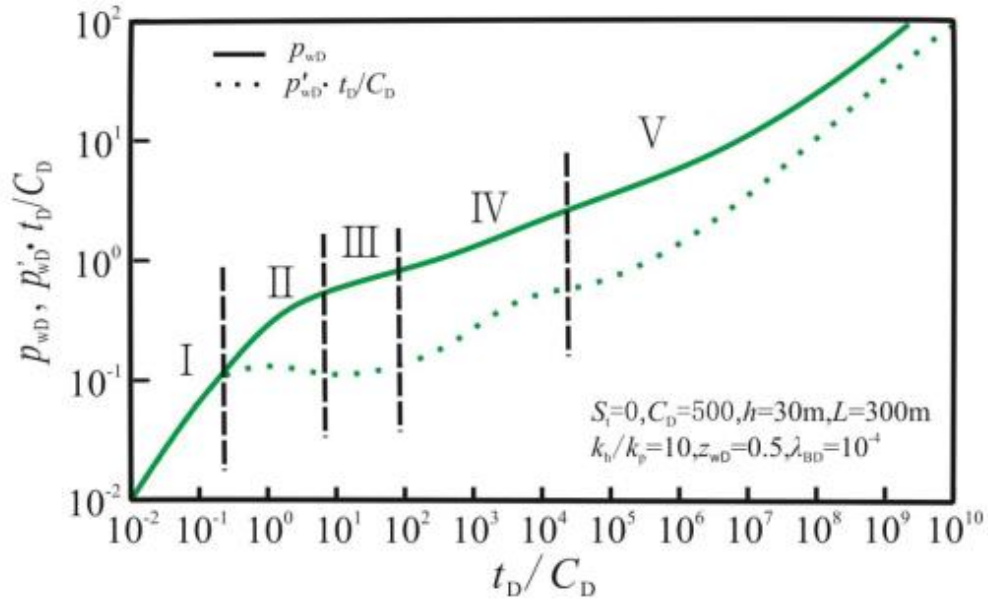


Figure 2.12 Log-log curves for flow regime recognition (Nie et al., 2018)

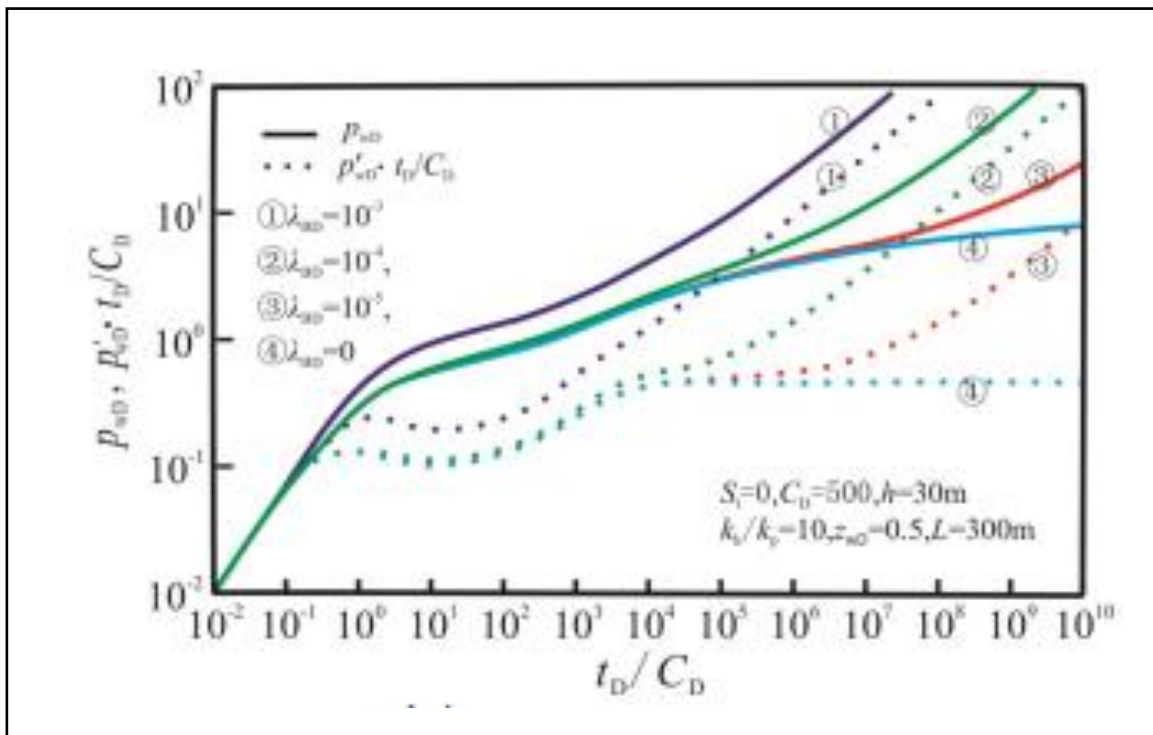


Figure 2.13 Log-log curve of pressure and pressure derivative showing effect of variable dimensionless threshold pressure (Nie et al., 2018)

positions, reservoir thickness, penetration ratio, interporosity flow parameter and storativity ratio on transient flow behaviour.

In the study for effects of penetration position, they considered four cases: bottom, top, intermediate and centre as shown on figure 2.15. For large values of interporosity flow parameter λ , they observed that the top and bottom penetrated wells have the same transient flow behaviour. Also, the behaviour of the intermediate and centre were also similar except for the fact that they differed at the beginning of early and late radial flow regime as shown on figure 2.15.

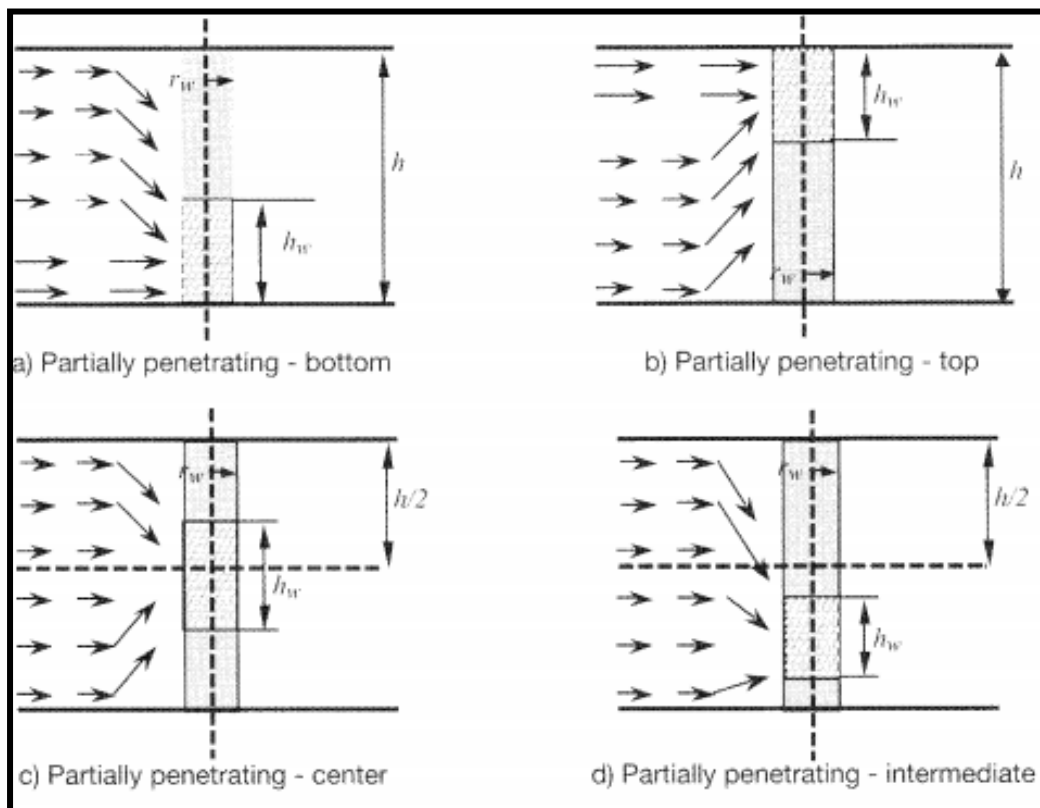


Figure 2.15 Different types of partially penetrating vertical wells based on the position in the perforated interval, h_w (Slimani & Tiab, 2008) .

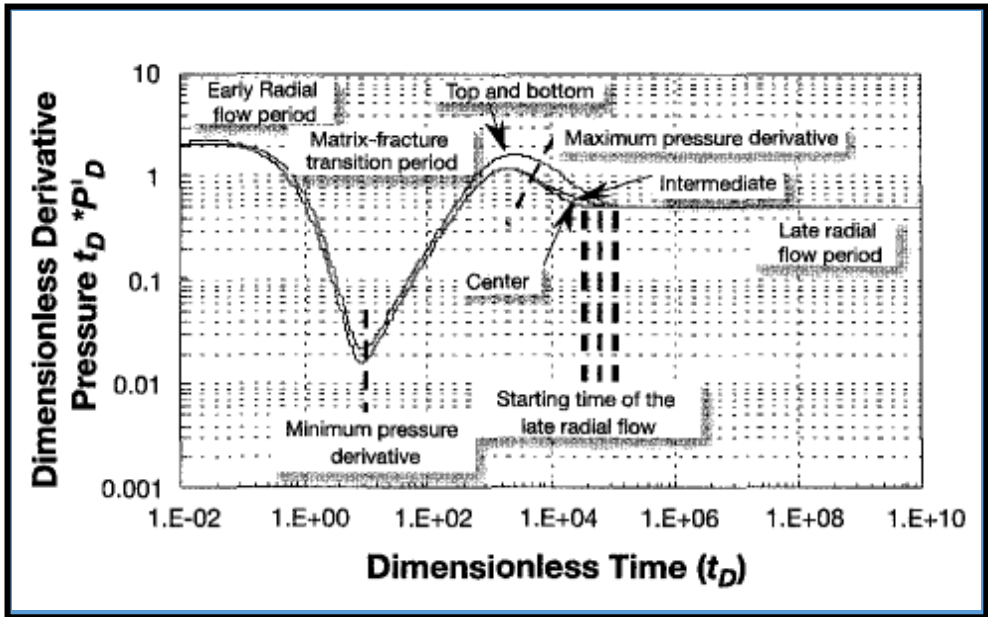


Figure 2.16 Different types of partially penetrating vertical wells based on the position in the perforated interval, h_w (Slimani & Tiab, 2008)

2.5.2.1 Storage capacity ratio (storativity)

Storage capacity ratio, also known as storativity is the ratio of the fracture storage capacity to the entire system storage capacity. Equation 2.6 gives a mathematical definition to storativity.

$$\omega = \frac{\phi_f C_f}{\phi_f C_f + \phi_m C_m} \quad (2.26)$$

ϕ_f = fracture porosity, C_f = fracture compressibility, ϕ_m = matrix porosity,

C_m = matrix compressibility

Storativity ratio of an infinite conductivity fracture system has an impact on the transient flow behaviour. At very low storativity ratio the fracture depletion period is small as compared with high storativity. This is because the storage capacity of the fracture will be very small in comparison to the entire formation system. Resultantly, it will take short amount of time before

the matrix system starts contributing to the flow. Thus, a small storage ratio is characterised by an early appearance of a trough on pressure derivative curve of the log-log plot.

2.5.2.2 Interporosity flow parameter (λ)

Interporosity flow parameter, also known as transmissivity defines the extent of communication between the matrix and fracture. The mathematical definition is given in equation 2.27:

$$\lambda = \alpha r_w^2 \frac{k_f}{k_m} \quad (2.27)$$

The parameter α is a shape factor and reflects the geometry of the matrix elements. Equation 2.28 gives a mathematical definition of α .

$$\alpha = \frac{4n(n+2)}{h_m^2} \quad (2.28)$$

$r_w =$ wellbore length

$h_m =$ length of a side of the cubic matrix

$n =$ number of fracture planes.

$k_f, k_m =$ permeability of fracture and matrix respectively.

Interporosity flow parameter is an important phenomenon especially in engineering analysis of NFR. This is because of the complexity in determining the amount of oil in the fractures and that in the matrix which makes the work of estimation oil in place difficult. There may be high production rates as a result of contribution from the fracture system but it is uncertain to predict those rates. As such, it is important to examine from various sources of data the level of matrix support for the fractures (Rebolledo & Ershaghi, 2015).

Pressure analysis techniques have been developed to estimate the interporosity flow parameters. Figure 2.17 shows diagnostic plot for a build-up test and its derivative plot.

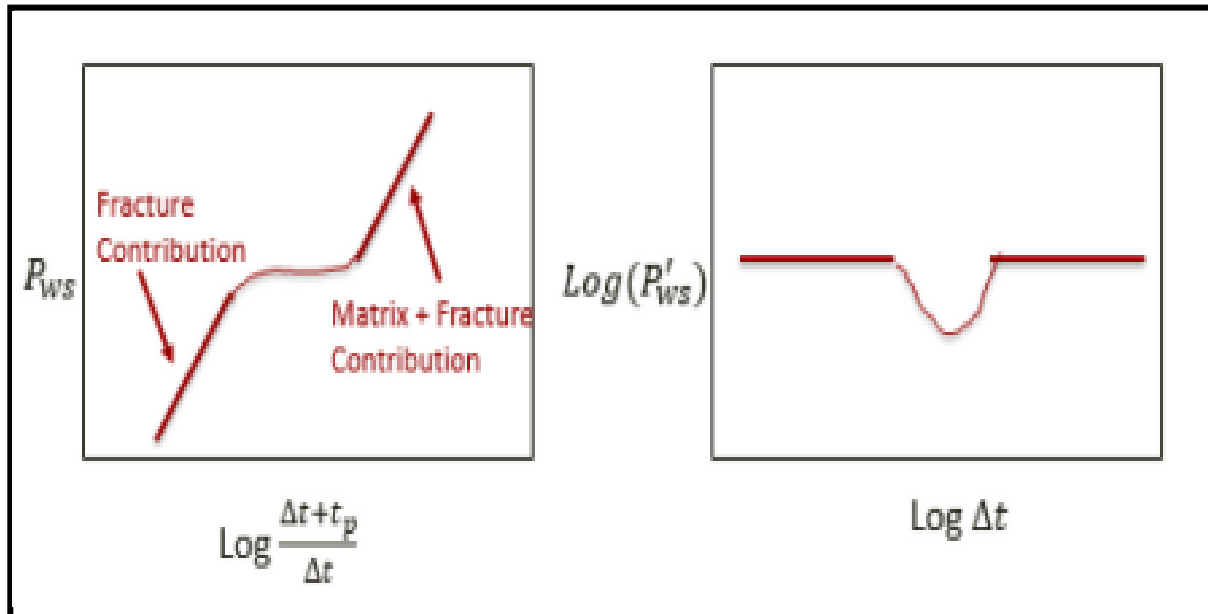


Figure 2.17 Dual porosity Model Diagnostic Plots; Build-up Test and its derivative.(Rebolledo & Ershaghi, 2015)

The first plot on figure 2.17 shows that at early time, the pressure response is due to fracture contribution. This response continues until the matrix begins to support the fracture contribution. This period is called matrix-fracture transition period. Thereafter, the whole system (matrix + fracture) contribution is observed as depicted on figure 2.17. Similarly, on the derivative plot shown on the right of figure 2.17, at early and late time, a horizontal straight line is observed which indicates radial flow. These flow regimes are connected by a trough which signifies the transition period. The duration of transition period is determined by the storativity ratio while the occurrence of the radial flow regimes is determined by the interporosity flow parameter.

(Slimani & Tiab, 2008) investigated the effect of interporosity flow parameter for two different values of dimensionless formation thickness $h_D = 200, h_D = 2000$. They observed that the behaviour of the pressure derivative for small values of h_D was similar to that of fully

penetrating wells. The only difference was of spherical flow which occurred just after early radial flow in partially penetrating well. As such, the minimum time coordinate was different though the pressure derivative coordinate of the trough was the same. It was also observed that for large h_D , a combination of partial penetration effect and matrix fracture transition occurs for an interporosity flow parameter greater than 10^{-5} . For λ less than 10^{-5} the fracture-matrix transition was shifted to the right (i.e. late radial flow) as shown on figure 2.18.

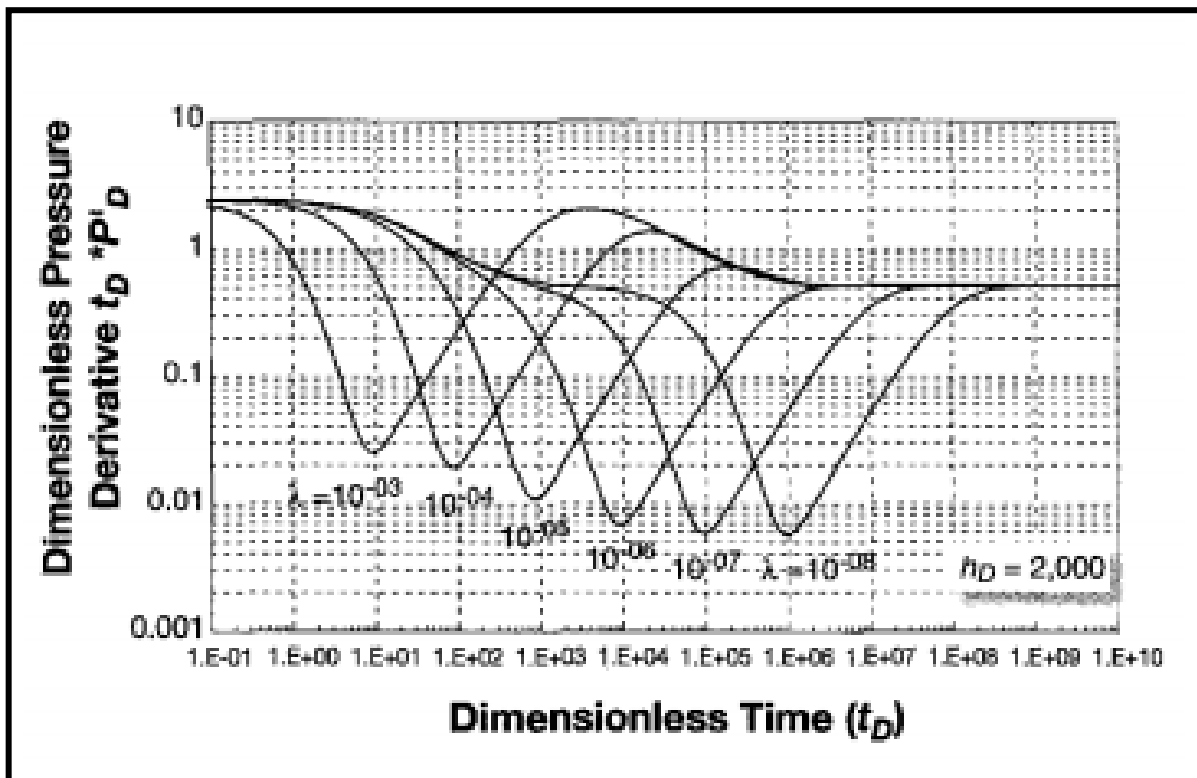


Figure 2.18 Pressure derivative response to various interporosity flow parameters. (Slimani & Tiab, 2008)

2.5.2.3 Penetration ratio, b

Penetration ratio is the portion of the formation thickness that is penetrated as a proportion of the entire formation thickness. The magnitude of the penetration ratio has an impact on the transient behaviour and causes a pseudo skin. (Slimani, Tiab, & Moncada, 2006) investigated the effect of penetration ratio and came up with a correlation as follows:

$$b = 0.97 \left\{ \frac{(t^*dp)_{lr}}{(t^*dp)_{er}} \right\}^{-1.0434} \quad (2.29)$$

This observation was for small penetration ratio and λ less than 10^{-6} .

2.5.2.4 Reservoir thickness, h

According to (Slimani et al., 2006), for the same reservoir thickness and wellbore radius, the higher the fracture permeability ratio k_f/k_z , the longer it takes to reach radial flow in the reservoir, when λ less than 10^{-6} . Figure 2.19 shows the effect of dimensionless reservoir thickness on generated type curve.

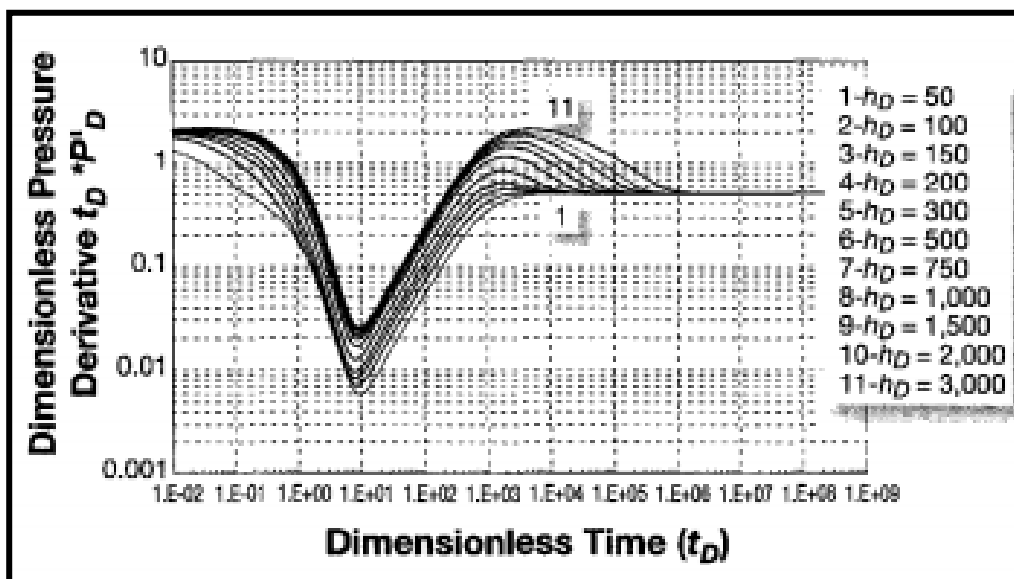


Figure 2.19 Effect of dimensionless storage coefficient on pressure derivative (Slimani et al., 2006)

2.5.3 Application of Tiab's Direct Synthesis Technique in Pressure Transient Analysis

Tiab's Direct Synthesis (TDS) method is a powerful technique that is used to estimate reservoir parameters without the use of type curve analysis. It makes use of log-log plot of

pressure and pressure derivative plot to estimate parameters like reservoir permeability, wellbore storage, skin effects, and fracture half-length among others. This method uses exact analytical solutions to estimate reservoir parameters, thus making it more accurate (Abel, Abdelghani, & Djebbar, 2007).

2.5.3.1 Use of TDS in determining penetration ratio, b for PPVW

(Slimani et al., 2006) presented an equation for determining the penetration ratio which was later simplified by (Slimani & Tiab, 2008) to equation 2.30.

$$b = \frac{(t*dp)_{lr}}{(t*dp)_{er}} \quad (2.30)$$

As observed from equation 2.30, penetration ratio is calculated as a ratio of the pressure derivative values of late time radial flow to early time radial flow. Equation 2.30 is applicable for all three types of partially penetrating wells (top and bottom, centre and intermediate) (Slimani & Tiab, 2008).

2.5.3.2 Using TDS to determine horizontal fracture permeability for PPVW

The fracture permeability can be determined from either late radial flow or early radial flow. Both early and late radial flow regimes are represented by a straight horizontal line on the pressure derivative curve of log-log plot. (Slimani & Tiab, 2008) calculated horizontal fracture permeability using equation 2.31 and 2.32.

Using the late radial flow, the equation for determining fracture permeability was given as:

$$k_f = \frac{70.6q\mu B}{h(t*dp)_{lr}} \quad (2.31)$$

Using the early radial flow, the equation was given as:

$$k_f = \frac{70.6q\mu B}{h_w(t*dp)_{er}} \quad (2.32)$$

2.5.3.3 Using TDS in determining vertical fracture permeability for PPVW

The expressions for vertical fracture permeability as presented by (Slimani & Tiab, 2008) are given as:

Centre partially penetrating vertical well:

$$k_{fz} = \frac{h^2(\phi c)_{T\mu}}{0.00087t_{br2}} \quad (2.33)$$

Intermediate partially penetrating vertical well:

$$k_{fz} = \frac{h^2(\phi c)_{T\mu}}{0.00018t_{br2}} \quad (2.34)$$

For top and bottom:

$$k_{fz} = \frac{h^2(\phi c)_{T\mu}}{0.000233t_{br2}} \quad (2.35)$$

t_{br2} = starting time of the late radial flow.

2.5.3.3 Using TDS to determining interporosity flow parameter (λ) for PPVW

For the fracture-matrix transition period that occurs during the early radial flow regime, λ can be obtained by knowing the maximum pressure derivative, penetration ratio and dimensionless reservoir thickness. For intermediate and centre partially penetrating vertical well, the equation for estimating λ , is given as:

$$\lambda = \frac{\left\{ \frac{(t^* \Delta p')_{max}}{(t^* dp)_{er}} \right\}^2}{c_1 * \left\{ \frac{(t^* \Delta p')_{max}}{(t^* dp)_{er}} \right\}^2 + c_2} \quad (2.36)$$

c_1 and c_2 are defined as:

$$c_1 = \frac{b}{(1.344 * 10^{-3} * e^{-0.0037h_D}) * b - \left(\frac{2.9478}{h_D^{1.5}} + 4.95 * 10^{-6} \right)} \quad (2.37)$$

$$C_2 = \frac{1}{\frac{0.336}{h_D^{1.1672}} \frac{0.0924}{h_D^{*e^b}}} \quad (2.38)$$

2.5.3.3 Using TDS to determining storage capacity ratio (ω) for PPVW

When the fracture-matrix transition period occurs during early radial flow regime, storage capacity ratio can be determined from the following equation given by (Slimani & Tiab, 2008):

$$\omega = 1.8083(\lambda * t_{Dwmin})^2 + 0.1299(\lambda * t_{Dwmin}) - 0.0004 \quad (2.39)$$

In real units equation 2.40 becomes:

$$\omega = 1.257 * 10^{-7} \left[\frac{\lambda k_{fr}}{(\phi c)_T \mu r_w^2} t_{min} \right]^2 + 3.425 * 10^{-5} \left[\frac{\lambda k_{fr}}{(\phi c)_T \mu r_w^2} t_{min} \right] - 0.0004 \quad (2.40)$$

Equation 2.39 and 2.40 are for the case of fracture-matrix transition period that occurs during early radial flow regime. It is also important to note that the work done on partially penetrated wells in NFR by (Slimani & Tiab, 2008; Slimani et al., 2006) did not provide for minimum threshold pressure.

2.6 Hydraulically fractured Wells

The main objective of hydraulic fracturing for well stimulation is to boost productivity and this is achieved by creating a highly conductive path at some considerable distance away from the skin zone into the reservoir. Wells with low permeability are particularly candidates for hydraulic fracturing. Pressure transient analysis is a tool that is used for evaluating the success of hydraulic fracturing job.

2.6.1 Flow patterns in hydraulically fractured wells

Basically, five flow regimes may occur in a hydraulically fractured reservoir. These are: fracture linear, bilinear, formation linear, elliptical and pseudo-radial flow regime.

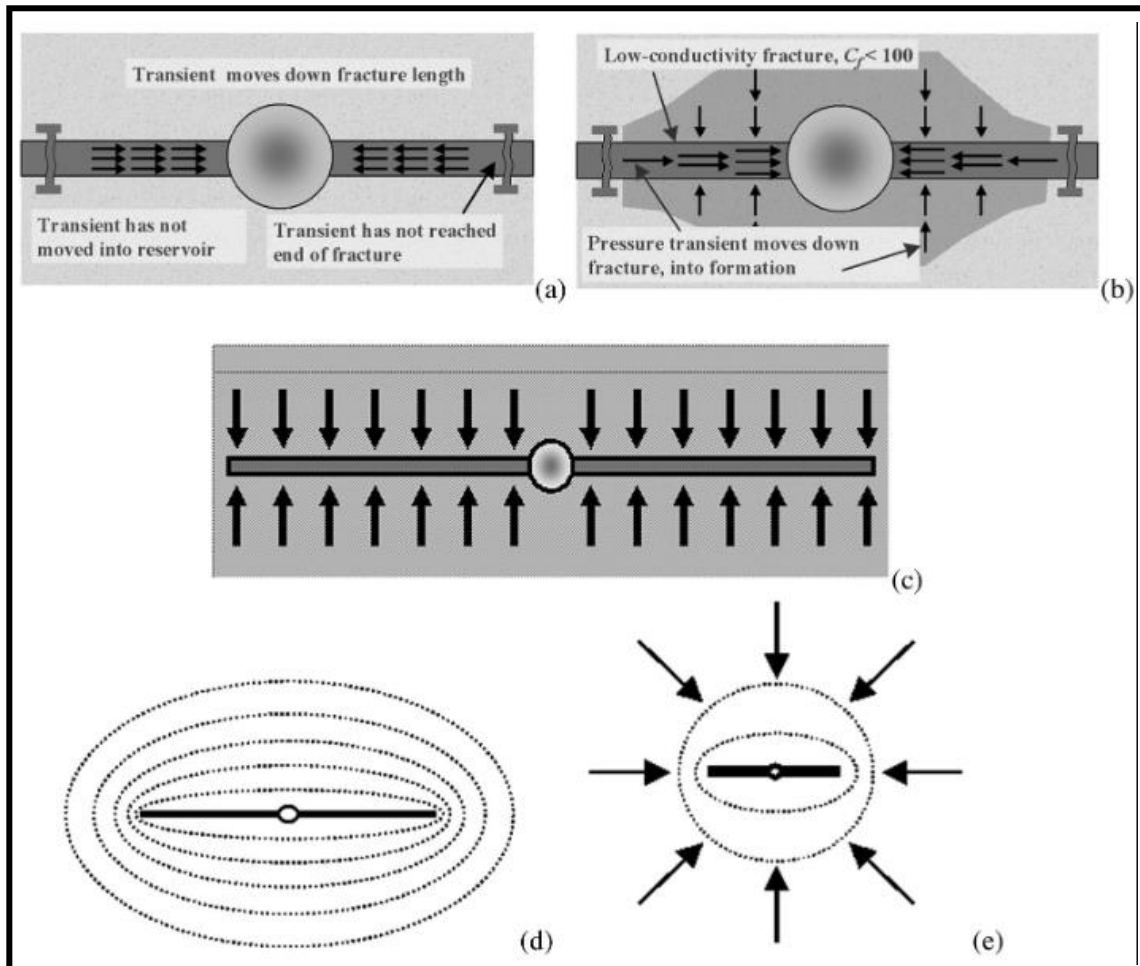


Figure 2.20 flow regimes in hydraulically fractured well

Fracture linear flow regime is the first flow regime and is usually obscured by wellbore effects and exists for a very short time. During this flow period fluid flows from the fracture into the wellbore as shown in figure 2.20a.

Figure 2.20b is bilinear flow regime which exists in finitely conductivity fractures. Fluids in formations surrounding fractures linearly flow into the fracture. The occurrence of this flow regime is characterised by a $\frac{1}{4}$ straight line slope on a derivative log-log plot.

Formation linear flow occurs in infinitely conductivity reservoirs. It is characterised by a $\frac{1}{2}$ straight line slope on a derivative log-log plot. Figure 2.20c shows the formation linear flow regime.

Pseudo-radial flow occurs with all range of fracture conductivities. After a long time, the fracture will appear like an extension to the wellbore radius. It is characterised by a horizontal line on the log-log derivative plot.

Elliptical flow is a transitional flow regime that may occur between formation linear and pseudo-radial flow regime.

2.6.2 Dual Porosity Behaviour in Pressure Transient Analysis

(Warren & Root, 1963) developed an idealized model (as shown in figure 2.21) so as to characterize behaviour of a porous medium that contains regions which contribute significantly to the pore volume of the system but negligibly to the flow capacity of the system such as a naturally fractured or vugular reservoir. The model is such that the blocks are able to transfer fluids into the fracture. In the study, it was observed that there are two parameters that are necessary to characterize the deviation of the behaviour of a double porosity medium from that of a homogenously porous medium. These parameters (storativity ratio and interporosity flow parameter) are obtainable from pressure transient analysis of build-up data. It was also observed that as storativity ratio approaches unity and similarly as interporosity flow parameter tends to infinity the reservoir behaves like an un-fractured reservoir.

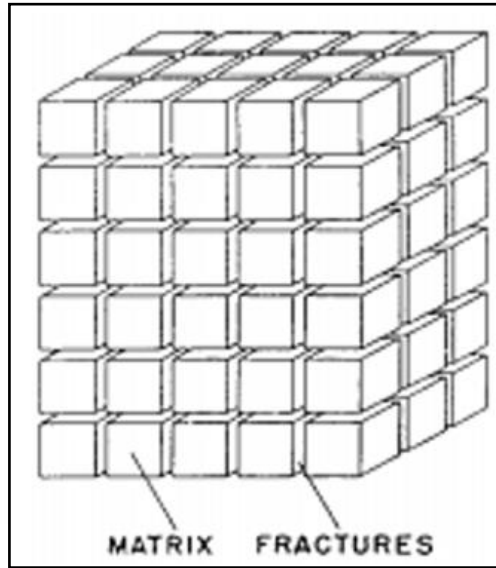
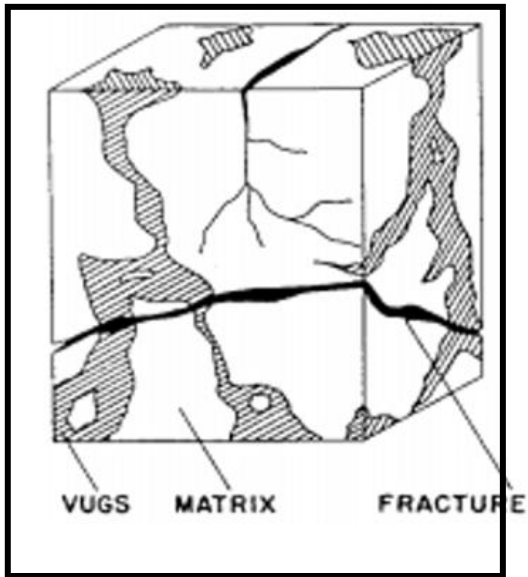


Figure 2.21 Model Reservoir (*Warren & Root, 1963*)

Figure 2.22 Actual reservoir

In dual porosity models, fluid flows from the matrix to the fracture and subsequently into the wellbore. Usually the fracture porosity is small since the fracture volume is small compared to the total volume. However, fracture compressibility is very large as a result of inflation/deflation effect as pressure changes in the fracture.

CHAPTER 3 METHODOLOGY

3.1 Incorporating minimum threshold pressure into inner boundary condition

Darcy's law is given by Equation 3.1

$$2\pi r h \frac{k}{\mu} \left(\frac{\partial P}{\partial r} \right) = -q \quad (3.1)$$

Incorporating a minimum threshold pressure to the Darcy's law gives the modified Darcy's law:

$$2\pi r h \frac{k}{\mu} \left(\frac{\partial P}{\partial r} + \frac{\lambda_B}{r} \right) = -q \quad (3.2)$$

Dimensionless pressure and dimensionless minimum threshold pressure are defined as:

$$P_D = \frac{2\pi k h \Delta P}{q \mu} \quad (3.3)$$

$$\lambda_{BD} = \frac{2\pi k h \lambda_B}{q \mu} \quad (3.4)$$

Therefore,

$$\Delta P = \frac{q \mu P_D}{2\pi k h} \quad (3.5)$$

Now, taking the derivative w.r.t. r gives:

$$\frac{\partial \Delta P}{\partial r} = \frac{q \mu}{2\pi k h} \frac{\partial P_D}{\partial r} \quad (3.6)$$

Rearranging Equation 0.4 gives:

$$\lambda_B = \frac{q\mu\lambda_{BD}}{2\pi kh} \quad (3.7)$$

Dividing Equation 0.7 throughout by r gives:

$$\frac{\lambda_B}{r} = \frac{q\mu\lambda_{BD}}{2\pi rkh} \quad (3.8)$$

Substituting for Equation 3.8 and 3.6 into the modified Darcy's equation gives:

$$r_w r_D \left(q_w \frac{\partial P_D}{r_w \partial r_D} + q_w \frac{\lambda_{BD}}{r_w r_D} \right) = -q \quad (3.9)$$

$$r_D = \frac{r}{r_w} \quad (3.10)$$

Simplifying Equation 3.10 gives:

$$r_D \left(\frac{\partial P_D}{\partial r_D} + \frac{\lambda_{BD}}{r_D} \right) = -\frac{q}{q_w} \quad (3.11)$$

At the wellbore, $r_D = 1$ and assuming $q = q_w$, Equation 3.11 becomes:

$$\frac{\partial P_D}{\partial r_D} + \lambda_{BD} = -1 \quad (3.12)$$

Dimensionless pressure gradient at the wellbore with minimum threshold pressure included is given as:

$$\frac{\partial P_D}{\partial r_D} = -(1 + \lambda_{BD}) \quad (3.13)$$

3.2 Physical Model formulation

Various inner wellbore and reservoir conditions were established which include horizontal well, partially completed vertical well, fully completed vertical well and hydraulically fractured well in a naturally fractured reservoir. Constant production was assumed in all cases and a pressure differential between the wellbore and formation was assumed to be sufficient to cause the Bingham fluid to flow into the wellbore.

3.2.1 Assumptions

- Flow of Bingham fluid with a minimum threshold pressure (Mendes et al., 2002b) was assumed.
- The formation has uniform thickness and is naturally fractured.
- Isotropic nature of the formation is assumed only in the horizontal plane thus horizontal permeability is not necessarily equal to the permeability in the vertical plane.
- The top and bottom boundaries of the reservoir are closed such that there is no flow across the boundaries.
- The flow of the Bingham fluid from the reservoir into the wellbore is assumed to be uniform and all point sources along the wellbore are assumed to be the same.
- At the wellbore, the pressure gradient is assumed to decrease with increasing fluid viscosity in the formation.
- Gravity effect is neglected.

3.2.2 Physical model for horizontal well

A single horizontal well with a constant rate when a pressure drop is induced between the wellbore and the formation was established as shown in fig 3-1. Heavy oil with Bingham fluid characteristics was assumed to be the reservoir fluid flowing from the formation to the wellbore. Other assumptions made are:

- The formation is naturally fractured.

- Bingham fluid in the formation flows towards the horizontal wellbore and the flow is uniform.
- Along the wellbore, every point source is same considering open-hole completions
- The horizontal well is perfectly horizontal and parallel to the upper and lower boundaries.
- The lateral boundaries are infinite.

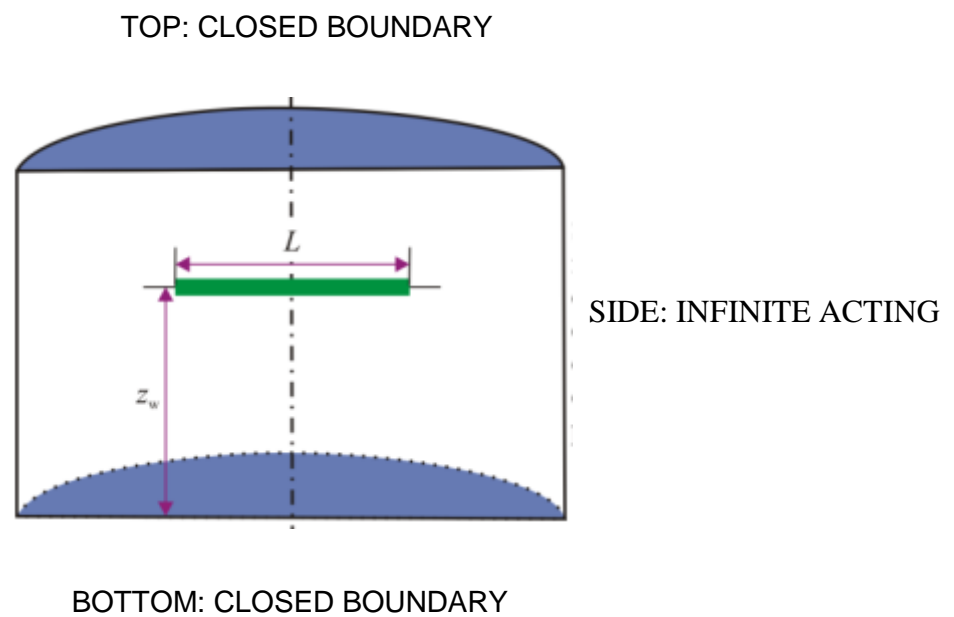


Figure 3.1 Horizontal well in an underground formation (Nie et al., 2018)

3.2.3 Physical Model for hydraulically fractured Model

The case considered was for dual porosity in hydraulically fractured well. The assumptions made are as follows:

- The formation is naturally fractured.
- The fractures have infinite conductivity therefore uniform pressure throughout.
- The formation has a uniform thickness and constant permeability.

- The fracture fully penetrates the vertical extent of the formation and is the same length on both sides of the well as shown in figure 3-2.
- Flow into the wellbore is only through the fracture

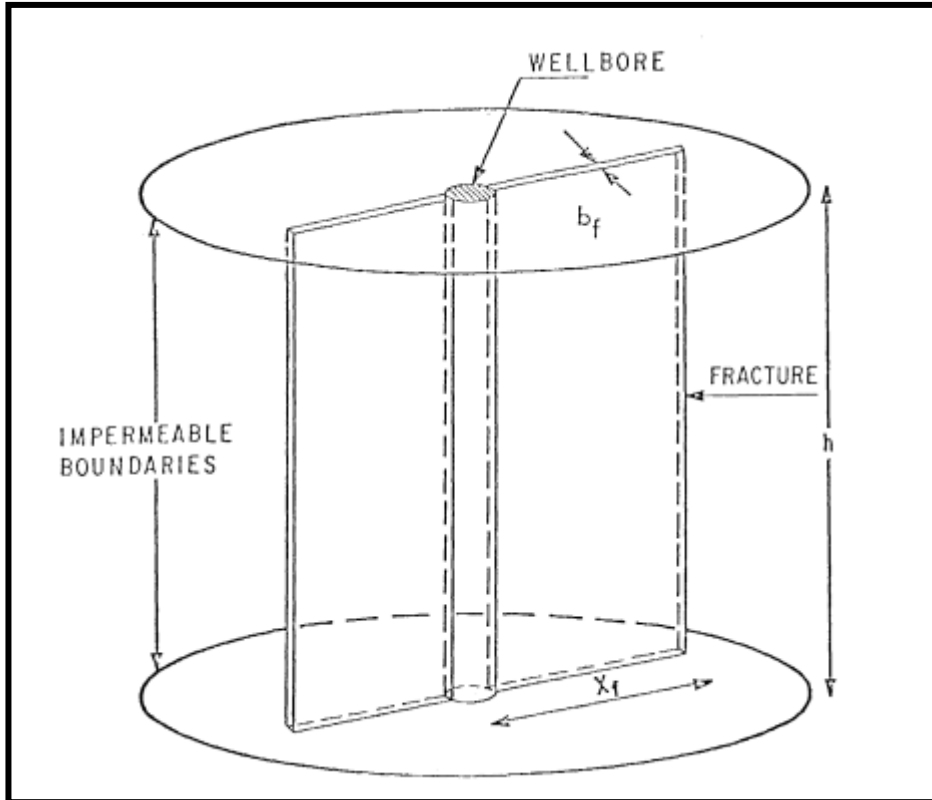


Figure 3.2 Infinite conductivity vertical fracture in an infinite slab reservoir (Tiab, 2015)

4.2.4 Physical model for partially penetrating vertical well

Assumptions made for the partially penetrating vertical well physical model are:

- The well is in a naturally fractured reservoir.
- The model assumes that the well produces from an interval that is less than the net drained interval as shown on the figure 3-3.
- The formation thickness is assumed uniform and permeability homogeneous.
- The top and bottom boundaries of the reservoir are closed such that there is no flow across the boundaries.

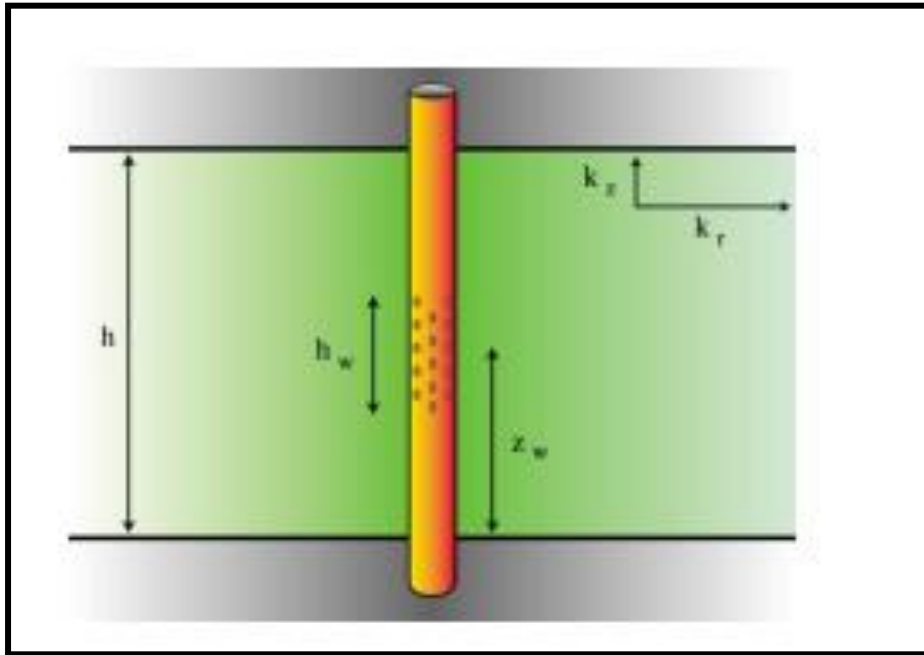


Figure 3.3. Partially penetrating vertical well schematic. (Houzé et al., 2018).

4.2.5 Physical Model for fully penetrating vertical well in a naturally fractured reservoir.

The physical model for fully penetrating is built from same assumption as the partially penetrating vertical well; however completed height is equivalent to formation thickness.

4.3 Mathematical models

The analytical model for pressure response of the four cases can be found by extending the point source solution.

Assumptions that are considered include:

- The reservoir is homogeneous and has a uniform thickness with two closed boundaries at the top and bottom of the reservoir.
- The permeability is constant in each direction but the formation is anisotropic.
- The effect of gravity and friction are negligible.

- Single phase fluid (Bingham fluid type) with constant compressibility and viscosity and formation volume factor flows towards the wellbore.
- Reservoir pressure is initially constant and is given as:

$$P|_{t=0} = P_i \quad (3.14)$$

- The lateral boundaries are infinite and the pressure is equal to the initial pressure

$$P_e = P_i \quad (3.15)$$

- Pressure at the upper and lower impermeable boundaries is assumed constant such that:

$$\left. \frac{\partial P}{\partial z} \right|_{z=0} = 0 \quad (3.16)$$

$$\left. \frac{\partial P}{\partial z} \right|_{z=1} = 0 \quad (3.17)$$

3.3.1 Dimensionless Mathematical Model

Horizontal well model used in this work was based on the model established by (Ozkan, Raghavan, & Joshi, 1989). The dimension distances were based on the well half-length but z_D was based on the thickness of the formation. The well was assumed to be placed at $(0, 0, z_w)$. The definition for x_D , y_D and z_D were given as follows:

$$x_D = \frac{2x}{L} \quad (3.18)$$

$$y_D = \frac{2y}{L} \quad (3.19)$$

$$z_D = \frac{z}{h} \quad (3.20)$$

$$L_D = \frac{L}{2h} \sqrt{\frac{k_z}{k}} \quad (3.21)$$

$$z_{wD} = \frac{z_w}{h} \quad (3.22)$$

Where:

z_w is the perpendicular distance from the bottom boundary to the mid-point of the horizontal strip.

Dimensionless radial radius of lateral boundary

$$r_{eD} = r/r_w \quad (3.23)$$

Where;

r_w is wellbore radius

r is radius of the reservoir

Dimensionless time

$$t_D = \frac{0.0002637k_h}{\phi\mu C_t L_w^2} t \quad (3.24)$$

Where

C_t is the total compressibility

Dimensionless formation thickness

$$h_D = \frac{h}{r_w} \sqrt{\frac{k_h}{k_p}} \quad (3.25)$$

Dimensionless pressure

$$p_D = \frac{k_h h}{141.2 q B \mu} (p_i - p) \quad (3.26)$$

Dimensionless threshold pressure

$$\lambda_{BD} = \frac{k_h h}{141.2 q B \mu} \lambda_B r_w \quad (3.27)$$

Where;

λ_B is the minimum threshold pressure

Now, the dimensionless governing equation for horizontal well expressed in cylindrical system is given as:

$$\frac{\partial^2 P_D}{\partial r_D^2} + \frac{1}{r_D} \frac{\partial P_D}{\partial r_D} + \frac{1}{h_D^2} \frac{\partial^2 P_D}{\partial z_D^2} = \frac{\partial P_D}{\partial t_D} \quad (3.28)$$

Initial Condition

$$P_D(r_D, z_D, t_D)|_{t_D=0} = 0 \quad (3.29)$$

Inner Boundary Condition

Production rate is assumed constant.

$$\left. \frac{\partial P_D}{\partial r_D} \right|_{r_D=1} = -(\lambda_{BD} + 1) \quad (3.30)$$

External boundary conditions:

Top

$$\left. \frac{\partial P_D}{\partial z_D} \right|_{z_D=1} = 0 \quad (3.31)$$

Bottom

$$\left. \frac{\partial P_D}{\partial z_D} \right|_{z_D=0} = 0 \quad (3.32)$$

Lateral Boundary Condition (Infinite boundary).

$$\lim_{n \rightarrow \infty} P_D(r_D, z_D, t_D) = 0 \quad (3.33)$$

3.3.1 Solution to the Dimensionless Mathematical Model

This section provides the solution to the horizontal well governing equation. The solution is presented in Laplace domain and inverted to the real domain by application of Stehfest algorithm (Stehfest, 2002) using Matlab.

Based on t_D , Laplace transform can be introduced as:

$$L[P_D(r_D, t_D)] = \int_0^{\infty} P_D(r_D, z_D, t_D) e^{-ut_D} dt_D = \bar{P}_D(r_D, u) \quad (3.34)$$

The Laplace transform as applied to governing equation gives:

$$\frac{\partial^2 \bar{P}_D}{\partial r_D^2} + \frac{1}{r_D} \frac{\partial \bar{P}_D}{\partial r_D} + \frac{1}{h_D^2} \frac{\partial^2 \bar{P}_D}{\partial z_D^2} = u \bar{P}_D \quad (3.35)$$

u is a Laplace variable.

Applying Laplace transform to the boundary and initial conditions gives:

Initial Condition

$$\bar{P}_D(r_D, z_D, t_D)|_{t_D=0} = 0 \quad (3.36)$$

Boundary conditions

For closed upper boundary system, the pressure gradient at the upper boundary in Laplace domain is given as:

Top

$$\left. \frac{\partial \bar{P}_D}{\partial z_D} \right|_{z_D=1} = 0 \quad (3.37)$$

For closed bottom boundary system, the pressure gradient at the lower boundary in Laplace domain is given as:

Bottom

$$\left. \frac{\partial \bar{P}_D}{\partial z_D} \right|_{z_D=0} = 0 \quad (3.38)$$

At the wellbore, the inner boundary condition is given as:

$$\left. \frac{\partial \bar{P}_D}{\partial z_D} \right|_{r_{D=1}} = -\frac{(\lambda_{BD}+1)}{u} \quad (3.39)$$

Assuming cylindrical lateral boundary to be infinite, the boundary condition is given as:

$$\lim_{n \rightarrow \infty} \bar{P}_D(r_D, z_D, t_D) = 0 \quad (3.40)$$

3.3.2 Transformation into Fourier space:

This section transforms the governing equation, initial and boundary conditions into Fourier space. Thereafter, Fourier back transform is made to obtain the solution in Laplace domain.

Forward Transform is given as:

$$\bar{\bar{P}}_D = \int_0^\infty \bar{P}_D \cos(n\pi z_D) dz_D \quad (3.41)$$

Back Transform is given as:

$$\bar{P}_D = \sum_{n=0}^{\infty} \frac{\bar{\bar{P}}_D \cos(n\pi z_D)}{N(n)} \quad (3.42)$$

Where:

$$N(n) = \int_0^1 \cos^2(n\pi z_D) dz_D \quad (3.43)$$

Applying the Fourier transform to the Governing equation gives:

$$\frac{\partial^2 \bar{P}_D}{\partial r_D^2} + \frac{1}{r_D} \frac{\partial \bar{P}_D}{\partial r_D} - \frac{(n\pi)^2}{h_D^2} \bar{P}_D = u \bar{P}_D \quad (3.44)$$

Transforming Boundary and Initial Conditions into Fourier space gives:

Initial Condition

$$\bar{P}_D(r_D, z_D, t_D)|_{t_D=0} = 0 \quad (3.45)$$

Boundary conditions

Top

$$\left. \frac{\partial \bar{P}_D}{\partial z_D} \right|_{z_D=1} = 0 \quad (3.46)$$

Bottom

$$\left. \frac{\partial \bar{P}_D}{\partial z_D} \right|_{z_D=0} = 0 \quad (3.47)$$

Inner Boundary Condition

$$\left. \frac{\partial \bar{P}_D}{\partial z_D} \right|_{r_D=1} = -\frac{(\lambda_D+1)}{u} \cos(n\pi z_D) \quad (3.48)$$

Lateral Boundary Condition (Infinite boundary)

$$\lim_{r_D \rightarrow \infty} \bar{P}_D(r_D, z_D, t_D) = 0 \quad (3.49)$$

3.3.3 Solution to Dimensionless Mathematical Model

Rearranging equation, the governing equation can be written as

$$\frac{\partial^2 \bar{P}_D}{\partial r_D^2} + \frac{1}{r_D} \frac{\partial \bar{P}_D}{\partial r_D} - \left(\frac{(n\pi)^2}{h_D^2} + u \right) \bar{P}_D = 0 \quad (3.50)$$

Let:

$$\xi_n = \frac{(n\pi)^2}{h_D^2} + u \quad (3.51)$$

Substitution of 3.51 into 3.50 gives

$$\frac{\partial^2 \bar{P}_D}{\partial r_D^2} + \frac{1}{r_D} \frac{\partial \bar{P}_D}{\partial r_D} - \xi_n \bar{P}_D = 0 \quad (3.52)$$

Multiplying equation throughout by r_D^2 gives

$$r_D^2 \frac{\partial^2 \bar{P}_D}{\partial r_D^2} + r_D \frac{\partial \bar{P}_D}{\partial r_D} - r_D^2 \xi_n \bar{P}_D = 0 \quad (3.53)$$

Let:

$$\eta = r_D \sqrt{\xi_n} \quad (3.54)$$

By substituting η for r_D 3.53 becomes:

$$\eta^2 \frac{\partial^2 \bar{P}_D}{\partial \eta^2} + \eta \frac{\partial \bar{P}_D}{\partial \eta} - \eta^2 \bar{P}_D = 0 \quad (3.55)$$

Equation 3.55 is a Modified Bessel Equation of Zero Order and the general solution is given by (Abramowitz & Stegun, I., 1964) as:

$$\bar{P}_D = A_n I_0(\eta) + B_n K_0(\eta) \quad (3.56)$$

From lateral boundary conditions

$$\lim_{r_D \rightarrow \infty} \bar{P}_D(r_D, z_D, t_D) = 0 \quad (3.57)$$

Therefore, combining Equation 3.56 and Equation 3.57 gives:

$$\bar{P}_D = A_n \lim_{r_D \rightarrow \infty} I_0(\eta) + B_n \lim_{r_D \rightarrow \infty} K_0(\eta) = 0 \quad (3.58)$$

According to (Abramowitz & Stegun, I., 1964)

$$\lim_{r_D \rightarrow \infty} I_0(\eta) = \infty; \quad (3.59)$$

$$\lim_{r_D \rightarrow \infty} K_0(\eta) = 0; \quad (3.60)$$

By considering Equations 3.58, 3.59 and 3.60, it follows that:

$$A_n = 0 \quad (3.61)$$

Differentiating Equation 3.58 w.r.t. η gives:

$$\frac{\partial \bar{P}_D}{\partial \eta} = B_n \frac{\partial K_0(\eta)}{\partial \eta} \quad (3.62)$$

According to (Abramowitz & Stegun, I., 1964) ,

$$\frac{\partial I_0(z)}{\partial z} = I_1(z) \quad (3.63)$$

$$\frac{\partial K_0(z)}{\partial z} = -K_1(z) \quad (3.64)$$

Therefore it follows that;

$$\frac{\partial \bar{P}_D}{\partial \eta} = -B_n K_1(\eta) \quad (3.65)$$

Note that Equation 3.65 can be written in terms of r_D as:

$$\frac{\partial \bar{P}_D}{\partial r_D} = -B_n K_1(r_D \sqrt{\xi_n}) \quad (3.66)$$

At the wellbore $r_D = 1$, combining Equation 3.48 and Equation 3.66 gives:

$$B_n \sqrt{\xi_n} K_1(\sqrt{\xi_n}) = \frac{(\lambda_{BD}+1)}{u} \cos(n\pi z_D) \quad (3.67)$$

Therefore:

$$B_n = \frac{(\lambda_{BD}+1)}{u \sqrt{\xi_n} K_1(\sqrt{\xi_n})} \cos(n\pi z_D) \quad (3.68)$$

$$\text{As } K_1(\sqrt{\xi_n}) \rightarrow 0, \quad K_1(\sqrt{\xi_n}) = \left(\frac{1}{\sqrt{\xi_n}}\right)$$

Therefore, Equation 3.68 become:

$$B_n = \frac{(\lambda_{BD}+1)}{u} \cos(n\pi z_D) \quad (3.69)$$

Substituting Equation 3.61 and 3.69 into Equation 3.58 gives:

$$\bar{P}_D = \frac{(\lambda_D+1)}{u} K_o(\eta) \cos(n\pi z_D) \quad (3.70)$$

Using Equation 3.42 to invert from Fourier domain gives:

$$\bar{P}_D = \sum_{n=0}^{\infty} \left(\frac{(\lambda_{BD}+1) K_o(r_D \sqrt{\xi_n}) \cos(n\pi z_{wD}) \cos(n\pi z_D)}{u N(n)} \right) \quad (3.71)$$

The point source solution for the radial flow problem is given in Laplace domain as

$$\bar{P}_D = \frac{(\lambda_{BD}+1)}{u} \left(K_o(r_D \sqrt{\xi_0}) + 2 \sum_{n=1}^{\infty} K_o(r_D \sqrt{\xi_n}) \cos(n\pi z_{wD}) \cos(n\pi z_D) \right) \quad (3.72)$$

3.3.4. Extension of Point Source Solution

The point source solution was extended to give solutions for four cases: horizontal well, partially penetrating vertical well, fully penetrating vertical well and hydraulically fractured wells.

Partially Penetrating Vertical Well

To obtain the solution for partially completed vertical well of length h_{wD} along the height of the well, the right hand side of the point source solution is integrated from $z_D - \frac{h_{wD}}{2}$ to $z_D + \frac{h_{wD}}{2}$ (Ozkan, 1988).

$$\bar{P}_D = \frac{(\lambda_{BD}+1)}{u} \left(\begin{array}{c} K_o(r_D\sqrt{u}) \\ + \\ \frac{2}{\pi h_{wD}} \sum_{n=1}^{\infty} \frac{K_o(r_D\sqrt{\xi_n}) \cos(n\pi z_{wD}) \cos(n\pi z_D) \sin(\frac{n\pi h_{wD}}{2})}{n} \end{array} \right) \quad (3.73)$$

Fully Penetrating Vertical Well

The solution corresponding to the fully completed vertical well may be obtained from the point source solution by integrating over the whole height of the pay-zone. The solution is given as:

$$\bar{P}_D = \frac{(\lambda_{BD}+1)}{u} \int_0^1 (K_o(r_D\sqrt{u}) + 2 \sum_{n=1}^{\infty} K_o(r_D\sqrt{\xi_n}) \cos(n\pi z_{wD}) \cos(n\pi z_D)) dz_D \quad (3.74)$$

Solving Equation 3.74 gives:

$$\bar{P}_D = \frac{(\lambda_{BD}+1)}{u} K_o(r_D\sqrt{u}) \quad (3.75)$$

Hydraulically Fractured Wells

The solution for fully penetrating hydraulically fractured well is obtained by integrating the right hand side of point source solution from 0 to 1 with respect to dz_D and then from -1 to 1 with respect to dx_{wD} (Ozkan, 1988). The solution is

$$\bar{P}_D = \frac{(\lambda_{BD}+1)}{u} \left[\int_{-1}^1 \int_0^1 \left(\begin{array}{c} K_o(\sqrt{(x_D - x_{wD})^2 + (y_D - y_{wD})^2} \sqrt{u}) \\ + \\ 2 \sum_{n=1}^{\infty} \left[\frac{K_o(\sqrt{(x_D - x_{wD})^2 + (y_D - y_{wD})^2} \sqrt{\xi_n})}{\cos(n\pi z_{wD}) \cos(n\pi z_D)} \right] \end{array} \right) dz_D dx_{wD} \right] \quad (3.76)$$

Therefore,

$$\bar{P}_D = \frac{(\lambda_{BD}+1)}{u} \int_{-1}^1 K_o\left(\sqrt{u} \sqrt{(x_D - x_{wD})^2 + (y_D - y_{wD})^2}\right) dx_{wD} \quad (3.77)$$

Matlab software was used to solve and transform the solution into real domain by using Stehfest algorithm (Stehfest, 2002).

Horizontal well

The solution for the horizontal well can be obtained by integrating over the entire length of horizontal well with respect to dx_{wD} . That is,

$$\bar{P}_D = \frac{(\lambda_{BD}+1)}{u} \int_{-1}^1 \left(K_o(r_D \sqrt{u}) + 2 \sum_{n=1}^{\infty} K_o(r_D \sqrt{\xi_n}) \cos(n\pi z_{wD}) \cos(n\pi z_D) \right) dx_{wD} \quad (3.78)$$

Where:

$$r_D = \sqrt{(x_D - x_{wD})^2 + (y_D - y_{wD})^2} \quad (3.79)$$

Following the solution to the 3D diffusivity equation for horizontal well in a naturally fractured reservoir, the Stehfest numerical inversion method (Stehfest, 2002) was used to transform the Laplace space solution \bar{p}_{wD} to real space solution p_{wD} .

The solution in Laplace domain is given as below:

$$\bar{P}_D = \frac{(\lambda_{BD}+1)}{u} \left[\int_{-1}^1 \left(K_o\left(\sqrt{u} \sqrt{(x_D - x_{wD})^2 + (y_D - y_{wD})^2}\right) + 2 \sum_{n=1}^{\infty} \left[\cos(n\pi z_{wD}) \cos(n\pi z_D) K_o\left(\sqrt{\left(\frac{(n\pi)^2}{h_D^2} + u\right) \sqrt{(x_D - x_{wD})^2 + (y_D - y_{wD})^2}}\right) \right] \right) dx_{wD} \right] \quad (3.80)$$

Incorporating Wellbore Storage and Skin effect

Duhamel's principle has been applied to incorporate the effect of skin and wellbore storage for horizontal well testing (Ozkan & Raghavan, 1991) as shown in

$$\bar{P}_{wD} = \frac{u\bar{P}_D + S}{u(1 + uC_D(u\bar{P}_D + S))} \quad (3.81)$$

3.4 Investigating effects of parameters on pressure transient analysis

3.4.1 Investigating effect of λ_{BD} on Pressure Transient Analysis

1. A plot of ΔP and $t * \Delta P'$ versus t was drawn on log-log plot with the following parameters held constant:
 - a) Interporosity flow parameter
 - b) Anisotropy
 - c) Storativity ratio
2. Three different values of λ_{BD} were considered and the discrepancies on the graphs was noted.

3.4.2 Effect of ω , on the pressure response

1. A plot of ΔP and $t * \Delta P'$ versus t was drawn on log-log plot with the following parameters held constant:
 - a) Interporosity flow paameter
 - b) Anisotropy
 - c) λ_{BD}
2. Three different values of ω were considered and the discrepancies on the graphs was noted

3.4.3 Effect of interporosity flow parameter, (λ) on the pressure response for the four cases

1. A plot of ΔP and $t * \Delta P'$ versus t was drawn on log-log plot with the following parameters held constant:

- d) storativity
- e) Anisotropy
- f) λ_{BD}

2. Three different values of λ were used and the discrepancies on the graphs were noted.

3.5 TDS Technique

This section presents an analytical technique referred to as Tiab's Direct Synthesis (TDS) technique for the interpretation of log-log plots of pressure and pressure derivative data. Steps for calculating certain reservoir parameters are described.

Steps to calculate $k_y k_z$ permeability product

3. A plot of ΔP and $t * \Delta P'$ versus t was drawn on log-log plot
4. The value of $(t * \Delta P')_{ERF}$ was taken from pressure derivative plot during early radial flow
5. Equation 3.82 was derived and used to compute the permeability product

$$\sqrt{k_y k_z} = \frac{70.6q\mu B(1+\lambda_{BD})}{L_w(t*\Delta P')_{ERF}} \quad (3.82)$$

2.1.1.1 Steps for calculating k_y , using TDS approach.

1. A plot of ΔP and $t * \Delta P'$ versus t was drawn on log-log plot.
2. The value of $(t * \Delta P')$ was taken from pressure derivative plot at one hour.
3. Equation 3.83 was derived and used to compute k_y

$$k_y = \left(\frac{4.066qB(1+\lambda_{BD})}{h_z L_w(t*\Delta P')} \right)^2 \frac{\mu}{\phi \omega C_t} \quad (3.83)$$

Steps for calculating k_h , using TDS approach.

1. A plot of ΔP and $t * \Delta P'$ versus t was drawn on log-log plot.
2. The value of $(t * \Delta P')_{LRF}$ was taken from pressure derivative during late radial flow.
3. Equation 3.84 was derived and used to compute k_h

$$k_h = \frac{70.6 * q \mu B_0 (1 + \lambda_{BD})}{h * (t * \Delta P')_{LRF}} \quad (3.84)$$

Steps for using TDS to calculate storativity

1. A plot of ΔP and $t * \Delta P'$ versus t was drawn on log-log plot.
2. The value of $(t * \Delta P')_{min}$ was taken from pressure derivative at the lowest point of the trough.
3. The value of $(t * \Delta P')_{LRF}$ corresponding to the zero slope fracture depletion period was taken from pressure derivative during late radial flow.
4. A relationship between $(t * \Delta P')_{min}$ and $(t * \Delta P')_{RF}$ was obtained from equation 3.85

$$R = \frac{(t * \Delta P')_{min}}{(t * \Delta P')_{RF}} \quad (3.85)$$

5. Storativity was estimated from equation 3.86

$$\omega = 0.5604R^6 - 1.3322R^5 + 1.7232R^4 - 0.827R^3 + 0.7287R^2 + 0.1469R \quad (3.86)$$

Steps for calculating interporosity flow parameter.

1. A plot of ΔP and $t * \Delta P'$ versus t was drawn on log-log plot.
2. The value of $(t * \Delta P')_{min}$ was taken from pressure derivative at the lowest point of the trough.
3. The value of t_{min} was taken from time co-ordinate at the lowest point of the trough.
4. Equation 3.87 was derived and used to estimate the interporosity parameter.

$$\lambda = \frac{45.5 \mu r_w^2 h (\phi C_t)_{m+f} (t * \Delta P')_{min}}{q B * (1 + \lambda_{BD}) t_{min}} \quad (3.87)$$

CHAPTER 4

RESULTS AND DISCUSSION

In this chapter, pressure and pressure derivative curves were drawn on log-log plots and the effect of minimum threshold pressure observed for the four well types. Effect of other parameters like storativity, interporosity flow parameter, horizontal well length, penetration ratio was also investigated from the log-log plots. Derivations of equations used in TDS to determine k_x , k_y , interporosity flow parameter, storativity ratio and fracture length were presented taking cognisance of the minimum threshold pressure. An example of application for some of the derived equations was also included.

4.1 Effect minimum threshold pressure on pressure transient response of HW

This section discusses the effect of minimum threshold pressure on the pressure response of a horizontal well in naturally fractured reservoir. A vertical isotropy was assumed and other constant parameters are: Dimensionless wellbore storage = 0.1, Skin = 2.0, interporosity flow parameter = 10^{-4} , storativity ratio = 0.01 and dimensionless length = 10. Dimensionless minimum threshold pressure was varied as follows: $\lambda_{BD} = 0, 0.1, 1.0, 2.0$

During the early time, little information can be extracted due to distortion caused by wellbore storage effects. All the three curves overlap for pressure and pressure derivative plots as shown on figure 1. However, the effects of minimum threshold pressure begin to show after wellbore effect period.

The curve for $\lambda_{BD} = 0.0$ is on the lowest position as compared to the other two. Since crude oil with $\lambda_{BD} = 0.0$ exhibits Newtonian characteristics, it follows that the oil experiences a minimal pressure loss due to fluid properties (yield shear stress).

The curve for $\lambda_{BD} = 0.1$ is slightly higher than for $\lambda_{BD} = 0.0$ due to the closeness of threshold values. A significantly large difference is observed for $\lambda_{BD} = 2.0$. The curve for $\lambda_{BD} =$

2.0 is the highest as shown on figure 4.1. Reservoirs with heavy crude oil that exhibit Bingham fluid characteristics indicate a minimum threshold pressure and experience an additional pressure drop. This pressure drop is responsible for the rise above the curve for $\lambda_{BD} = 0.0$. The pressure derivative value for a fluid with any value of λ_{BD} at any given time is equivalent to $(1 + \lambda_{BD})$ times pressure derivative value of the Newtonian fluid at that particular time. The same is true for the pressure change curves as well. As such, for low values of λ_{BD} , we can say $(1 + \lambda_{BD}) \approx 1$ and thus a very small rise on the log-log plot is observed for small λ_{BD} .

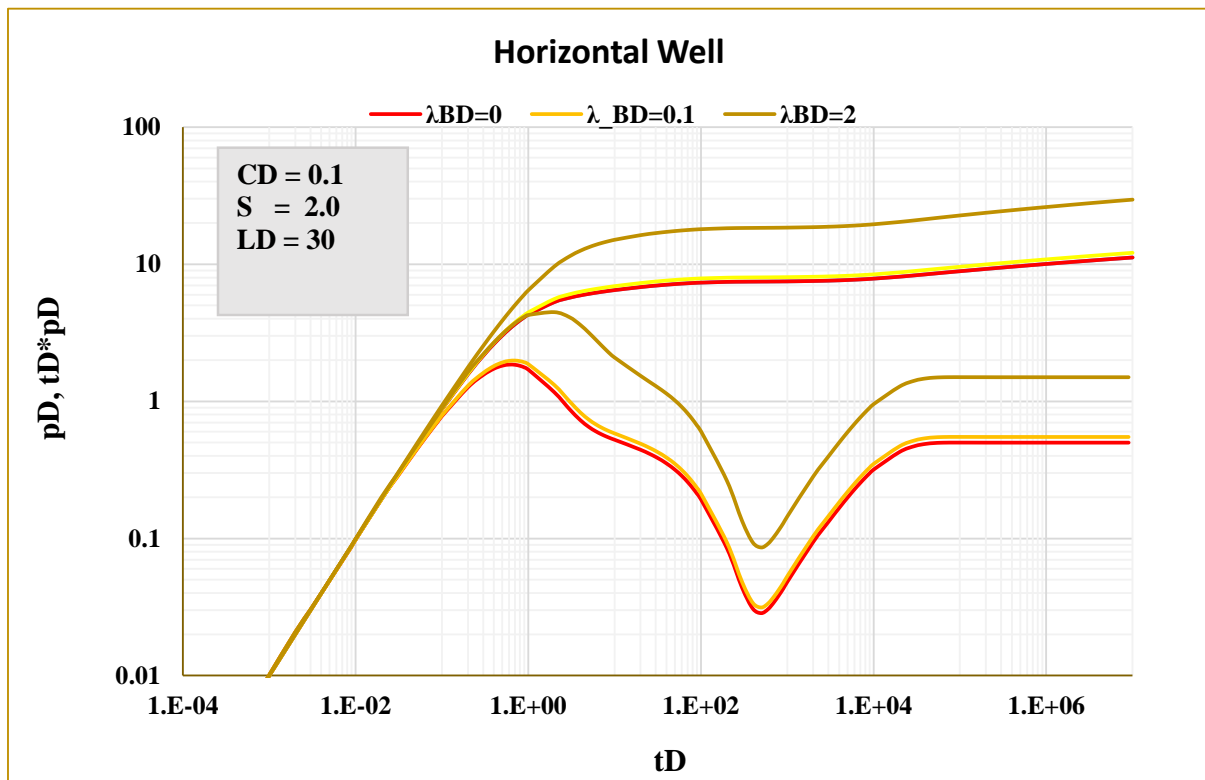


Figure 4.1 Effect of λ_{BD} pressure on reservoir pressure response of horizontal well

4.2 Effect of well length on the flow regimes of HW in NFR

This section discusses the effect of horizontal well length on fluid flow regimes. Two cases were considered.

CASE 1:

A vertical isotropy was assumed and other constant parameters are: Dimensionless wellbore storage = 0.0, Skin = 0.0, inter-porosity flow parameter $\lambda = 100$, storativity ratio = 0.01 and dimensionless length = 1.0. Figure 4.2 represents case 1.

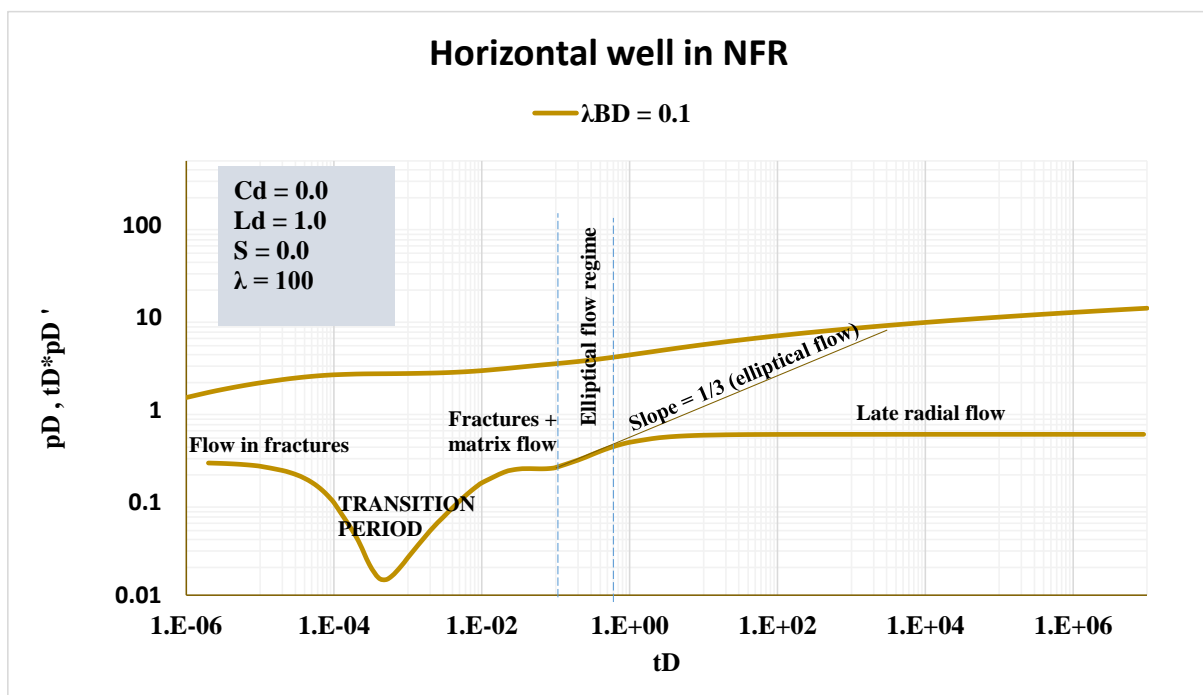


Figure 4.2 CASE1: Effect of LD on flow regimes in horizontal wells

CASE 2:

A vertical isotropy was assumed and other constant parameters are: Dimensionless wellbore storage = 0.0, Skin = 0.0, inter-porosity flow parameter = 100, storativity ratio = 0.01 and dimensionless length = 30.0 represents case 1.

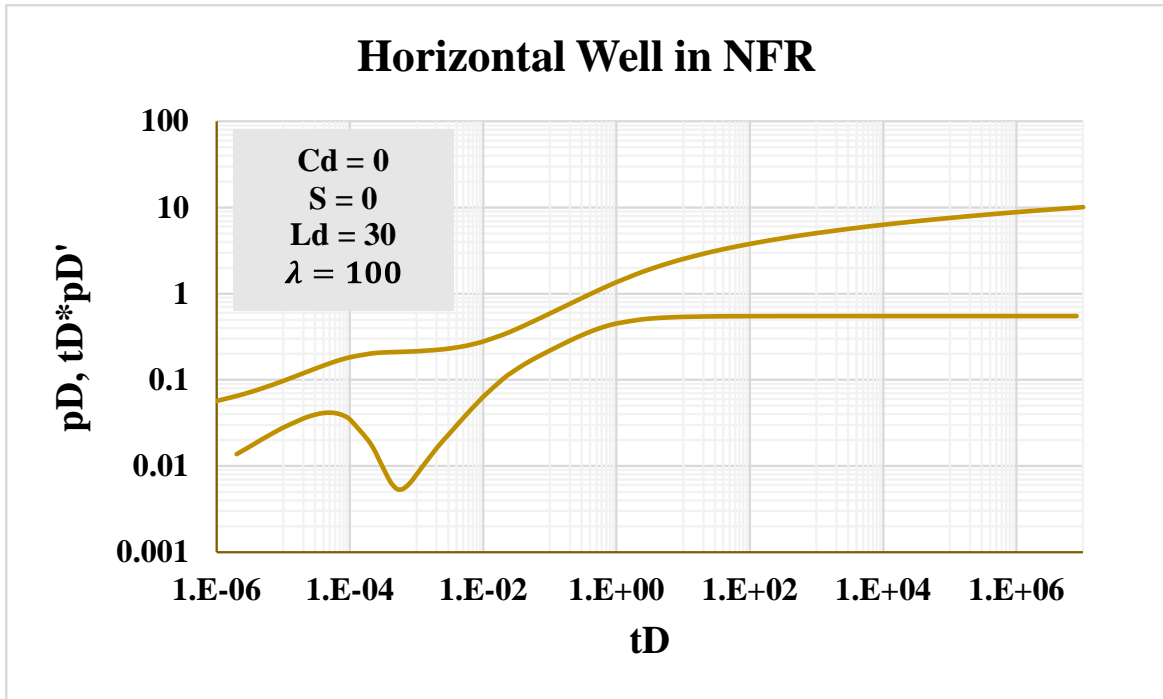


Figure 4.3 CASE2: Effect of LD on flow regimes in horizontal wells

Three flow regimes can be observed in case 1. The flow regimes are early radial flow, elliptical flow and late radial flow regime. Figure 4.2 shows these flow regimes for short well length. However, there is a difference for case 2 as shown on figure 4.3.

4.3 Effect of minimum threshold pressure in hydraulically fractured well in naturally fractured reservoir

This section discusses the effect of minimum threshold pressure on the pressure response of a hydraulically fractured well in a naturally fractured reservoir. A vertical isotropy was assumed and other constant parameters are: Dimensionless wellbore storage = 0, Skin = 0, interporosity flow parameter = 100, storativity ratio = 0.01 and dimensionless penetration ratio = 0.6. Dimensionless minimum threshold pressure was varied as follows: $\lambda_{BD} = 0, 0.1, 2.0$

Just as the case for horizontal wells and partially penetrating vertical well, minimum threshold pressure has an impact on the pressure response in a hydraulically fractured reservoir. The curve for $\lambda_{BD} = 0$ was at the bottom most position as compared to $\lambda_{BD} = 0.1$

and $\lambda_{BD} = 2.0$ as shown in figure 4.4. The curve for $\lambda_{BD} = 0.0$ was considered as a reference point representing Newtonian fluid. Other curves, $\lambda_{BD} = 0.1$ and $\lambda_{BD} = 2.0$ are shifted upwards by a factor of $(\lambda_{BD} + 1)$. Figure 4.4 shows the pressure response due to minimum threshold pressure on the pressure derivative curve.

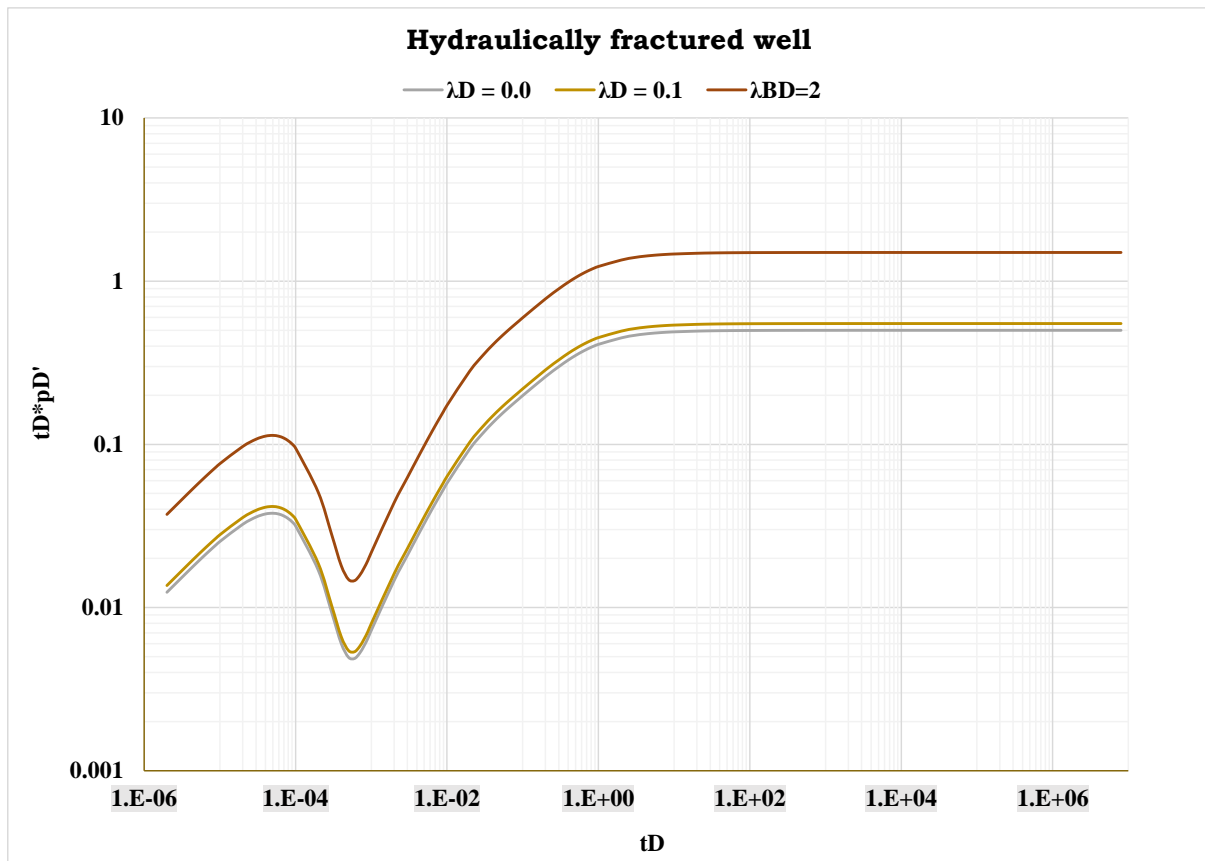


Figure 4.4 Effect of λ_{BD} pressure on reservoir pressure response of hydraulically fractured well

4.4 Effects of minimum threshold pressure on partially penetrating vertical wells in NFR

This section discusses the effect of minimum threshold pressure on the pressure response of a partially penetrating vertical well in a naturally fractured reservoir. A vertical isotropy was assumed and other constant parameters are: Dimensionless wellbore storage =

0, Skin = 0 , interporosity flow parameter = 100 , storativity ratio = 0.01 and dimensionless penetration ratio = 0.6. Dimensionless minimum threshold pressure was varied as follows:
 $\lambda_{BD} = 0, 0.1, 2.0$

The $\lambda_{BD} = 0$ curve was the lowest in terms of position as shown in figure 4.5. At $\lambda_{BD} = 0$, the oil behaves like a Newtonian fluid; and in this case it was taken as a reference point. As the value for λ_{BD} increases, an upward shift is observed. Just as the case for horizontal wells, the magnitude of increase or an upward shift factor was equivalent ($\lambda_{BD} + 1$). A small value of λ_{BD} will cause a minimal upward shift on the log-log plot because $1 \approx (1 + \lambda_{BD})$ when λ_{BD} is small. As such, the curve for $\lambda_{BD} = 2$ is clearly higher than the two lower ones because it is of a higher order.

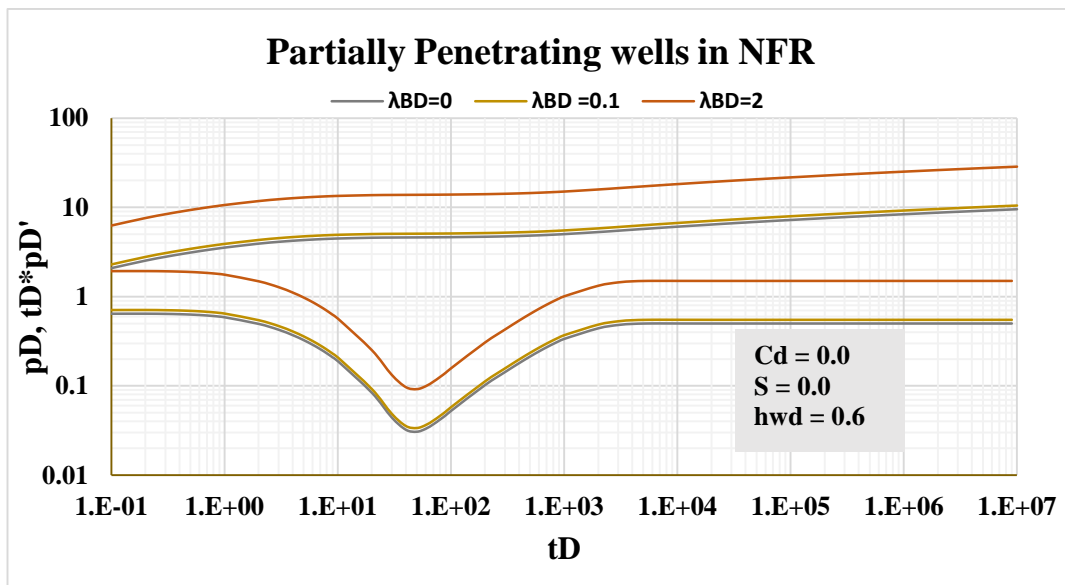


Figure 4.5 Effect of λ_{BD} on pressure response of Partially Penetrating well

4.5 Effect of penetration ratio in partially penetrating vertical wells in NFR

This section discusses the effect of penetration ratio on the pressure response of a partially penetrating vertical well in naturally fractured reservoir. A vertical isotropy was assumed and other constant parameters are: Dimensionless wellbore storage = 0, Skin = 0, interporosity flow parameter $\lambda = 100$, storativity ratio $\omega = 0.01$ and dimensionless penetration ratio was varied as follows: $h_D = 0.2, h_D = 0.6, h_D = 0.8$

Penetration ratio significantly affects the pressure behaviour in a partially penetrating vertical well as shown in figure 4.6. The effect is observed at early time, i.e., near the wellbore. The curve for $h_D = 0.2$ is higher than that for $h_D = 0.6$ and $h_D = 0.8$. Partial penetration causes a pseudo-skin near the wellbore and this effect causes an upward shift that is observed on the pressure and pressure derivative log-log plot. A low penetration ratio causes a greater pseudo-skin and thus a higher curve on the log-log plot.

However, as the transient travels further away from the wellbore, the effect of partial penetration is almost minimal. This can be observed by an overlap for all the three cases at late radial flow as shown in figure 4.6.

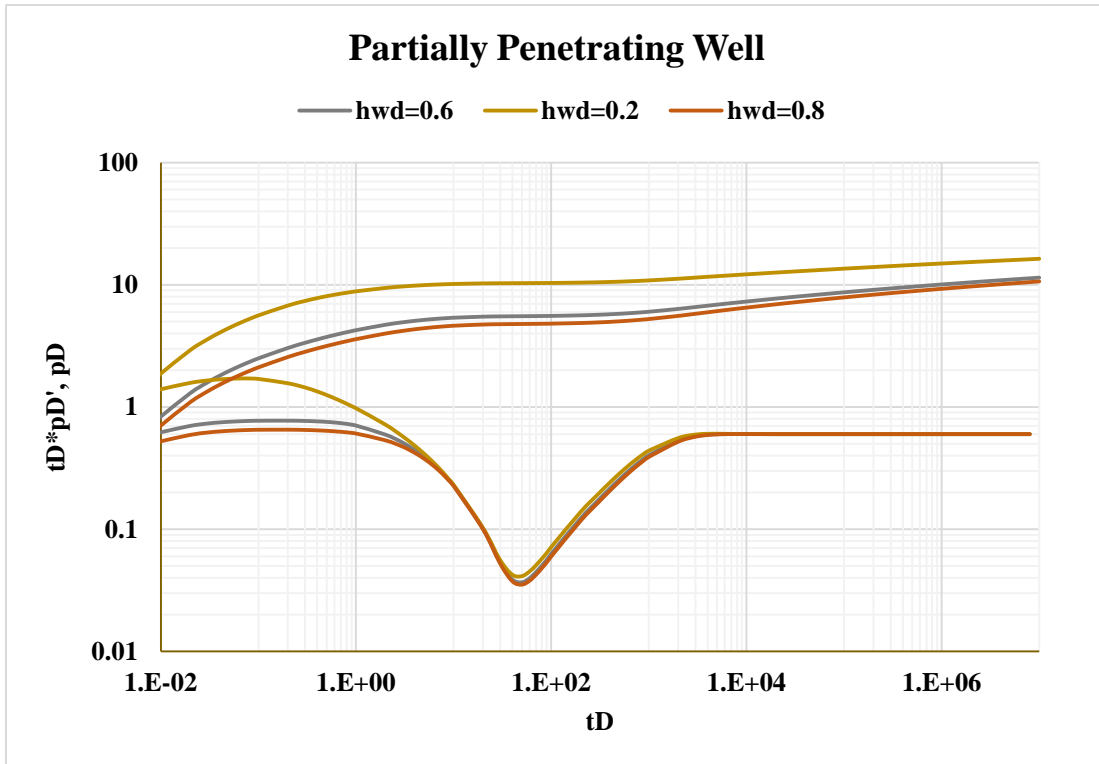


Figure 4.6 Pressure response to completed interval in a PPVW in NFR

4.6 Effect of minimum threshold pressure on a fully penetrating vertical well in NFR

This section discusses the effect of minimum threshold pressure on the pressure response of a fully penetrating vertical well in a naturally fractured reservoir. A vertical isotropy was assumed and other constant parameters are: Dimensionless wellbore storage = 0, Skin = 0, interporosity flow parameter = 100, storativity ratio = 0.01 and dimensionless penetration ratio = 1.0. Dimensionless minimum threshold pressure was varied as follows: $\lambda_{BD} = 0, 0.1, 2.0$

The curve for $\lambda_{BD} = 0$ was taken to be the reference point since the fluid will behave like a Newtonian fluid. An additional pressure drop was experienced due to existence of the minimum threshold pressure. Like in the three previous cases, all the curve were raised above the $\lambda_{BD} = 0$ by a factor $(\lambda_{BD} + 1)$. Unlike the partial penetration ratio effect that is significantly felt during early time, i.e., close to the wellbore, minimum threshold pressure is felt through

the life of the reservoir. This is because λ_{BD} is a factor of the reservoir fluid itself and the formation geometry. As long as these parameters are unaltered, the effect will remain the same within the entire reservoir. Figure 4.7 shows the effect of minimum threshold pressure in fully penetrating vertical well.

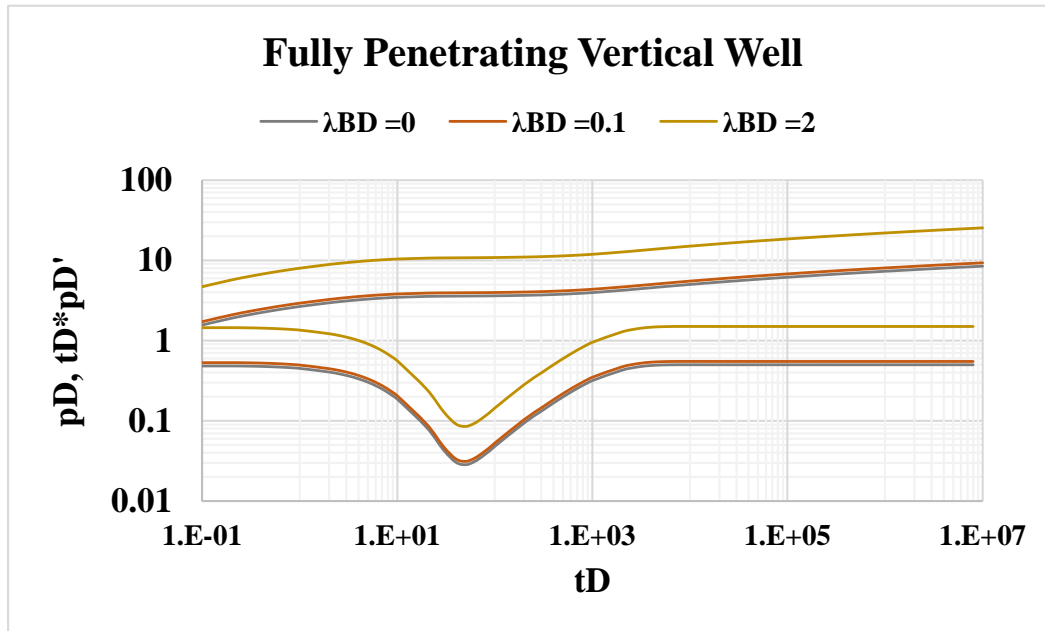


Figure 4.7 Effect of λ_{BD} pressure on reservoir pressure response of fully penetrating vertical well

5.7 Effects of Storativity ratio

This section discusses the effect of storativity ratio for horizontal well, hydraulically fractured well, partially penetrating vertical well and fully penetrating vertical well. A vertical isotropy was assumed and other constant parameters are: Dimensionless wellbore storage = 0, Skin = 0, storativity ratio = 0.01 interporosity flow parameter $\lambda = 100$, $\lambda_{BD} = 0.1$.

A general trend was also observed for all the four cases. The depth of the tough decreases with increasing storativity ratio and the transition period took longer to appear. This

is because, for a high storativity ratio the storage capacity of the fracture will be high and thus the depletion period will take long before transition period commences.

The trough tend to disappear into a straight line as shown on figure 4.8 and figure 4.9 for $\omega=1$. This is because as storativity ratio approaches unit, the porosity will be mostly from the fractures and thus dual porosity is replaced by single porosity. Figure 4.8 to figure 4.9 show effect of storativity ratio on the four cases under discussion.

4.7.1 Horizontal Well

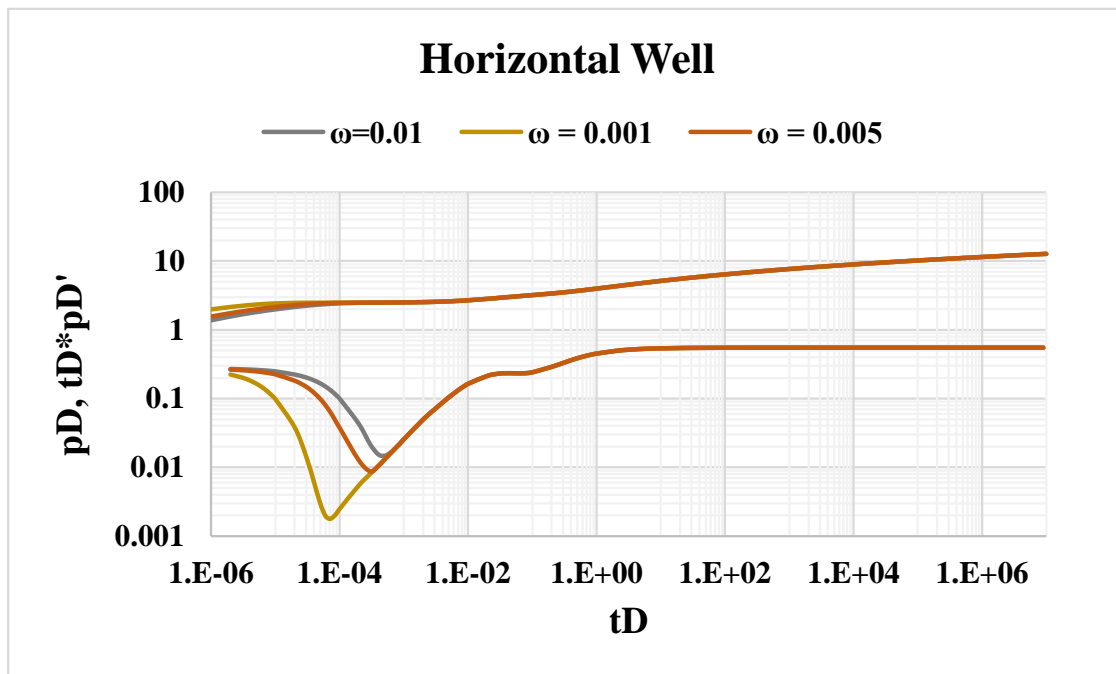


Figure 4.8 Effect of storativity on pressure response of a horizontal well

4.7.2 Hydraulically fractured well

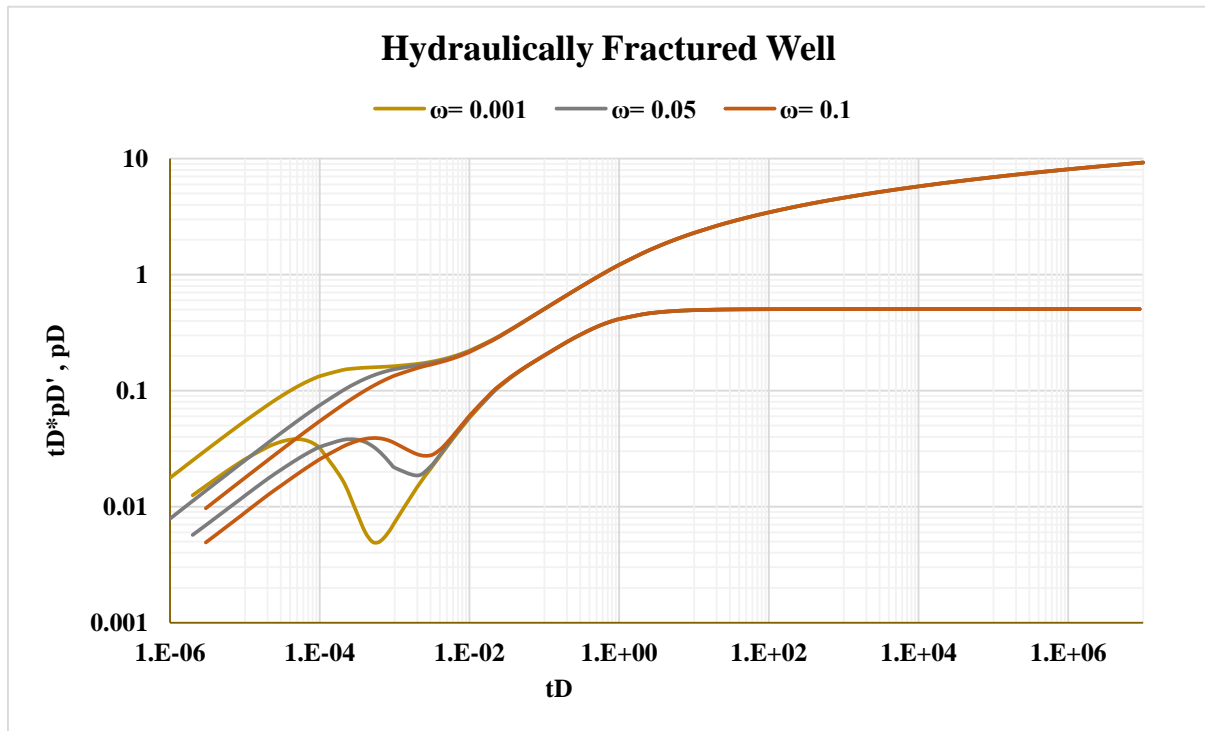


Figure 4.9 Effect of storativity ratio on pressure response of hydraulically fractured well

4.7.3 Partially Penetrating Vertical Well

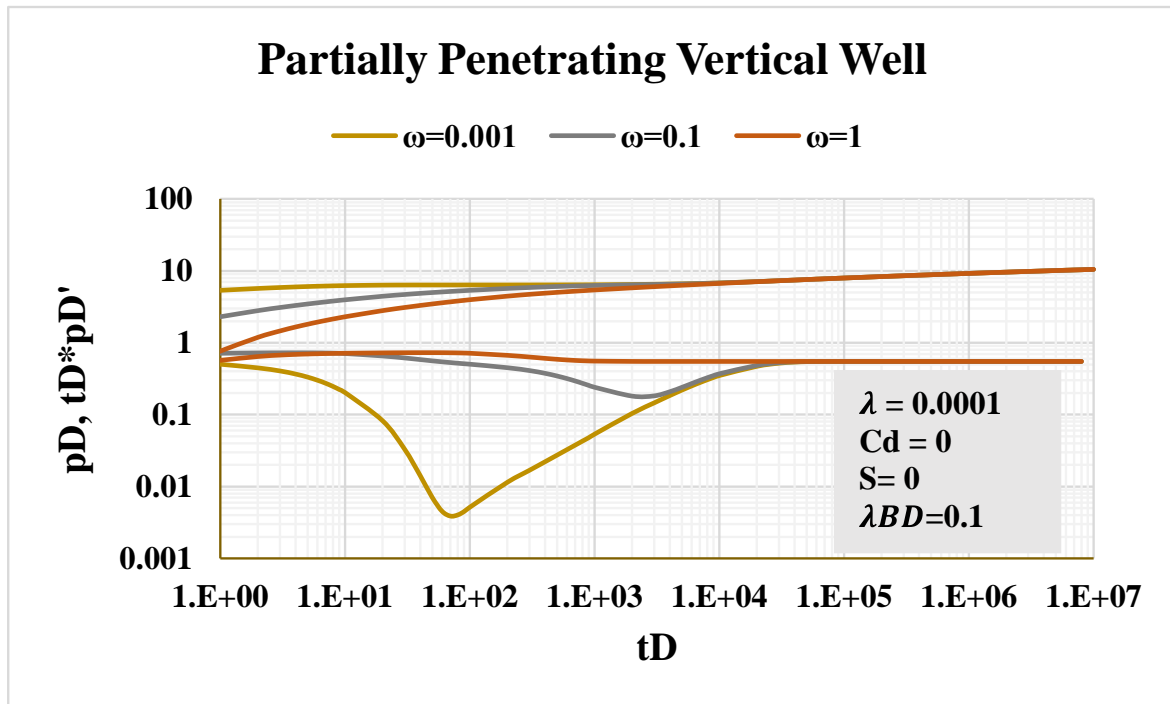


Figure 4.10 Effect of storativity on pressure response of a partially penetrating vertical well

4.7.4 Fully Penetrating Vertical Well

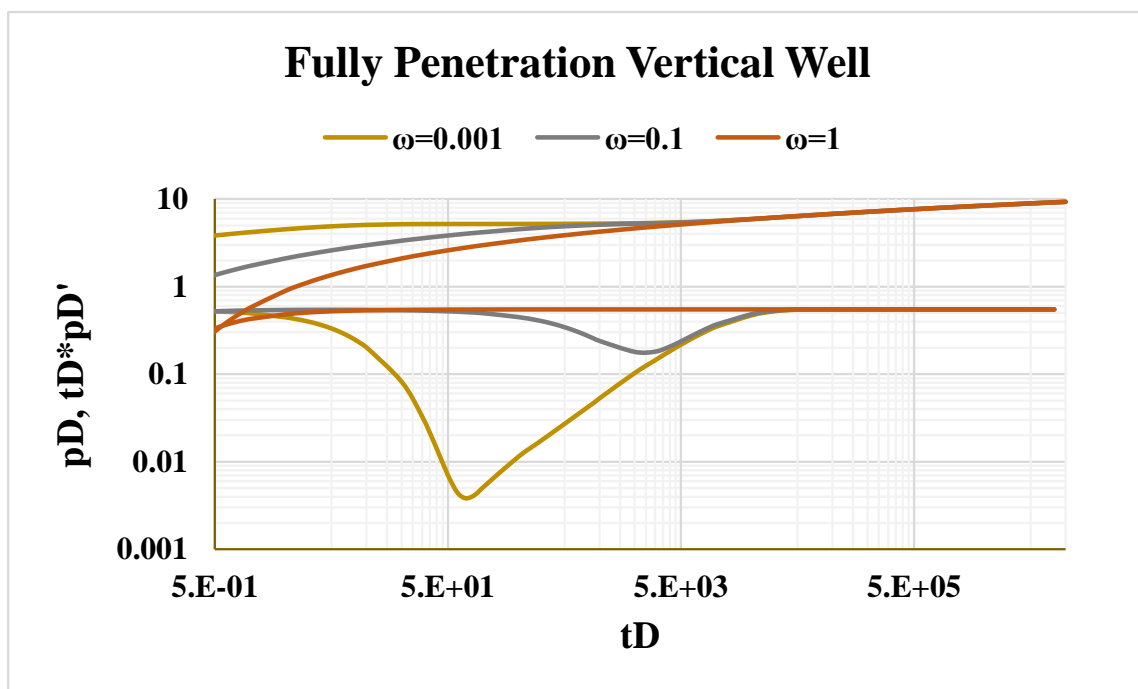


Figure 4.12 Effect of storativity ratio on pressure response of a fully penetrating vertical well

4.8 Effects of interporosity flow parameter, λ

This section discusses the effect of interporosity flow parameter for horizontal well, hydraulically fractured well, partially penetrating vertical well and fully penetrating vertical well. A vertical isotropy was assumed and other constant parameters are: Dimensionless wellbore storage = 0, Skin = 0, storativity ratio = 0.01, $\lambda_{BD} = 0.1$

A general trend observed was made for all the three curves. The curves were shifted to the left as the value of λ increases. The ratio of the matrix permeability to fracture permeability is one of the factors that influence interporosity permeability. A higher λ implies that fracture depletion takes a short time before transition period begins. This may be due to a relatively high matrix permeability as compared to fracture permeability. From figure 4.12 to figure 4.15, a shift to the left with increasing λ is observed.

4.8.1 Horizontal well

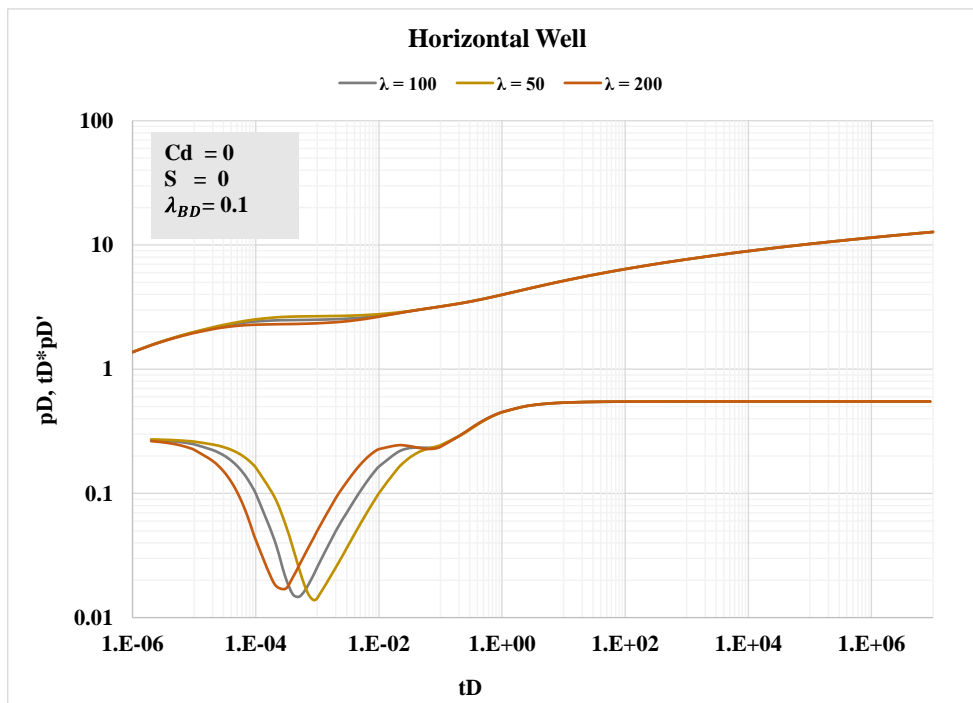


Figure 4.12 Effect of interporosity flow parameter on horizontal well

4.8.2 Hydraulically fractured well

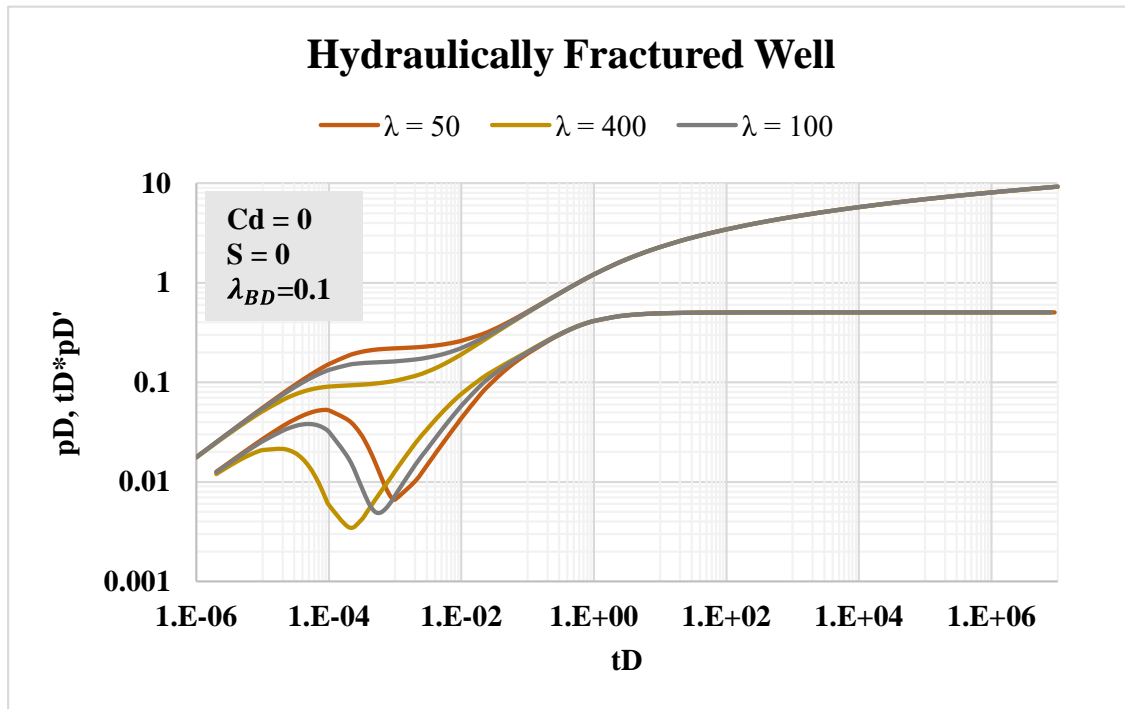


Figure 4.13 Effects of interporosity flow parameter in hydraulically fractured well.

4.8.3 Partially penetrating vertical well

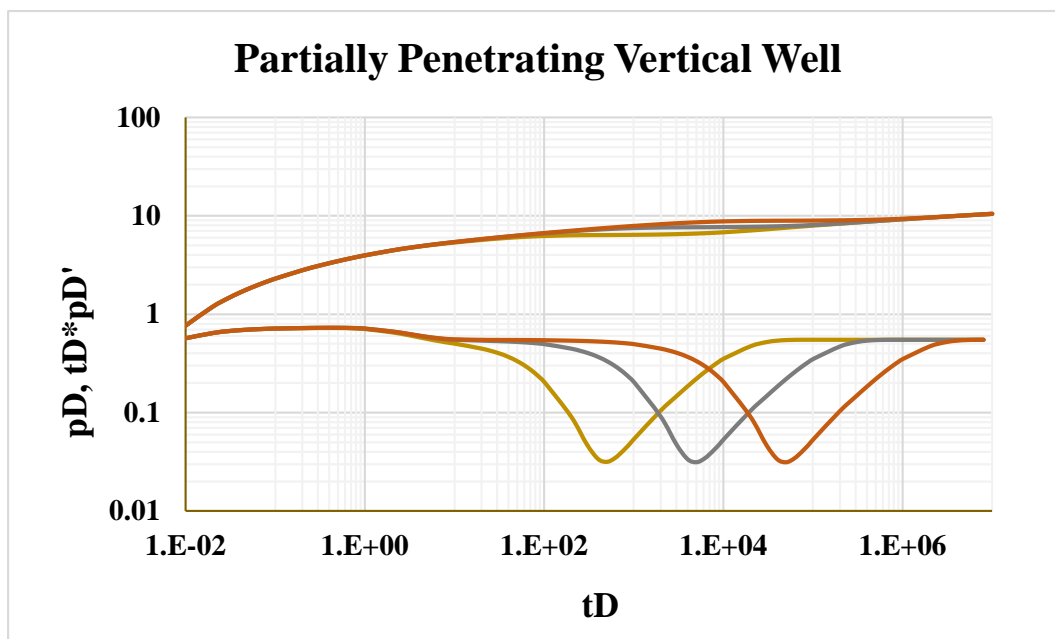


Figure 4.14 Effect of interporosity flow parameter in a partially penetrating vertical well

4.8.4 Fully penetrating vertical well

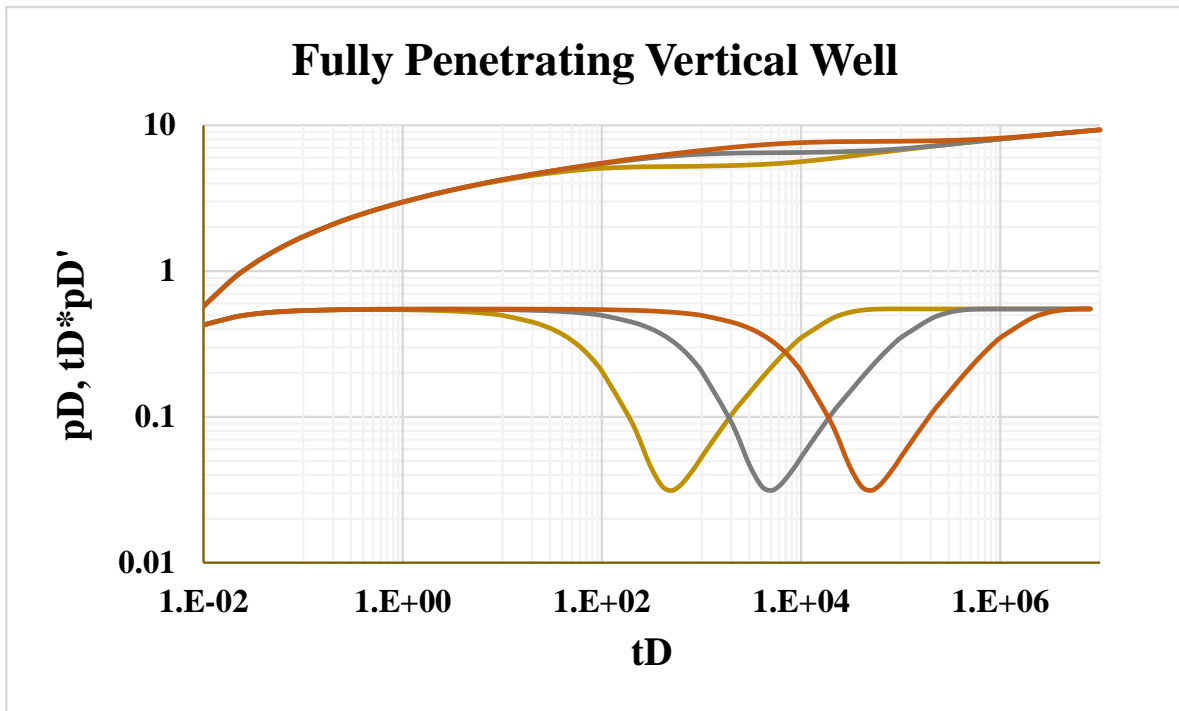


Figure 4.15 Effect of interporosity flow parameter for vertical well

4.9 Establishment of the pressure derivative at late radial flow

This section discusses a unique value for the pressure derivative plot at late radial flow regime for horizontal well, hydraulically fractured well, partially penetrating vertical well and fully penetrating vertical well. A curve of $t * \Delta P' / (1 + \lambda_{BD})$ versus time was drawn for all the four cases. An interesting observation was made on the late radial flow regime for all cases. The value of $t * \Delta P' / (1 + \lambda_{BD})$ is equivalent to 0.5 during late radial flow for all the four cases and for any value of λ_{BD} . Figures 4.16 to 4.19 show this phenomenon.

4.9.1 Horizontal Well

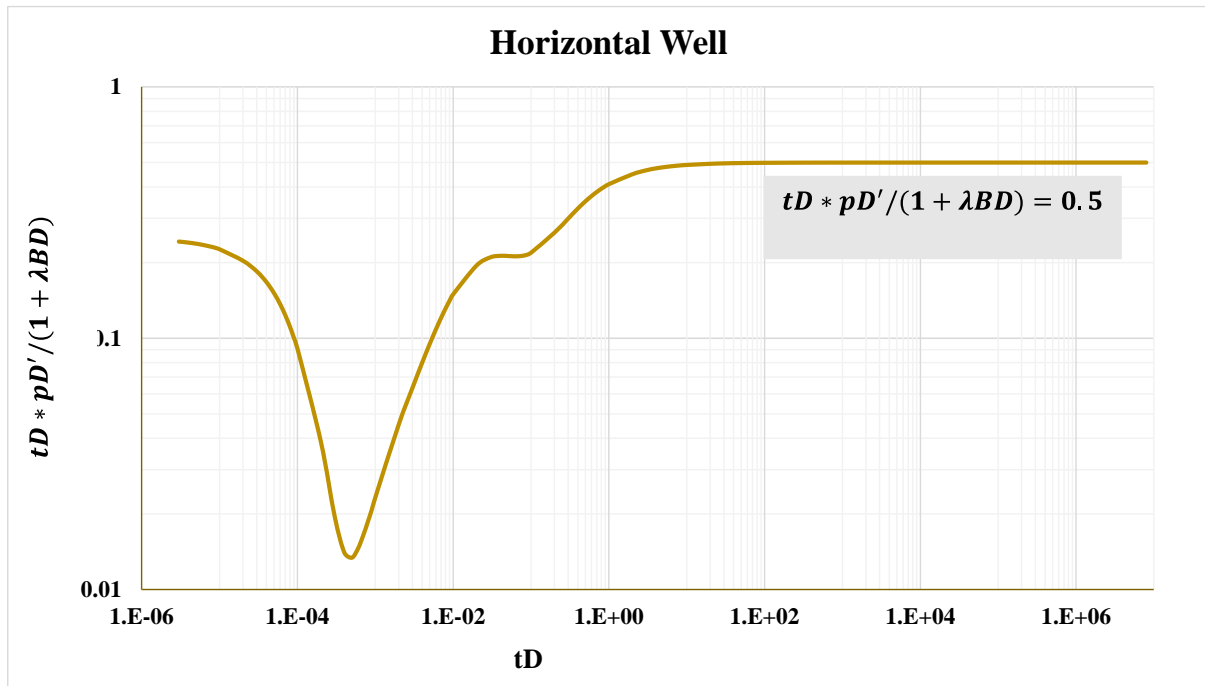


Figure 4.16 Pressure derivative value for Horizontal well in a reservoir with minimum threshold pressure

4.9.2 Hydraulically Fractured Well

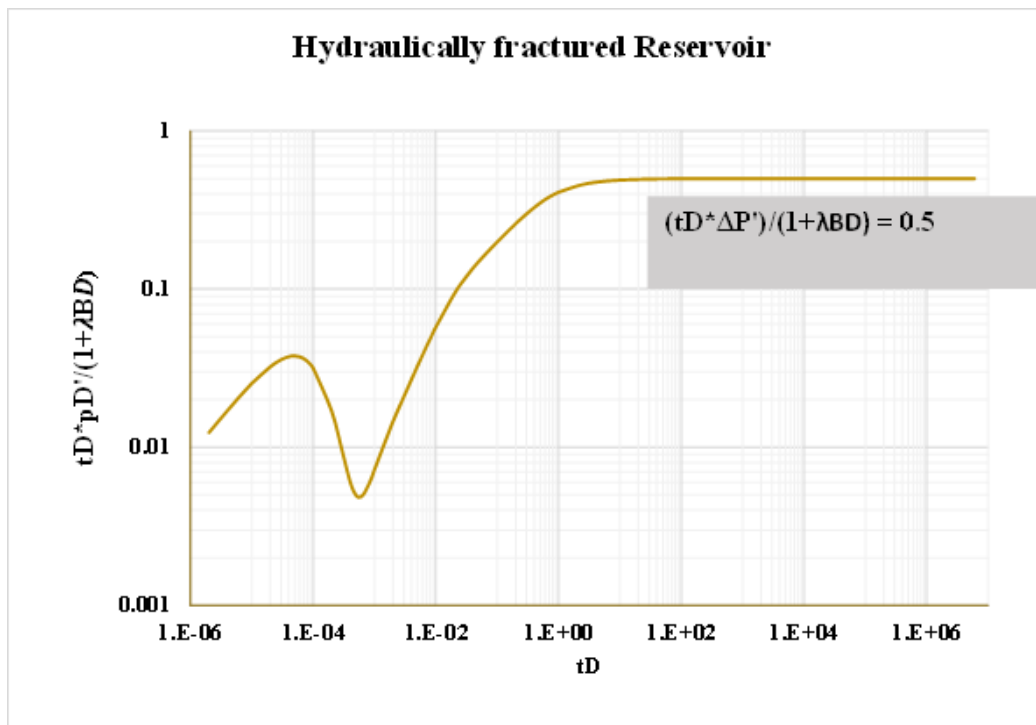


Figure 4.17 Pressure derivative value for hydraulically fractured well in a reservoir with minimum threshold pressure

4.9.3 Partially Penetrating Vertical Well

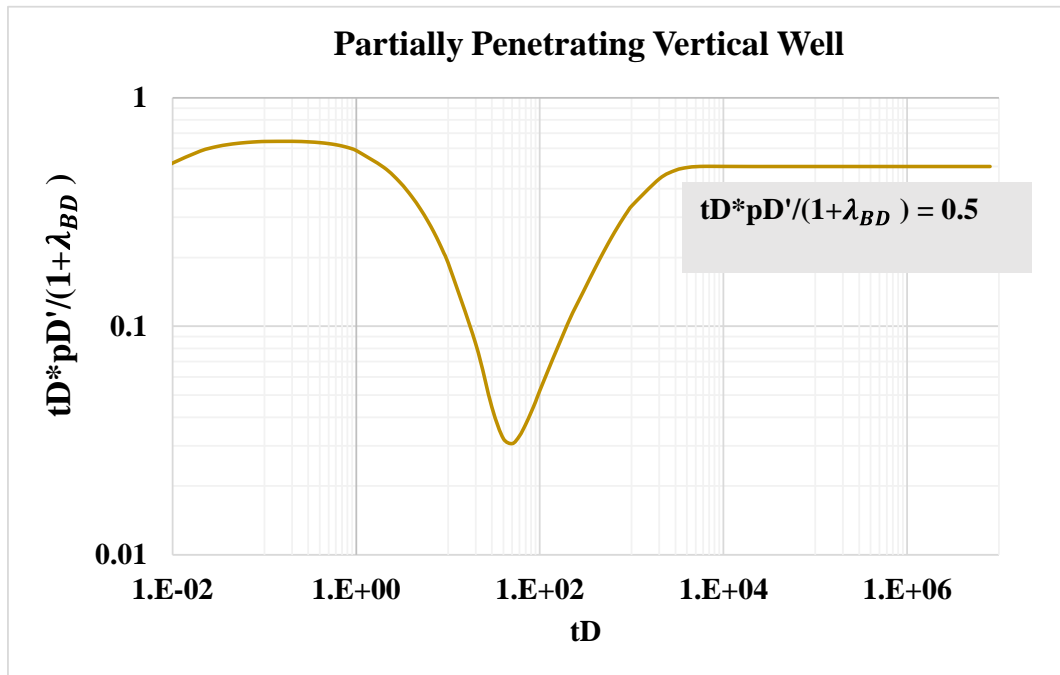


Figure 4.18 Pressure derivative value for partially penetrating vertical well in a reservoir with minimum threshold pressure

4.9.4 Fully penetrating vertical well

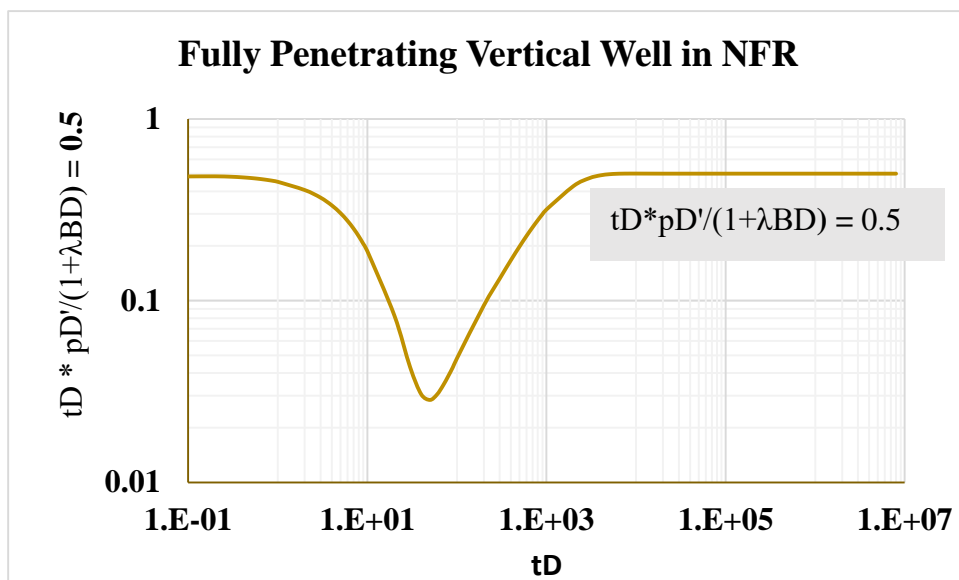


Figure 4.19 Pressure derivative value for fully penetrating vertical well in a reservoir with minimum threshold pressure

5.10 Derivation of permeability formular during early radial flow

Horizontal well model was used to estimate k_{yz} permeability. Infinte acting, early time radial flow regime in the yz plane is used for calculating k_{yz} permeability product for horizontal well. During early radial flow:

$$t_D * P_D' = 0.5 * (1 + \lambda_{BD}) \sqrt{\frac{k_y}{k_z}} \quad (4.1)$$

Where:

$$p_D = \frac{k_y L_w}{141.2 q B \mu} \Delta P \quad (4.2)$$

Therefore,

$$t_D * P_D' = \frac{k_y L_w}{141.2 q B \mu} t * \Delta P' \quad (4.3)$$

Substituting Equation 4.2 into Equation 4.1 and manipulating gives the permeability product as:

$$\sqrt{k_y k_z} = \frac{70.6 q \mu B (1 + \lambda_{BD})}{L_w (t * \Delta P')_{ER}} \quad (4.4)$$

Derivation of equation for permeability in the y-direction

$$P_D = \left(\frac{2r_w}{h_z} \sqrt{\pi t_D} + \left(S_t \sqrt{\frac{k_y}{k_z}} \right) \right) * (1 + \lambda_{BD}) \quad (4.5)$$

Taking the derivative of Equation 4.5 gives:

$$P_D' = \frac{r_w \sqrt{\pi}}{h_z \sqrt{t_D}} (1 + \lambda_{BD}) \quad (4.6)$$

Multiplying Equation 4.6 by t_D gives:

$$t_D * P_D' = \frac{r_w}{h_z} \sqrt{\pi t_D} * (1 + \lambda_{BD}) \quad (4.7)$$

By definition, dimensionless pressure and time are given as:

$$P_D = \frac{k_y L_w \Delta P}{141.2 q \mu B} \quad (4.8)$$

$$t_D = \frac{0.0002637 k_y t}{\phi \mu \omega C_t r_w^2} \quad (4.9)$$

Substituting for dimensionless terms and rearranging gives:

$$k_y = \frac{141.2 q \mu B (1 + \lambda_{BD})}{h_z (t * \Delta P')} \sqrt{\frac{\pi * 0.000263 k t}{\phi \omega \mu C_t L_w^2}} \quad (4.10)$$

Equation 4.10 is simplified to:

$$k_y = \left(\frac{4.066 q B (1 + \lambda_{BD})}{h_z L_w (t * \Delta P')} \right)^2 \frac{\mu t}{\phi \omega C_t} \quad (4.11)$$

At 1 hour,

$$k_y = \left(\frac{4.066q\mu B(1+\lambda_{BD})}{h_z L_w(t*\Delta P')} \right)^2 \frac{\mu}{\phi\omega C_t} \quad (4.12)$$

4.11 Derivation of equation for average radial permeability

At late time when t_D is large enough, a radial flow regime is observed and is characterised by a zero slope on the pressure derivative plot.

During late radial flow, dimensionless pressure derivative is given as

$$t_D * P'_D = 0.5 (1 + \lambda_{BD}) \quad (4.13)$$

Substituting Equation 4.8 into Equation 4.13 gives:

$$\left(\frac{k_h h}{141.2qB\mu} \right) t * \Delta P' = 0.5 (1 + \lambda_{BD}) \quad (4.14)$$

Therefore,

$$t * \Delta P' = \frac{70.6qB_0\mu}{k_h h} (1 + \lambda_{BD}) \quad (4.15)$$

Average horizontal permeability is given by Equation 4.16.

$$k_h = \frac{70.6*q\mu B_0(1+\lambda_{BD})}{h*(t*\Delta P')_{LRF}} \quad (4.16)$$

4.12 Derivation of equation for fracture length in hydraulically fractured well

If $t_{Dxf} < 0.1$;

$$P_D = (1 + \lambda_{BD})\sqrt{\pi t_{Dxf}} \quad (4.17)$$

Taking derivative w.r.t. t_{Dxf} gives

$$P'_D = 0.5 * (1 + \lambda_{BD}) \frac{\sqrt{\pi}}{\sqrt{t_{Dxf}}} \quad (4.18)$$

Multiplying by t_{Dxf} gives

$$t_{Dxf} * P'_D = 0.5 * (1 + \lambda_{BD})\sqrt{\pi t_{Dxf}} \quad (4.19)$$

Rearranging gives:

$$t_{Dxf} = 0.5 * (1 + \lambda_{BD}) \frac{P_D}{P'_D} \quad (4.20)$$

t_{Dxf} is also defined as:

$$t_{Dxf} = t_D \left(\frac{r_w}{x_f} \right)^2 = \frac{0.000263kt}{\phi \mu C_t X_f^2} \quad (4.21)$$

Substituting for t_{Dxf} gives:

$$\frac{0.0002637k}{\phi \mu C_t X_f^2} t = 0.5 * (1 + \lambda_{BD}) \frac{P_D}{P'_D} \quad (4.22)$$

Fracture length is given by:

$$X_f = \sqrt{\left(\frac{0.0002637k t_{L1} \Delta P'_{L1}}{0.5 \phi \mu C_t (1 + \lambda_{BD}) \Delta P'_{L1}} \right)} \quad (4.23)$$

At time = 1hr, X_f can be determined from:

$$X_f = \sqrt{\left(\frac{0.0002637k t_{L1} \Delta P'_{L1}}{0.5 \phi \mu C_t (1 + \lambda_{BD}) \Delta P'_{L1}} \right)} \quad (4.24)$$

4.13 Derivation of equation for storativity ratio

Storativity ratio is calculated from $(t * \Delta P')_{min}$ and $(t * \Delta P')_{FD}$ on the derivative plot during naturally fractured reservoir, NFR response.

At the lowest point of the trough:

$$(t_D * P'_D)_{min} = 0.5 * (1 + \lambda_{BD}) * \left(1 + \omega^{\frac{1}{1-\omega}} - \omega^{\frac{\omega}{1-\omega}} \right) \quad (4.25)$$

During fracture depletion, the flow is radial and the derivative is given as:

$$(t_D * P'_D)_{RF} = 0.5 * (1 + \lambda_{BD}) \quad (4.26)$$

Normalising Equation 4.25 by dividing by Equation 4.26 gives:

$$R = \frac{(t * \Delta P')_{min}}{(t * \Delta P')_{RF}} = \left(1 + \omega^{\frac{1}{1-\omega}} - \omega^{\frac{\omega}{1-\omega}} \right) \quad (4.27)$$

Storativity is estimated from the following empirical correlation:

$$\omega = 0.5604R^6 - 1.3322R^5 + 1.7232R^4 - 0.827R^3 + 0.7287R^2 + 0.1469R \quad (4.28)$$

4.14 Derivation of equation for interporosity flow parameter

Interporosity parameter is calculated during transition period, at the point corresponding to the minimum of the trough. At the minimum point:

$$(t_D * P'_D)_{min} = 0.63 * (1 + \lambda_{BD}) * \lambda * t_{Dmin} \quad (4.29)$$

Where:

$$p_D = \frac{k_f h}{141.2 q B \mu} \Delta P \quad (4.30)$$

$$t_D = \frac{0.0002637 k_f}{\mu r_w^2 (\phi C_t)_{m+f}} t_{min} \quad (4.31)$$

Substituting Equations 4.30 and 4.31 into Equation 4.29 and rearranging gives:

$$\lambda = \frac{42.6 \mu r_w^2 h (\phi C_t)_{m+f} (t * \Delta P')_{min}}{q B * (1 + \lambda_{BD}) t_{min}} \quad (4.32)$$

4.15 Example of Application

A data set of pressure draw down of horizontal well in a naturally fractured reservoir is given on table-1 in Appendix C. Other known well and reservoir data are:

$$Q = 500 \text{ STB/D} \quad \mu = 0.5 \text{ cp} \quad h = 20 \text{ ft} \quad L_w = 4000 \text{ ft} \quad B_o = 1.2 \text{ RB/STB}$$

$$\phi = 0.2 \quad C_t = 3 * 10^{-5} \quad \lambda_{BD} = 0.1, \quad \lambda = 10^{-4}, \quad \omega = 0.001, \quad x_D = 0.708, \quad z_D = 0.5, \quad y_D = 0.5$$

$$k_x = 100, \quad k_y = 100, \quad L_D = 100,$$

Example 1:

Calculate permeability in x and y direction, interporosity flow parameters, storativity ratio from pressure and pressure derivative log-log plot using TDS technique.

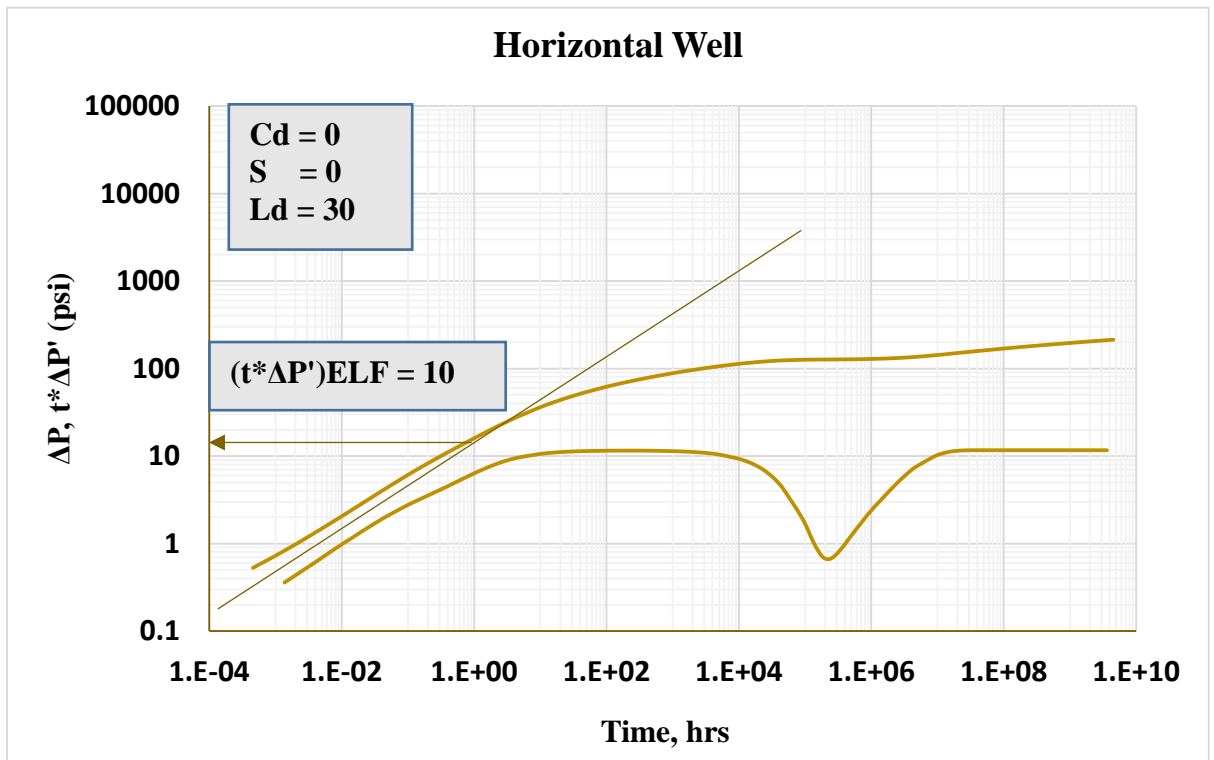


Fig. 4-20. Graph of pressure and pressure derivative against time for example 4-1

The value of $(t * \Delta P')_{ELF}$ is read from fig. 4-2 at time = 1 hour. Calculating permeability in y direction gives:

$$k_y = \left(\frac{4.066 * 500 * 1.2 * (1 + 0.1)}{20 * 4000 * 10} \right)^2 \frac{0.5}{0.2 * 0.01 * 0.00003} = 93.7mD$$

Permeability in y-direction is 93.7mD

4.15.1 Calculating permeability during infinitely acting late radial flow

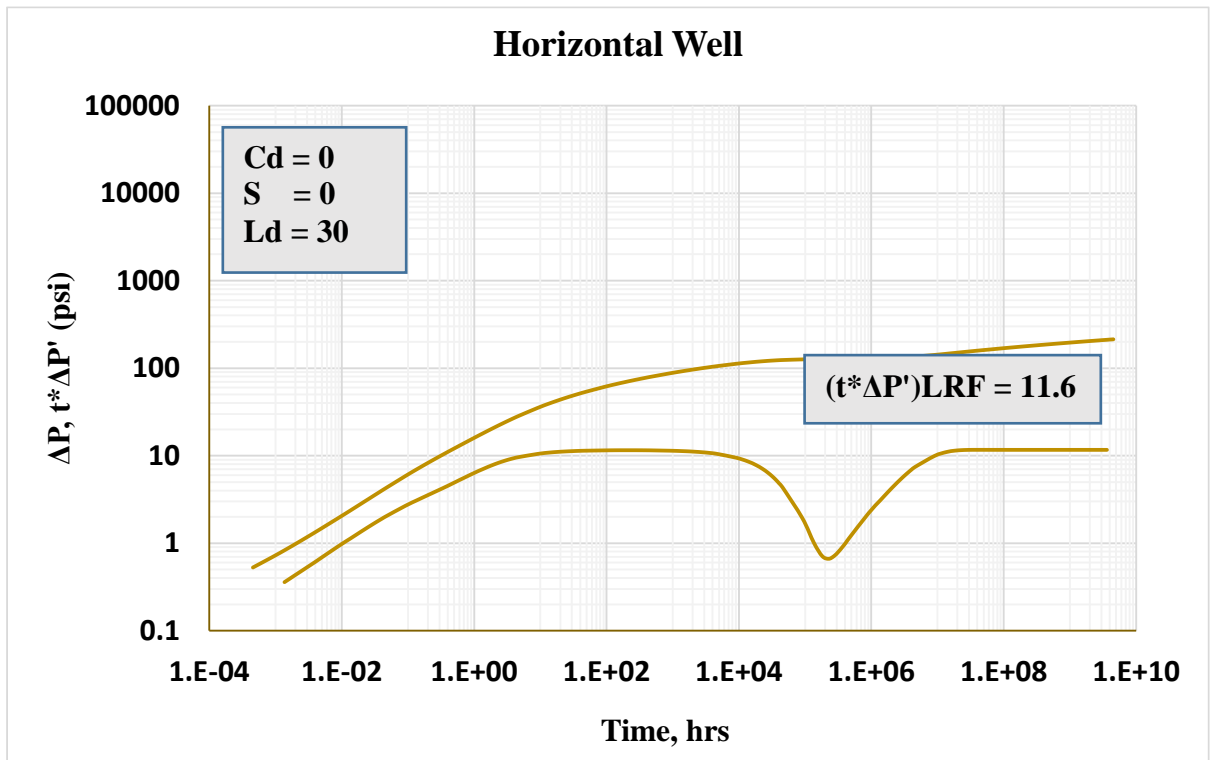


Fig. 4-21. Graph of pressure and pressure derivative against time for example 4-1

From fig.4-3, the $(t * \Delta P')_{LRF} = 4.66$

k_H is calculated from:

$$k_H = \frac{70.6 * q\mu B_0(1 + \lambda_{BD})}{h * (t * \Delta P')_{LRF}}$$

$$k_H = \frac{70.6 * 500 * 0.5 * 1.2 * (1 + 0.1)}{20 * 11.6} = 100.4mD$$

Which is approximately equivalent to the average of k_x and k_y used in the model.

Calculating permeability in the x-direction, k_x

$$k_H = \sqrt{k_x k_y}$$

$$k_x = \frac{(\sqrt{k_x k_y})^2}{k_y} = \frac{k_H^2}{k_y} = \frac{(100.4)^2}{93.7} = 107.6mD$$

4.15.2 Calculating storativity ratio

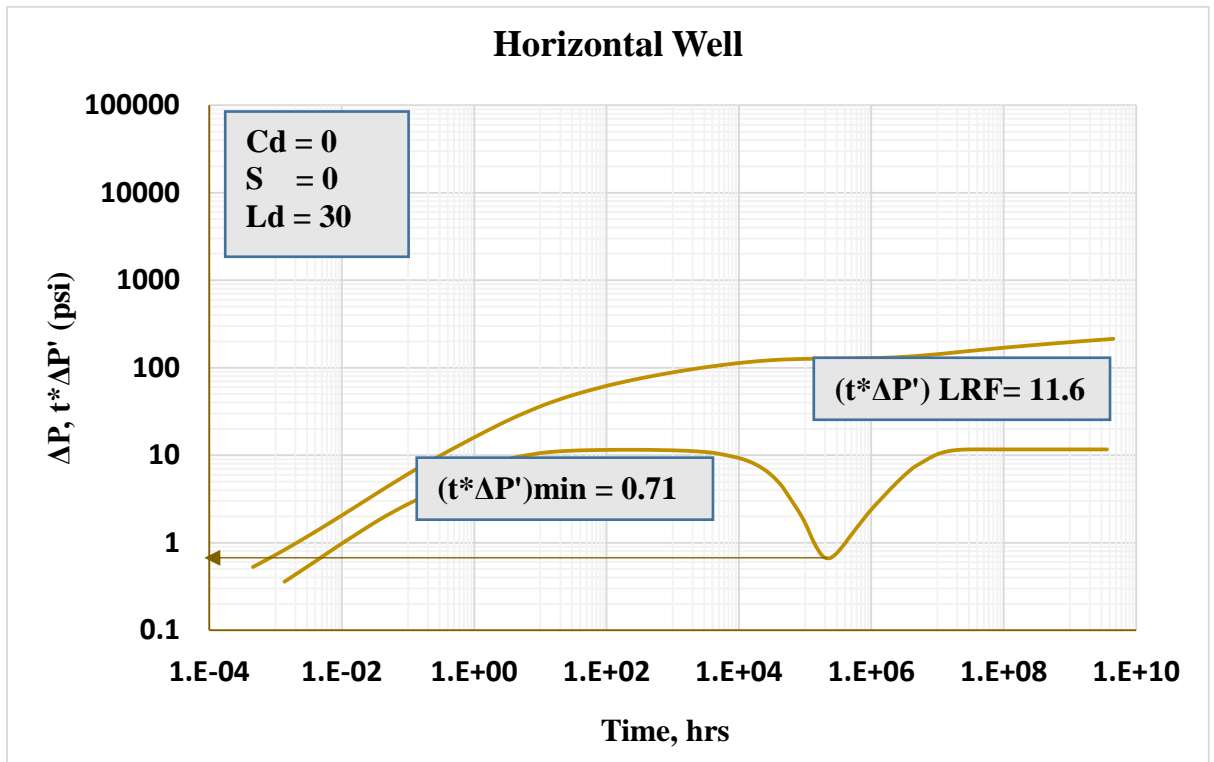


Fig.4-22 Graph of pressure and pressure derivative against time for example 4-1

$$R = \frac{(t * \Delta P')_{min}}{(t * \Delta P')_{RF}} = \frac{0.71}{11.6} = 0.0612$$

$$\omega = 0.5604 * 0.061^6 - 1.3322 * 0.061^5 + 1.7232 * 0.061^4 - 0.827 * 0.061^3 + 0.7287 * 0.061^2 + 0.1469 * 0.061 = 0.01$$

This is the same as the original value used as input data.

4.15.3 Calculating interporosity flow parameter

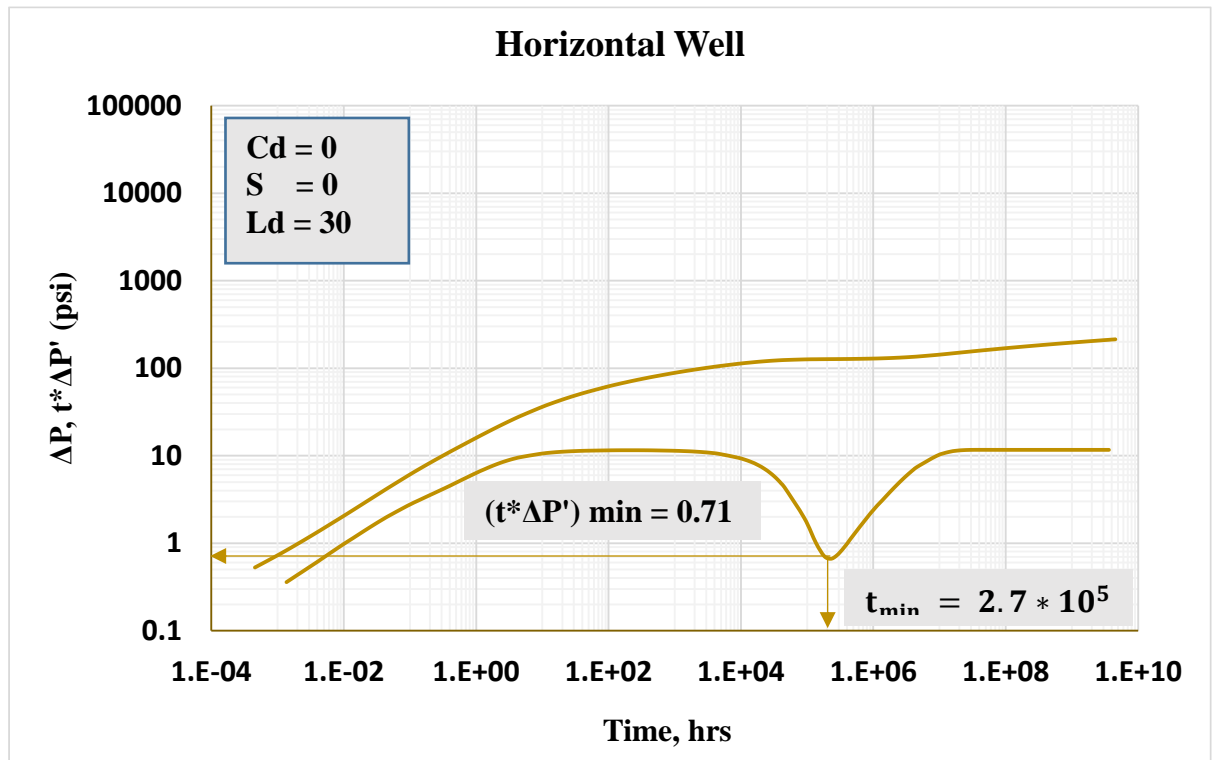


Fig. 4-23 Graph of pressure and pressure derivative against time for example 4-1

$$(\phi C_t)_{m+f} = (\phi C_t)_m \left(1 + \frac{\omega}{1 - \omega}\right)$$

$$(\phi C_t)_{m+f} = 0.2 * 0.00003 * \left(1 + \frac{0.01}{1 - 0.01}\right) = 6.0 * 10^{-6}$$

$$\lambda = \frac{45.5 \mu L_w^2 h (\phi C_t)_{m+f} (t * \Delta P')_{min}}{qB * (1 + \lambda_{BD}) t_{min}}$$

$$\lambda = \frac{45.5 * 0.5 * 4000^2 * 20 * 6.06 * 10^{-6} * 0.71}{500 * 1.2 * (1 + 0.1) * 2.7 * 10^5} = 1.76 * 10^{-4}$$

This value is in the same order as the original one used as input data.

CHAPTER 5

CONCLUSION AND RECOMMENDATIONS

This section presents insights that were derived from the research and some recommendations that may advance the work.

5.1 Conclusions

1. The presence of minimum threshold pressure in a Bingham fluid causes an additional pressure drop which is characterised by an upward shift on both pressure and pressure derivative response on the log-log plot.
2. If $t_D * P'_D / (1 + \lambda_{BD})$ vs time is plotted on a log-log plot, during the late radial flow regime, the pressure derivative coordinate is equal to 0.5 for all the four cases considered in this study.
3. For high values of L_D , horizontal wells behave like hydraulically fractured wells, an early radial flow disappears.
4. Small h_{wD} causes a pseudo-skin and this is characterised by an upward shift in both pressure and pressure derivative on the log-log plot of partially penetrating well.
5. For high values of h_{wD} , partially penetrating wells behave similar to fully penetrating vertical well

Recommendations

To advance the study presented in this work, the following recommendations are made:

1. Further works should consider the effect of skin and wellbore storage effects in the analysis of pressure transient analysis of horizontal well with long well length.

2. An investigation should be made to estimate the impact of λ_{BD} on the economics of heavy oil production.

REFERENCES

- Abel, C., Abdelghani, D., & Djebbar, T. (2007). Determining the Average Reservoir Pressure from Vertical and Horizontal Well Test Analysis Using the Technique. <https://doi.org/10.2523/88619-ms>
- Abramowitz, M., & Stegun, I., A. (1964). *Handbook of Mathematical Functions With Formulas, Graphs and Mathematical Tables*.
- Escobar, F. H. (2012). Transient Pressure and Pressure Derivative Analysis for Non-Newtonian Fluids.
- Goode, P. A., & Thambynayagam, R. K. . (1985). Pressure Drawdown and Buildup Analysis of Horizontal Wells in Anisotropic Media. *SPE Formation Evaluation*, 2(4), 683–697. <https://doi.org/10.2118/14250-PA>
- Gringarten, A. C., & Ramey, H. J. (1973). The Use of Source and Green's Functions in Solving Unsteady-Flow Problems in Reservoirs. *Society of Petroleum Engineers Journal*, 13(05), 285–296. <https://doi.org/10.2118/3818-pa>
- Guo, J. C., Nie, R. S., & Jia, Y. L. (2012). Dual permeability flow behavior for modeling horizontal well production in fractured-vuggy carbonate reservoirs. *Journal of Hydrology*, 464–465, 281–293. <https://doi.org/10.1016/j.jhydrol.2012.07.021>
- Houzé, O., Viturat, D., & Fjaere, O. (2018). *Dynamic Data Analysis*. KAPPA.
- Lee, L., Rollins, J. ., & Spivy, J. . (2003). *Pressure Transient Testing*. Society of Petroleum Engineers.
- Mattar, L., & Dean, L. (2008). Well Test Interpretation. *Reservoir Engineering for Geologists, Part 6*, 1–3. <https://doi.org/10.1016/j.jpeds.2009.06.015>
- Mendes, P. R. S., Naccache, M. F., Braga, C. V. M., Nieckele, A. O., & Ribeiro, F. S. (2002a). Flows of Bingham Materials Through Ideal Porous Media: an Experimental and Theoretical Study. *Journal of the Brazilian Society of Mechanical Sciences*, 24(1), 40–45. <https://doi.org/10.1590/S0100-73862002000100006>
- Mendes, P. R. S., Naccache, M. F., Braga, C. V. M., Nieckele, A. O., & Ribeiro, F. S. (2002b). Flows of Bingham Materials Through Ideal Porous Media: an Experimental and Theoretical Study. *Journal of the Brazilian Society of Mechanical Sciences*, 24(1). Retrieved from http://www.scielo.br/scielo.php?script=sci_arttext&pid=S0100-73862002000100006
- Nie, R. S., Wang, Y. M., Kang, Y. L., & Jia, Y. L. (2018). Modeling the characteristics of Bingham porous-flow mechanics for a horizontal well in a heavy oil reservoir. *Journal of Petroleum Science and Engineering*, 171(July), 71–81. <https://doi.org/10.1016/j.petrol.2018.07.026>
- Owayed, J. F., & Tiab, D. (2008a). Transient pressure behavior of Bingham non-Newtonian fluids for horizontal wells. *Journal of Petroleum Science and Engineering*, 61(1), 21–32. <https://doi.org/https://doi.org/10.1016/j.petrol.2007.10.003>
- Owayed, J. F., & Tiab, D. (2008b). Transient pressure behavior of Bingham non-Newtonian fluids for horizontal wells. *Journal of Petroleum Science and Engineering*, 61(1), 21–32. <https://doi.org/10.1016/j.petrol.2007.10.003>
- Ozkan, E. (1988). *Perfomance of horizontal wells*. University of Tulsa.
- Ozkan, E., & Raghavan, R. (1991). New Solutions for Well-Test-Analysis Problems: Part 1-Analytical Considerations, (September).

- Ozkan, E., Raghavan, R., & Joshi, S. D. (1989). Horizontal Well Pressure Analysis. *SPE Formation Evaluation*, 4(04), 567–575. <https://doi.org/10.2118/16378-pa>
- Rebolledo, L. C., & Ershaghi, I. (2015). Errors in Estimating Interporosity Flow Coefficient in Naturally Fractured Reservoirs. <https://doi.org/10.2118/178737-stu>
- Slimani, K., & Tiab, D. (2008). Pressure transient analysis of partially penetrating wells in a naturally fractured reservoir. *Journal of Canadian Petroleum Technology*, 47(5), 63–69.
- Slimani, K., Tiab, D., & Moncada, K. (2006). Pressure Transient Analysis of Partially Penetrating Wells in a Naturally Fractured Reservoir. *Society of Petroleum Engineers Journal*.
- Stehfest, H. (2002). Algorithm 368: Numerical inversion of Laplace transforms [D5]. *Communications of the ACM*. <https://doi.org/10.1145/361953.361969>
- Tiab, P. D. (2015). ADVANCED WELL TEST – Hydraulically Fractured Wells Class Notes.
- Warren, J. E., & Root, P. J. (1963). The Behavior of Naturally Fractured Reservoirs. *Society of Petroleum Engineers Journal*, 3(03), 245–255. <https://doi.org/10.2118/426-pa>
- Wu. (1990). *Lawrence Berkeley National Laboratory Lawrence Berkeley National Laboratory*. <https://doi.org/10.1007/978-3-319-46448-0>
- Wu, Y. S., Pruess, K., & Witherspoon, P. A. (1992). *Flow and Displacement of Bingham Non-Newtonian Fluids in Porous Media*.
- Zhao, Zhang, L.-H., Wu, F., ZHANG, B.-N., & Liu, Q.-G. (2013). Analysis of horizontal well pressure behaviour in fractured low permeability reservoirs with consideration of the, 10. <https://doi.org/10.1088/1742-2132/10/3/035014>

APPENDIX A

Darcy's law

$$\vec{v} = -\frac{k}{\mu}(\nabla P) \quad A 1$$

Continuity Equation

$$\nabla(\rho\vec{v}) = -\frac{\partial(\rho\phi)}{\partial t} \quad A 2$$

Substituting A1 into Equation A2

$$\nabla\left(\rho\left(-\frac{k}{\mu}\nabla P\right)\right) = -\frac{\partial(\rho\phi)}{\partial t} \quad A 3$$

Heavy oil is a slightly compressible fluid, therefore,

$$\rho = \rho_o e^{c_o(\Delta P)} \quad A 4$$

Using the McLaurin Expansion,

$$e^{c_o(\Delta P)} = 1 + (c_o(\Delta P)) + \frac{(c_o(\Delta P))^2}{2!} + \dots + \frac{(c_o(\Delta P))^n}{n!} \quad A 5$$

Taking the first two terms

$$e^{c_o(\Delta P)} = 1 + (c_o(\Delta P)) \quad A 6$$

Therefore, substituting for ρ , using Maclaurin expansion of the exponent gives;

$$-\frac{k}{\mu}\rho_o\nabla\left([1 + (c_o(\Delta P))](\nabla P)\right) = \frac{\partial(\rho_o\phi_r[1+(c_o(\Delta P))]*[1+(c_r(\Delta P))])}{\partial t} \quad A 7$$

Considering LHS of A7,

$$-\frac{k}{\mu}\rho_o\nabla\left([1 + (c_o(\Delta P))](\nabla P)\right) = -\frac{k}{\mu}\rho_o[(\nabla P) + C_o\Delta P(\nabla P)] \quad A 8$$

$C_o\Delta P(\nabla P) \ll (\nabla P)$ and can be neglected. So LHS becomes

$$-\frac{k}{\mu}\rho_o\nabla\left([1 + (c_o(\Delta P))](\nabla P)\right) = -\frac{k}{\mu}\rho_o\nabla(\nabla P) \quad A 9$$

Now considering the RHS of A7,

$$-\frac{\partial(\rho_o \varphi_r [1+(c_o(\Delta P))] * [1+(c_r(\Delta P))])}{\partial t} = -\frac{\rho_o \varphi_r \partial([1+(c_o(\Delta P))] * [1+(c_r(\Delta P))])}{\partial t} \quad A 10$$

Expanding and taking out negligible terms gives

$$-\frac{\rho_o \varphi_r \partial([1+(c_o(\Delta P))] * [1+(c_r(\Delta P))])}{\partial t} = -\frac{\rho_o \varphi_r \partial(1+c_t \Delta P)}{\partial t} \quad A 11$$

$c_t = c_r + c_o$, assuming that oil is the only fluid in the reservoir such that $c_w s_w + c_g s_g = 0$

Now, combining LHS and RHS gives,

$$-\frac{k}{\mu} \rho_o \nabla(\nabla P) = -\frac{\rho_o \varphi_r c_t \partial(1+\Delta P)}{\partial t} \quad A 12$$

Therefore,

$$-\frac{k}{\mu} \nabla(\nabla P) = -\frac{\varphi_r c_t \partial(1+\Delta P)}{\partial t} = -\frac{\varphi_r c_t \partial(\Delta P)}{\partial t} \quad A 13$$

Rearranging A13 gives,

$$-\frac{k}{\mu} \nabla(\nabla P) = -\frac{\varphi_r c_t \partial(\Delta P)}{\partial t} \quad A 14$$

$$-\frac{k}{\mu \varphi_r c_t} \nabla(\nabla P) + \frac{\partial \Delta P}{\partial t} = 0 \quad A 15$$

In cylindrical form,

$$-\frac{k}{\mu \varphi_r c_t} \nabla(\rho \vec{v}) = \frac{\eta}{r} \frac{\partial}{\partial r} \left(r \frac{\partial(\nabla P)}{\partial r} \right) + \frac{\eta \partial(\nabla P)}{\partial z^2} \quad A 16$$

Where $\eta_h = \frac{k_h}{\mu \varphi_r c_t}$ and $\eta_v = \frac{k_v}{\mu \varphi_r c_t}$

A16 can be written as

$$-\frac{\eta_h}{r} \frac{\partial}{\partial r} \left(r \left(\frac{\partial}{\partial r} P \right) \right) - \frac{\eta_v \partial}{\partial z} \left(\frac{\partial}{\partial z} P \right) + \frac{\partial(\Delta P)}{\partial t} = 0 \quad A 17$$

Using chain rule equation A17 becomes,

$$-\eta_h \left(\frac{\partial^2 P}{\partial r^2} + \frac{1}{r} \frac{\partial P}{\partial r} \right) - \eta_v \left(\frac{\partial^2 P}{\partial z^2} \right) + \frac{\partial(\Delta P)}{\partial t} = 0 \quad A 18$$

$$\frac{\eta_v}{\eta_h} = \frac{K_v}{K_h}$$

Dividing throughout by η_h gives,

$$-\frac{\partial^2 P}{\partial r^2} - \frac{1}{r} \frac{\partial P}{\partial r} - \frac{K_v}{K_h} \left(\frac{\partial^2 P}{\partial z^2} \right) + \frac{1}{\eta_h} \frac{\partial(\Delta P)}{\partial t} = 0$$

A 19

APPENDIX B

STEHFEST ALGORITHM

$$\forall t \in R_+^*, f(t) \approx \frac{\ln(2)}{t} \sum_{n=1}^N \left(K_n \hat{F} \left(\frac{n \ln(2)}{t} \right) \right) \quad B 1$$

APPENDIX C

Table 1: Pressure drawdown data

| time, hrs | ΔP (psi) | $t^*\Delta P'$ (psi) |
|-----------|------------------|----------------------|
| 0.001024 | 5.823907426 | |
| 0.002048 | 6.619817599 | 1.14091896 |
| 0.003072 | 7.080680293 | 1.12968521 |
| 0.004096 | 7.404253507 | 1.11862628 |
| 0.005119 | 7.652806145 | 1.10803646 |
| 0.006143 | 7.853956248 | 1.09669437 |
| 0.007167 | 8.022155269 | 1.08565779 |
| 0.008191 | 8.16649125 | 1.07544637 |
| 0.009215 | 8.292592523 | 1.06470124 |
| 0.010239 | 8.404211843 | 1.05276109 |
| 0.020478 | 9.103639364 | 0.94742351 |
| 0.030717 | 9.473167332 | 0.86019912 |
| 0.040956 | 9.710186909 | 0.7790908 |
| 0.051195 | 9.876281274 | 0.7044756 |
| 0.061433 | 9.998784064 | 0.63628748 |
| 0.071672 | 10.09222607 | 0.57433807 |
| 0.081911 | 10.16523586 | 0.51832864 |
| 0.09215 | 10.22333226 | 0.46788017 |
| 0.102389 | 10.27023736 | 0.42400891 |
| 0.204778 | 10.46756537 | 0.1805485 |
| 0.307167 | 10.5160724 | 0.09138001 |
| 0.409556 | 10.53659395 | 0.06541632 |
| 0.511945 | 10.5501669 | 0.06237191 |
| 0.614334 | 10.56176892 | 0.06783687 |
| 0.716724 | 10.57277367 | 0.07654033 |
| 0.819113 | 10.58359 | 0.08645788 |
| 0.921502 | 10.59434008 | 0.09678076 |
| 1.023891 | 10.60505631 | 0.10826702 |
| 2.047782 | 10.71000122 | 0.21138162 |
| 3.071672 | 10.80993481 | 0.2954974 |
| 4.095563 | 10.90495198 | 0.37250318 |
| 5.119454 | 10.99538088 | 0.44223166 |
| 6.143345 | 11.08151833 | 0.50508562 |
| 7.167235 | 11.16363137 | 0.56158648 |
| 8.191126 | 11.24196437 | 0.61226921 |
| 9.215017 | 11.31674341 | 0.65765059 |
| 10.23891 | 11.38817914 | 0.69673002 |

| | | |
|----------|-------------|------------|
| 20.47782 | 11.95646964 | 0.90745959 |
| 30.71672 | 12.34518753 | 0.97732408 |
| 40.95563 | 12.63014834 | 0.9914144 |
| 51.19454 | 12.85152729 | 0.98988084 |
| 61.43345 | 13.0316745 | 0.98717932 |
| 71.67235 | 13.18373224 | 0.98793483 |
| 81.91126 | 13.31582745 | 0.99314395 |
| 92.15017 | 13.43320807 | 1.00250711 |
| 102.3891 | 13.53939104 | 1.019677 |
| 204.7782 | 14.30030986 | 1.22550912 |
| 307.1672 | 14.82750755 | 1.39464311 |
| 409.5563 | 15.24799248 | 1.52989665 |
| 511.9454 | 15.60119478 | 1.63392793 |
| 614.3345 | 15.90670433 | 1.71517821 |
| 716.7235 | 16.17625029 | 1.78001125 |
| 819.1126 | 16.41757246 | 1.83279144 |
| 921.5017 | 16.63609965 | 1.87651839 |
| 1023.891 | 16.83580693 | 1.91121947 |
| 2047.782 | 18.23240033 | 2.09287585 |
| 3071.672 | 19.09949279 | 2.16960962 |
| 4095.563 | 19.7299978 | 2.20849164 |
| 5119.454 | 20.22571951 | 2.23209714 |
| 6143.345 | 20.63425202 | 2.24797869 |
| 7167.235 | 20.98172483 | 2.25940375 |
| 8191.126 | 21.28403832 | 2.26802141 |
| 9215.017 | 21.55159179 | 2.27475494 |
| 10238.91 | 21.79156047 | 2.27974193 |
| 20477.82 | 23.3815432 | 2.30352146 |
| 30716.72 | 24.31783225 | 2.31271257 |
| 40955.63 | 24.98388068 | 2.31707372 |
| 51194.54 | 25.5012409 | 2.31964777 |
| 61433.45 | 25.92433241 | 2.32135125 |
| 71672.35 | 26.28227098 | 2.32256359 |
| 81911.26 | 26.5924708 | 2.32347087 |
| 92150.17 | 26.8661802 | 2.32417541 |
| 102389.1 | 27.11108776 | 2.32469375 |
| 204778.2 | 28.72345427 | 2.32714203 |
| 307167.2 | 29.66726371 | 2.32807946 |
| 409556.3 | 30.33708371 | 2.32852108 |
| 511945.4 | 30.85671052 | 2.32878088 |
| 614334.5 | 31.28131458 | 2.32895255 |
| 716723.5 | 31.64033435 | 2.32907435 |
| 819112.6 | 31.95134536 | 2.32916563 |
| 921501.7 | 32.22568601 | 2.32923639 |

| | | |
|----------|-------------|------------|
| 1023891 | 32.47109867 | 2.32928822 |
| 2047782 | 34.08573987 | 2.32953394 |
| 3071672 | 35.0303081 | 2.32962784 |
| 4095563 | 35.7005076 | 2.32967208 |
| 5119454 | 36.22036214 | 2.32969804 |
| 6143345 | 36.64511802 | 2.32971522 |
| 7167235 | 37.00424623 | 2.32972742 |
| 8191126 | 37.31533862 | 2.32973653 |
| 9215017 | 37.58974251 | 2.32974373 |
| 10238908 | 37.83520583 | 2.32974898 |
| 20477816 | 39.4500748 | 2.3297734 |
| 30716724 | 40.39471898 | 2.32978285 |
| 40955631 | 41.06495648 | 2.32978718 |
| 51194539 | 41.58483377 | 2.32978978 |
| 61433447 | 42.00960486 | 2.32979155 |
| 71672355 | 42.36874391 | 2.32979271 |
| 81911263 | 42.67984443 | 2.32979355 |
| 92150171 | 42.95425463 | 2.3297945 |
| 1.02E+08 | 43.19972304 | 2.3297952 |
| 2.05E+08 | 44.8146148 | 2.32979733 |
| 3.07E+08 | 45.75926656 | 2.32979828 |
| 4.1E+08 | 46.42950783 | 2.32979868 |
| 5.12E+08 | 46.94938741 | 2.329799 |
| 6.14E+08 | 47.37416002 | 2.32979911 |
| 7.17E+08 | 47.73330013 | 2.3297993 |
| 8.19E+08 | 48.0444015 | 2.32979939 |
| 9.22E+08 | 48.31881233 | 2.32979938 |
| 1.02E+09 | 48.56428121 | 2.32979948 |
| 2.05E+09 | 50.17917526 | 2.32979974 |
| 3.07E+09 | 51.12382778 | 2.32979983 |
| 4.1E+09 | 51.79406943 | 2.3297999 |
| 5.12E+09 | 52.31394927 | 2.32979989 |
| 6.14E+09 | 52.738722 | 2.32979988 |
| 7.17E+09 | 53.09786224 | 2.32979985 |
| 8.19E+09 | 53.40896365 | 2.32979992 |
| 9.22E+09 | 53.68337457 | 2.32979993 |
| 1.02E+10 | 53.92884349 | |